CO_2 LASER GLASS PROCESSING FOR HIGH POWER FIBER LASER APPLICATIONS

A THESIS SUBMITTED TO
THE GRADUATE SCHOOL OF ENGINEERING AND SCIENCE
OF BILKENT UNIVERSITY
IN PARTIAL FULFILLMENT OF THE REQUIREMENTS FOR
THE DEGREE OF
MASTER OF SCIENCE
IN
MATERIAL SCIENCE AND NANOTECHNOLOGY

By
Bartu Şimşek
January 2016

CO_2 LASER GLASS PROCESSING FOR HIGH POWER FIBER LASER APPLICATIONS
By Bartu Şimşek
January 2016

We certify that we have read this thesis and that in our opinion it is fully adequate, in scope and in quality, as a thesis for the degree of Master of Science.

Bülend Ortaç(Advisor)

Mehmet Bayındır

Hakan Altan

Approved for the Graduate School of Engineering and Science:

Levent Onural
Director of the Graduate School

ABSTRACT

CO_2 LASER GLASS PROCESSING FOR HIGH POWER FIBER LASER APPLICATIONS

Bartu Şimşek
M.S. in Material Science and Nanotechnology
Advisor: Bülend Ortaç
January 2016

High power lasers have been extensively used in industry, military, astrophysics and medicine for decades. Thanks to developments in optical fiber technology in terms of transmittance, heat resistance, robustness, stability and power endurance, fiber lasers have recently become more favourable compared to conventional laser types such as gas and solid state lasers. Furthermore, high power fiber lasers possess advantageous features like compactness, robustness, all-fiber and alignment-free operation. Besides advances in high power fiber lasers, the structure and power endurance of the critical components as well as their integration quality have been improved. CO_2 laser is one the most effective source in glass processing of optical fibers since it provides stable and homogeneous radiation resulting in a clean process. We have tailored optical fibers to attain low-loss, high quality, mechanically stable integration points by using CO_2 laser radiation. Moreover, we have produced high power fiber laser components such as end-cap and ball lens for manipulating the fiber laser output beam. By tapering the optical fibers, we have fabricated pump and signal combiners which have mode field adapting properties. The 7x1 pump combiner was integrated to the high power fiber laser system developed in our laboratory. Pump source limited power handling capacity of this pump combiner was measured as 850 W with an overall efficiency of 98%. In addition, the same pump combiner was adapted to a high power fiber laser system which was built by using an in-house fabricated active fiber. Finally, we have fabricated a 3x1 laser combiner to combine two in-house fiber lasers with an output power of 1 kW and 690 W at 1080 nm wavelength. The maximum combined power was measured as 893 W by using two ports of this combiner with a launched power of approximately 500 W from each of them. The overall efficiency of the combiner was calculated as 93%. On the whole, we have performed successful glass processing by using CO_2 laser radiation. As a consequence of optimized, high quality tapering and splicing of optical fibers, we have fabricated critical components for high power fiber lasers such as end-cap, ball lens, pump and laser combiners.

Keywords: CO_2 laser glass processing, high quality fiber integration, end-cap, ball lens, tapering, pump combiner, laser combiner, high power fiber laser.

ÖZET

YÜKSEK GÜÇLÜ FIBER LASER UYGULAMALARI IÇIN CO_2 LAZER CAM IŞLEME

Bartu Şimşek
Malzeme Bilimi ve Nanoteknoloji Bölümü, Yüksek Lisans
Tez Danışmanı: Bülend Ortaç
Ocak 2016

Yüksek güçlü lazerler endüstri, sanayi, bilim ve sağlık alanında yıllardır sıklıkla kullanılmaktadır. Optik fiberlerin ışık iletimi, ısıya dayanıklılık, sağlamlık, kararlılık ve yüksek güce dayanıklılık özelliklerinin teknolojiyle birlikte gelişimi, son yıllarda fiber lazerlerin gaz ve katı hal gibi geleneksel lazerlerden daha fazla rağbet görmesine sebep olmuştur. Bu yönelim yekpare yapıdaki yüksek güçlü fiber lazerlerin kompaktlık ve sağlamlık gibi özellikleriyle pekişmiş, hizalama gerektirmeyen yapısıyla daha da avantajlı hale getirmiştir. Yüksek güçlü fiber lazerlerdeki ilerlemeler, kritik komponentlerin hem yapısal ve güç dayanımları yönünde, hem de bu komponentlerin entegrasyon kalitesinin arttırılması yönünde gelişimlere yol açmıştır. Karbondioksit lazerler, sunduğu istikrarlı ve homojen ışıma ile optik fiberleri temiz bir şekilde işleyebilen en etkili kaynaklardan biridir. Karbondioksit lazerin avantajları kullanılarak, optik fiber entegrasyon noktaları düşük kayıp, yüksek kalite ve mekanik stabilite oluşturabilmek amacıyla işlenmiştir. Ayrıca, yüksek güçlü fiber lazer komponentlerinden olan ve lazer çıkışını yönlendirmeye yarayan fiber uç başlığı ve kresel mercek geliştirilmiştir. Mod alan adaptörü özellikleri gösteren pompalama ve sinyal kombinarı, optik fiber inceltme tekniği ile üretilmiştir. Üretilen 7x1 pompalama kombinarı laboratuvarda geliştirilen yüksek güçlü lazere entegre edilmiştir. Pompalama kombinarlarının, pompalama kaynağı limitli güç dayanım değerleri 850 W olarak ölçülmüş ve ortalama verimliliği % 98 olarak belirlenmiştir. Buna ek olarak, üretilen bu kombinar, enstitümüz bünyesindeki fiber üretim merkezinde çekilen aktif fiber ile entegre edilip, yüksek güçlü fiber lazer sistemi kurulmuştur. Son olarak, yüksek güçlü iki fiber lazeri birleştirmek amacıyla 3x1 lazer kombinar üretimi gerçekleştirilmiştir. Üç adet giriş fiberine sahip olan bu kombinarın iki girişinden her birisine 500 W güç verilmesi ile 893 W lazer gücü kombine edilmiş olup, bu kombinarın ortalama verimliliği % 93 olarak hesaplanmıştır. Sonuç olarak, karbondioksit lazer ile başarılı bir şekilde cam işlenmesi gerçekleştirilmiştir. Optimize edilmiş yüksek kalitede entegrasyon ve fiber esnetme işlemleri sonucu yüksek güçlü, lazerler için kritik öneme sahip olan bileşenlerden uç başlığı, küresel mercek, pompalama ve lazer kombinarı üretilmiştir.

Anahtar sözcükler: CO_2 lazer cam işleme, yüksek kaliteli fiber entegrasyonu, uç başlık, yuvarlak mercek, fiber inceltme, pompalama kombinarı lazer kombinarı yüksek güçlü fiber lazer.

Acknowledgement

I acknowledge that apart from my effort, the encouragement and guidance of many other people contributed to the success and existence of this study. First, I would like to express my sincere gratitude to my advisor Assist. Prof. Dr. Bülend Ortaç for giving me this opportunity and his endless help, support, encouragement, guidance, and supervision for this study. I also would like to thank Prof. Mehmet Bayındır and his group for sharing their knowledge and supplying high quality capillaries and active fibers.

I would like to thank our research group members for their friendship, encouragement and support. I would like to thank my talented laboratory buddy Yakup Midilli for his encouragement, patience, guidance and friendship, also his support for all works in the laboratory. I would like to thank Dr. Tolga Bağcı for his encouragement, guidance, friendship, and support for my experimental and theoretical work. I would like to thank Canan Kurşungöz for her sincere friendship, support, patience and positive attitude. I would like to thank again everyone above for helping me to complete my thesis with their endless patience. I would like to thank Levent Ersoy for his sincere friendship, honesty, and support for all technical problems in laboratory. I would like to thank Refik Tuzaklı as my undergraduate and graduate fellow for his sincerity, honesty and friendship. I would like to thank to the new member of our research group O. Benjamin Efunbajo for his friendliness and support. The last and most important, I would like to thank my wife, love, friend, group member and the only one who always supports me, helping me about all problems, encourages me all times, loves me deeply, makes me feel cheerful with her existence, Elif Uzcengiz Şimşek.

I would like to thank Sebahattin Uğur, Toshiki Kubo and Nasir Usman for helping all technical problems of AFL LAZERMaster LZM-100 splicer with their endless patience. In addition, I would like to thank to UNAM members, friends and staff for their support and friendship.

I would like to thank my family, my father Özer Şimşek, my lovely mother Leyla

Şimşek, my little sweet sister Tuana Şimşek, my mother in-law Şükran Uzcengiz, my sister in-law Yasemin Uzcengiz and my father in-law Orhan Uzcengiz who passed away eight years ago, for their endless love, encourage and support.

I would like to thank TUBITAK. This work is partially supported by TUBITAK under the project number of 113A055. B. O. acknowledges support from the Turkish Academy of Sciences under the TUBA-GEBiP program and Bilim Akademisi - The Science Academy, Turkey under the BAGEP program.

Contents

List of Figures

List of Tables

Chapter 1

Introduction

In 1970, Corning scientists developed a highly pure optical glass which transmitted light signals over long distances with low-attenuation. Highly transmissive optical fibers were then demonstrated and they were firstly developed for optical telecommunications so as to substitute low-loss, high-capacity and fast data transfer cable for conventional cables [1,2]. Subsequently, optical fiber technology has been developed and the first low-loss rare-earth element doped double-clad fiber was fabricated in early 1980's [3]. By the invention of this optical fiber, the first high power fiber laser operations were performed in 1988 [4]. These results sparked a revolution in high power fiber laser industry. The evolution of high power fiber lasers has undergone sudden increment over the past 25 years. During quarter century, the optical fibers have been improved in terms of transmittance, heat resistance, robustness, stability and power endurance as well as developing the critical components for the high power fiber laser. The fiber-coupled laser diode as a pump source, the fiber bragg grating (FBG) as a mirror and the combiner as a light coupler have also been developed to reach highest laser powers on the fiber laser concept [5]. Today, fiber lasers have numerous advantages over gas or solid state lasers. Firstly, an alignment-free waveguide structure can guide light over long distances with high stability. Secondly, high single-pass gains can be realized not only in amplifier concepts but also in simple resonators with efficient double-clad active medium of an optical fiber. Another advantage of the fiber laser is that an active fiber can be easily cooled due to its large surface-to-volume ratio. Yet another advantage is the high power-handling capacity of optical fibers arising from the efficient rare-earth dopants in the active medium. Last but not the least, high beam quality can be achieved with single-mode (SM) or large-mode area (LMA) optical fibers [2].

With the developing technology on optical fibers, the diversity of fiber types has increased and their integration for constructing high power fiber laser has gotten complicated. There are basically two methods to integrate fibers, namely mechanical splicing and fusion splicing. Fusion splicing of optical fibers is a welding process of two fibers and has advantages over mechanical splicing in terms of loss, compactness, mechanical strength and stability. There are also several heat sources for fusing optical fibers such as flame torch, filament, electrode arc discharge and CO_2 laser radiation [6–8]. Although, all heat sources are used for fusion splicing of optical fibers effectively, CO_2 laser has several advantages for manipulating optical fibers to fabricate critical components, such as end-cap [9], fiber ball lens [10] and fused pump/signal combiners, by using strong absorption feature of silica (SiO_2) at 10.6 μm wavelength. CO_2 laser source allows long tapering processes of optical fibers with clean, stable and homogeneous laser radiation. By tapering the optical fibers, high quality mode field adapter (MFA), axicon and pump/signal combiners can be fabricated. Fused, monolithic, all-fiber pump combiners, which guide light coming from fiber coupled laser diodes into a double-clad active fiber, are critical components for constructing monolithic fiber laser systems. Fused laser combiners are, also, key components for scaling fiber laser power. The output power of fiber lasers can be limited by thermal effects, non-linearity of fiber, facet damage and brightness of the fiber-coupled pump diodes. In order to overcome these limitations, a laser combiner can be used to add the outputs of multiple high power fiber lasers.

In this thesis, by using CO_2 laser source, high power fiber laser integration of same diameter optical fibers, different diameter optical fibers and core offset fibers was studied and optimized for low loss, robust, stable and long-lasting joints. High quality integration of any kind of fiber splicing is an important step to gain the ability of building up stable, robust high power fiber laser systems with high beam quality. Then, the optical fibers were tailored by CO_2 laser radiation to fabricate ball lens and end-cap. Both laser light guiding components were designed and fabricated. The fiber tapering is another CO_2 laser glass processing which is necessary for optimizing pump and laser combiner production. The fiber tapering was developed and optimized for the optical fibers, the fiber bundles and the capillary tubes. A 7x1 pump combiner was designed, fabricated and optimized in terms of tapering, cleaving and splicing. Afterwards, the structural, optical and thermal characterizations were performed. As an application of this combiner, a high power laser system was constructed by using the in-house fabricated 7x1 pump combiner which was operated at the maximum powers of the fiber coupled laser diodes. Also, optical and thermal characterization of this laser was performed and results were discussed. Another application of 7x1 pump combiner is building a high power fiber laser with both in-house fabricated active fiber and 7x1 pump combiner. The fiber laser was constructed and operated to characterize its optical and thermal performance.

In the rest of this thesis, a 3x1 signal combiner was fabricated and characterized as above. Then, two lasers with an output power of 1 kW and 690 W were constructed and incoherently combined by the fabricated 3x1 laser combiner. Thermal and optical characterization of this setup was carried out. By exploiting CO_2 laser glass processing technology, we are able to develop state-of-art key components for powerful fiber laser systems.

Finally, preliminary studies were conducted in order to obtain all-fiber beam combining with higher quality. For this purpose, 7x1 laser combiner was fabricated and characterized structurally. Additionally, a laser combiner with tapered bridge fiber concept was studied and preliminary data were demonstrated.

Chapter 2

Theoretical Background

In this chapter, ray tracing fundamentals, basic properties of step-index fibers and tapering of optical fibers will be introduced. High power fiber laser concepts are discussed and fusion splicing types of the optical fibers are demonstrated. Finally, CO_2 laser radiation - silica interaction will be described.

2.1 Light guiding principles in uniform and non-uniform optical fibers

Light travels through material at a speed which is less than its speed in a vacuum. Therefore *index of refraction* can be defined as the ratio of the speed of light in vacuum to the speed of light in the material in Equation 2.1.

$$n = \frac{Speed\ of\ light\ in\ vacuum}{Speed\ of\ light\ in\ the\ material} = \frac{c}{\nu} \tag{2.1}$$

Optical fibers are composed of high refractive index cylindrical core covered by low refractive index cylindrical cladding. According to their profile of the refractive index, optical fibers are classified into two main types which are *step-index fibers* and *graded index fibers*. The step-index fiber is the most preferred type of optical fiber. The standard fiber is generally referred as the step-index fiber. The index profiles of both the step index fiber and the graded index fiber with respect to their radii are shown in Figure 2.1. In a step-index fiber, the refractive index

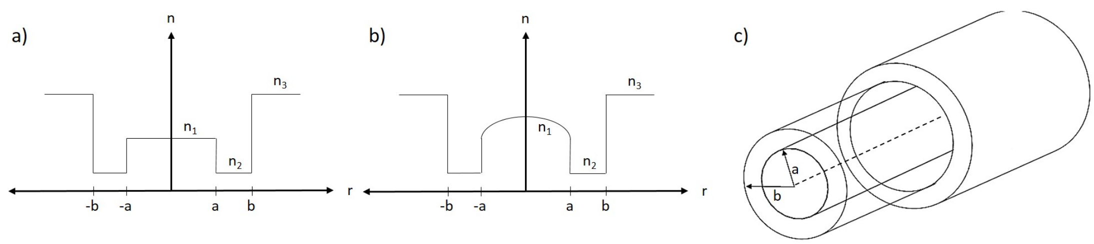

Figure 2.1: Index profiles of a) step-index fiber and b) graded index fiber according to their c) core and cladding radius.

of the core is uniform up to the boundary of core-cladding and the refractive index decreases abruptly at this boundary. However, in graded index fiber, the refractive index decreases gradually away from the center of core and it drops to the same value of cladding as in the step-index fiber boundary [11].

In order to explain the physics behind light guiding in the optical fibers, the behavior of light should be investigated at the boundary of media. When light travels from a material with one index of refraction to a material with a different index of refraction, the angle of incidence is related to the angle of refraction by Snell's law which is shown in Equation 2.2 [12].

$$n_1 \sin \theta_1 = n_2 \sin \theta_2 \tag{2.2}$$

In Figure 2.2, the refraction of light from both lower refractive index to higher one and higher refractive index to lower one is shown. If the light comes from the medium with lower refractive index, the angle of incidence is bigger than the angle of refraction. Also, if the light comes from the medium with higher refractive index, three cases may occur; the first one is light refraction with smaller angle of refraction, the second one is *critical angle (θ_c)* principle when the angle of refraction $\theta_2 = 90^0$ and the last one is *total internal reflection*(TIR) which is the explanation of light guiding mechanism inside the optical fibers. The total internal reflection principle is shown in Figure 2.3. If light is guided into the core with the angle of incidence larger than critical angle (θ_c), it continues to be guided inside the fiber due to total internal reflection (TIR).

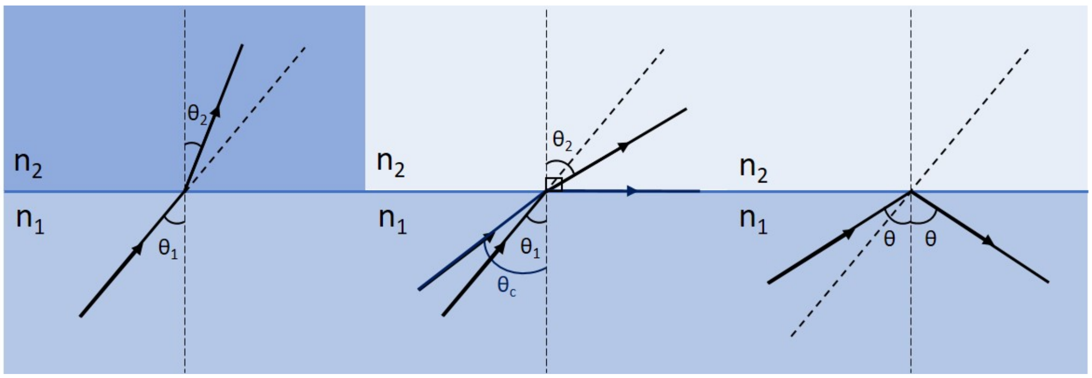

Figure 2.2: Refractive indices a) $n_1 < n_2$ then $\theta_1 > \theta_2$, b) $n_1 > n_2$ then $\theta_1 < \theta_2$ and when $\theta_2 = 90^0$ then θ_c: Critical angle, d) total internal reflection (TIR); $n_1 > n_2$ and $\theta > \theta_c$.

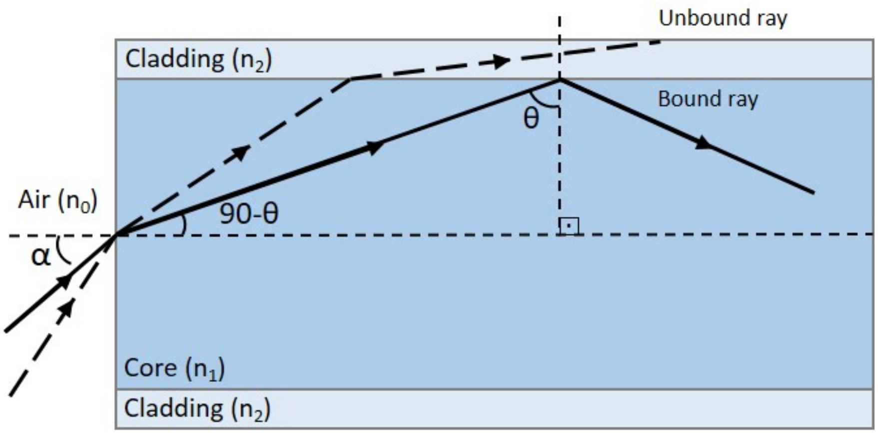

Figure 2.3: Total internal reflection (TIR) in an optical fiber which has $n_1(core)>n_2(cladding)>n_0(air)$ occurs when $\theta>\theta_c$ (Critical angle).

The critical angle is derived in Equation 2.4 from Snell's law, which is shown in equation 2.2.

$$n_1 \sin\theta_c = n_2 \sin 90^0 \tag{2.3}$$

$$\theta_c = \arcsin(\frac{n_2}{n_1}) \tag{2.4}$$

As the light guiding inside the core is limited by critical angle (θ_c), the fiber accepts light only for entrance angles within the range $0 < \alpha < \alpha_{max}$. This maximum angle ($\alpha_{max}$) is called *acceptance angle* which can be calculated also from the Snell's law. For optical fiber, the *numerical aperture (NA)* is commonly used to express this angle. Derived numerical aperture (NA) is shown in Equation 2.6 in terms of the maximum acceptance angle (α_{max}) and it is also shown in terms of the index of refractions of fiber in Equation 2.7 [12].

$$n_\circ \sin\alpha_{max} = n_1 \sin(90 - \theta_{critical}) \tag{2.5}$$

Using $\cos\theta_c$=$\sin(90-\theta_c)$, $\cos\theta_c$=$\sqrt{1-\sin^2\theta_{critical}}$ and Equation 2.4,

$$n_\circ \sin\alpha_{max} = NA \tag{2.6}$$

Also numerical aperture can be defined with respect to the refractive index of fibers,

$$NA = \sqrt{n_{core}^2 - n_{clad}^2} \tag{2.7}$$

Fiber optical modes are described as a discrete set of electromagnetic fields which can propagate in a cylindrical waveguide. Optical fibers can be classified as *single mode fiber (SM)* or *multi mode fiber(MM)* based on the number of modes that propagates through the fiber. The geometry and composition of the fiber designate the V-parameter which determines the number of guided modes in step-index fiber. V-parameter is defined as follows,

$$V = \frac{2\pi a}{\lambda_0}\sqrt{(n_{core})^2 - (n_{clad})^2} \tag{2.8}$$

where a is the radius of core, n_{core} is the refractive index of core, n_{clad} is the refractive index of cladding and λ_0 is the free space wavelength. Single-mode fiber is a fiber that only allows a single propagating mode. This mode is supported only in the case of V-parameter$<$ 2.405. For V-parameter$>$ 2.405, the optical fiber begins to support more modes and it turns out to be a multi-mode fiber. In multi-mode fiber, the V-parameter is related to the *total numbers of mode* , M, when it is large. The total number of modes M allowed in the fiber is given by

$$M \cong \frac{2\pi^2 a^2}{(\lambda_0)^2}\Omega = \frac{2\pi^2 a^2}{(\lambda_0)^2}((n_{core})^2 - (n_{clad})^2) = \frac{V^2}{2} \tag{2.9}$$

where A is the core cross-section πa^2 and ω is the acceptance solid angle of fiber which equals to $\pi\theta^2 = \pi((n_{core})^2 - (n_{clad})^2)$ with assumption sin$\theta \cong \theta$ for common numerical apertures. The plane waves can be in two polarization orientations, so Equation 2.9 is multiplied by a factor of 2 [13].

The fundamental mode of an optical fiber, which has a circular symmetry, is bell shaped. Therefore, this fundamental mode could be well described by a single parameter which is *mode field diameter* [14]. Mode field diameter (MFD) can be approximated by electric field which varies with radial distance r from the fiber axis $E(r) = E_0 e^{-(\frac{r}{w})^2}$ and the optical intensity $I(r) = I_0 e^{-2(\frac{r}{w})^2}$ varies as the square of E [12] [15]. For $1.2 < V < 2.4$, the mode waist size (w) is given by

$$w \simeq a(0.65 + \frac{1.619}{V^{1.5}} + \frac{2.879}{V^6}) \tag{2.10}$$

where a is radius of the fiber core.

It is clear from Equation 2.10 that the mode field diameter (2w) is related with the V-parameter. When V-parameter decreases below the limit of 1.2, the mode guided inside the core will spread out of the core and expand into the cladding of the fiber.

According to the geometry and the refractive index composition of the single-clad fibers, light is generally guided into the core as it is the case for most of the fibers as shown in Figure 2.1a and b. However, if the fiber has a second cladding with a low refractive index fluorine doped polymer, then this fiber is called double-clad. Light can be guided into the first cladding of fiber and these types of fiber are generally used as the active fiber and low brightness pump light delivery fiber. Double clad fiber will also be mentioned in Section 2.2.1.

2.1.1 Light guiding in non-uniform optical fibers: Tapering

Tapering of optical fiber is a stretching process to make fiber thinner by heat source. The high quality fabrication examples of fiber tapering, capillary tapering and fiber bundle tapering by using CO_2 laser technology are given in the Section 3.4. In this section, theory behind single-mode fiber tapering and multi-mode fiber tapering will be briefly introduced. The adiabatic limits for both fiber will also be calculated.

2.1.1.1 Single mode fiber tapering

The taper can be described as an adiabatic taper so that power of fundamental mode propagates along the taper region without coupling to the higher order modes (HOM). Adiabaticity criterion indicates the limits for light propagation inside tapered fibers [16]. In single-mode fiber, fundamental mode propagating inside the core can be conserved until the core of the fiber is tapered down to specific radius. Values that are below this limit lead to coupling from the fundamental mode (LP_{01}) to next higher order mode (LP_{02}) according to geometry of the core. Since coupling between the modes is an undesirable case during tapering process, the local change in taper radius should vary with little steps, which means that the taper local length should be much larger than the coupling length between LP_{01} mode and LP_{02} mode [17]. This can be demonstrated by

$$\frac{\delta r}{r} \ll 1 \tag{2.11}$$

where r is the core radius. The local change of the radius can be formulated in terms of beat length between the fundamental mode and the dominant coupling mode as

$$\delta r = L_B \frac{dr}{dz} \tag{2.12}$$

where $\frac{dr}{dz}$ is local slope of taper and the beat length can be formulated as,

$$L_B = \frac{2\pi}{\beta_1 - \beta_2} \tag{2.13}$$

The low loss tapering (adiabatic) criterion can be derived by inserting the Equation 2.13 and 2.12 into Equation 2.11. The adiabatic criterion for single mode fibers can be formulated as

$$|\frac{dr}{dz}| < \frac{r}{L_B} = \frac{r(\beta_1 - \beta_2)}{2\pi} \tag{2.14}$$

For linear tapers, the taper angle is Ω which is same along the taper, as shown in Figure 2.4. Before tapering the fiber, the core has initial radius r_0 and length

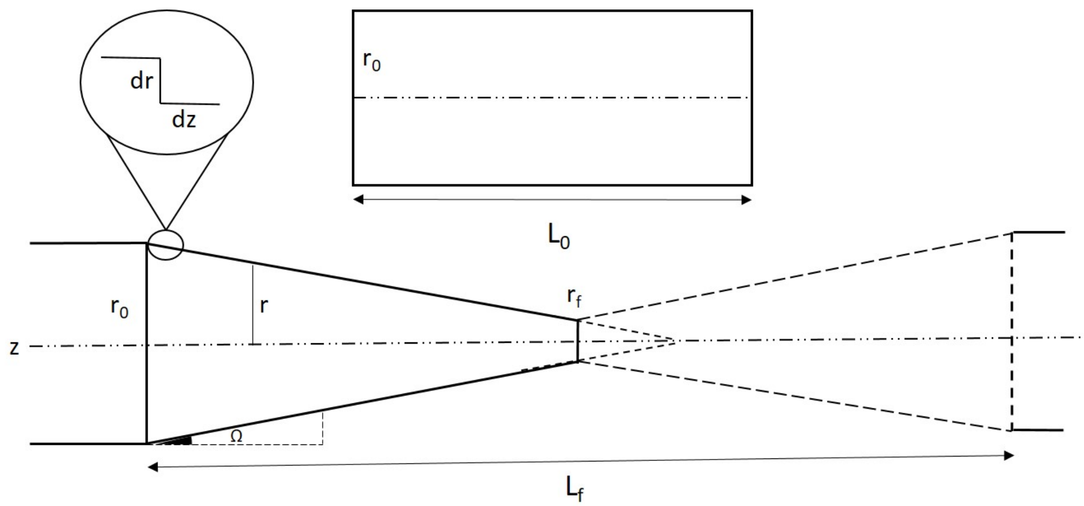

Figure 2.4: Adiabatic taper geometry and its parameters for linear tapering of single mode fiber core.

L_0. The tapering process reduces waist radius and increases the initial length of fiber. The final radius of single mode fiber core is r_f and the final length is L_f. Therefore the taper ratio (TR) can be defined as $TR = \frac{r_0}{r_f}$ and the elongation ratio (ER) can be defined as $ER = \frac{L_0}{L_f}$ and $L_f = 2L$. The adiabatic criterion for single-mode fibers can be formulated in terms of the taper length (L), the taper ratio (TR) and the beat length (L_B) as in the Equation 2.15,

$$\frac{L}{2} \geq (1 - TR)L_B \tag{2.15}$$

2.1.1.2 Multi-mode fiber tapering

In the multi-mode fiber tapering, the number of propagating modes is much more than that of single-mode fiber. Therefore, instead of using the beat length, L_B, a new parameter is defined, namely half-ray period z_p which is shown in Figure2.5 [18]. Adiabatic criterion for the single-mode fibers were shown in Equation 2.14.The adiabatic criterion for multi-mode fiber can be modified as

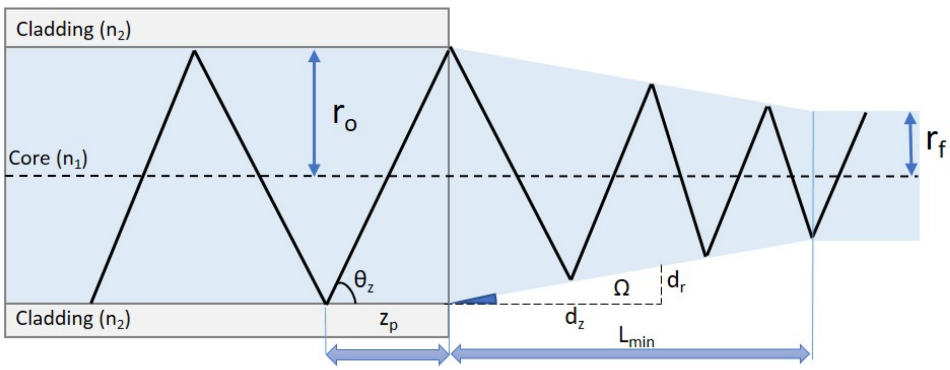

Figure 2.5: Structure of the tapered multi-mode fiber and its parameters.

$$\frac{dr}{dz} < \frac{r}{z_p} \tag{2.16}$$

where z_p is maximum half ray period and is equals to $z_p = \frac{2r}{tan\theta_z}$. Then, adiabatic criterion can be resulted in terms of ray angle with inserting z_p into Equation 2.16, as

$$\frac{dr}{dz} < \frac{tan\theta_z}{2} \tag{2.17}$$

The local slope of taper can be expressed in terms of the solid angle (Ω) in the Equation 2.18 and it is demonstrated as

$$tan\Omega < \frac{tan\theta_z}{2} \tag{2.18}$$

In Figure 2.5, the minimum taper length is shown and it can be calculated in terms of untapered (r_0) and tapered(r_f) radius of fiber and the ray angle (θ_z). It is demonstrated as

$$\frac{r_0 - r_f}{L_{min}} < \frac{2r_0}{2z_p} \tag{2.19}$$

Finally, it can be deduced in terms of the untapered and tapered diameter of fiber and ray angle (θ_z) as

$$L_{min} \geq \frac{D_{untapered} - D_{tapered}}{tan\theta_z} \tag{2.20}$$

Therefore, minimum taper length for multi-mode fibers depends on the numerical aperture (NA) of propagated light and the diameter of the tapered and untapered fiber.

In this section, light guiding principles in uniform and non-uniform optical fibers were introduced. In the following section, high power fiber laser systems will be described in terms of their components and power limitations.

2.2 High power fiber lasers systems

In 1960's, the first rare-earth doped fiber lasers were demonstrated which produced a few milliwatts at a wavelength of 1 μm [19, 20]. Since the beginning of the decade, there have been rapid developments which led to high-power fiber lasers with output powers of hundreds of watts or few kilowatts. The average output power of continuous-wave fiber lasers, having diffraction-limited beam quality has been increasing since in the early 1990s [2]. In 1999, 110 W fiber laser using Yb doped fiber which had a rectangular inner cladding was demonstrated [21]. In early 2004, 306 W all-fiber linearly polarized ytterbium (Yb) doped fiber laser was demonstrated [22]. Shortly after, Yb doped 610 W fiber laser, which has D-shaped active fiber, was shown [23]. In late 2004, kilowatt levels were reached by using the cladding pumped approach on fiber lasers and using a simple end-pumped ytterbium doped fiber laser [24]. Additionally, large-core design and fabrications refinements have led to reached single-mode operation. In 2009, multi-kW level fiber laser was demonstrated with near diffraction limited light [25]. Besides improvements in the output power, well known monolithic structure, compactness, low running cost, high efficiency and beam quality of fiber lasers are of great interest in various applications [26].

In this chapter, basic principles of a fiber laser will be introduced. The main components of high power fiber lasers such as double-clad active fibers, fused combiners and laser diodes will be described briefly. The power limitations of fiber lasers and high power beam combining as a solution for these limitations will be investigated.

2.2.1 Principles and main components of fiber lasers and amplifiers

In order to build highly efficient, long-term stable, compact and robust high power fiber laser system, it is crucial that the fiber laser system should have monolithic architecture [27]. There are two concepts to reach high power levels with high quality light and all-fiber architecture. The first concept is the double-clad fiber laser which is shown in Figure 2.6.

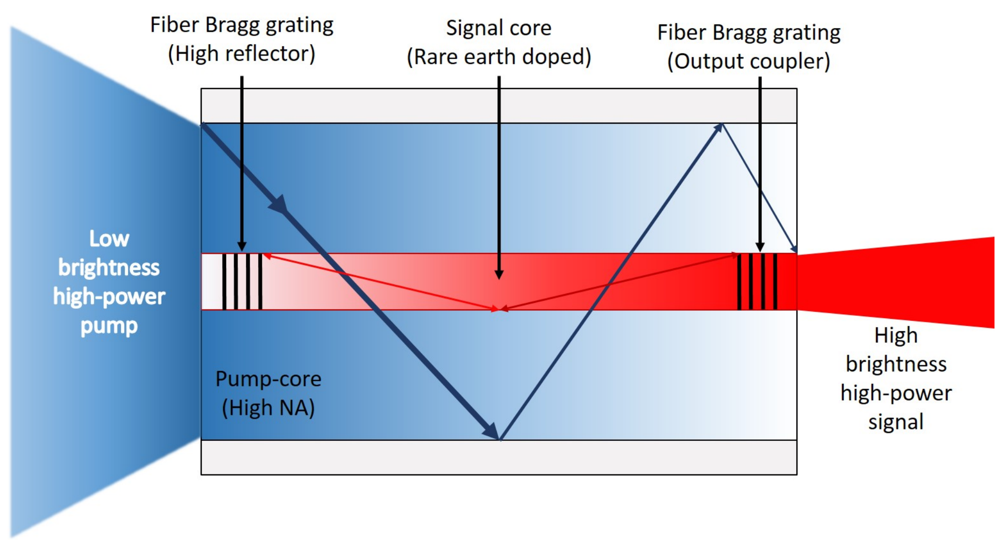

Figure 2.6: Illustration of double-clad fiber laser.

In this structure, the low brightness multi-mode light is guided from the beginning and it is taken out from the output as high brightness near single-mode light. The brightness is converted from low to high inside the fiber structure. In order for a fiber laser oscillator to operate, there are several main components such as fiber coupled laser diode, pump combiner, fiber bragg gratings (FBG) and active fiber [5]. In principle, the pump light that comes from the fiber-coupled laser diodes is directed through the active medium with or without the pump combiner. When the coupled light passes through the rare-earth atom doped core, the pump photons are absorbed by these active ions and bring them to the excited state. Then, the emission occurs through stimulated emission and emitted signal photons are guided into the core of fiber. The fiber laser resonator is built up by confinement of emitted signal photons within the core of the fiber using fiber bragg grating (FBG) as a mirror. These mirrors cause the fiber lase dominantly at a specific wavelength [28].

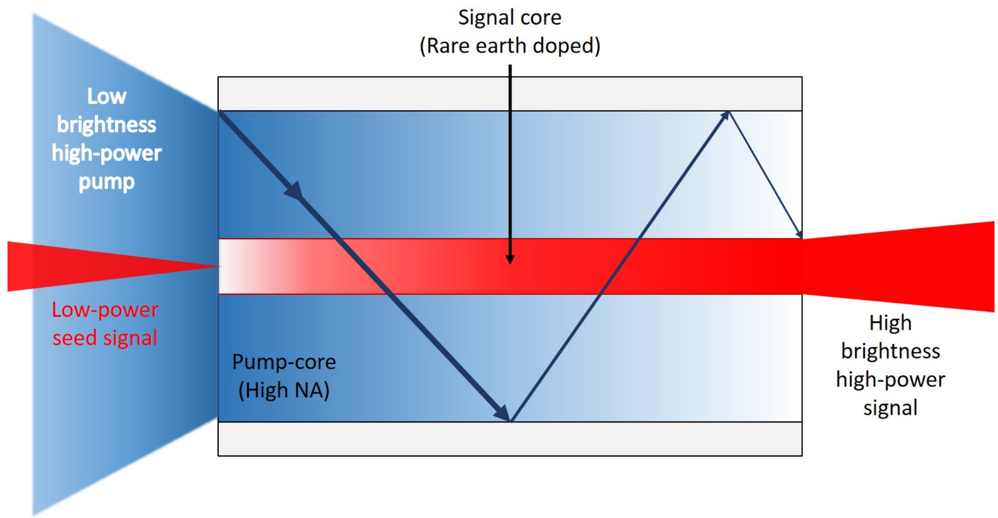

Figure 2.7: Illustration of double-clad fiber amplifier

The second concept is the fiber amplifier which is commonly called as master oscillator power amplifier (MOPA). The MOPA architecture is shown in Figure 2.7. This structure contains mainly fiber oscillator that generates low power seed signal and the amplifier part which is composed of the pump diodes and double-clad active fiber. The pump light is also absorbed by rare-earth atoms and emission occurs again through stimulated emission as in the case of fiber laser resonator. However, the emitted signal photons is not confined by FBG, the seed signal are amplified by domination of seed source wavelength. The production of high brightness fiber laser is introduced briefly on these two concepts. Also, all the main components of fiber lasers and amplifiers are basically introduced below based on the order of light passing through them.

The fiber-coupled laser diode is the main and the first element of the fiber laser. The fiber-coupled laser diodes are produced with several configurations, which are single-emitter, vertical stack, horizontal stack or bar modules so that the light can be coupled into the fiber with high efficiency and high power output levels can be achieved. There are fiber-coupled laser diodes with different characteristics in terms of output power, wavelength range and diameter of the coupling fiber. The maximum delivered output power commercially available in the market is 1 kW fiber-coupled laser. Moreover the wavelength range of this diodes varies between 790 nm and 1940 nm [29–33]. Also, the laser diodes can be used in high power laser systems with the output fibers having diameter from 100 μm to 600 μm. For instance, high brightness, 160 W light coming from the laser diode can be coupled into the 100 μm core fibers [31]. The ability of highly efficient light coupling to fibers with different diameters enables the use of a variety of combiners and active fibers in the fabrication of novel high power lasers [34].

Combiner is a device that provides very high coupling efficiency over a wide wavelength range from multiple sources into one output fiber. It is a critical component for pumping high power fiber lasers and amplifiers and for combining laser outputs incoherently. All-fiber combiners are necessary to build monolithic, alignment free and robust fiber laser systems. There are mainly two types of combiners; the first one is pump combiner and the second one is laser signal combiner. Pump combiner is generally fabricated with MM single-clad fibers, while laser combiner is fabricated with SM fibers. The principle of pump combiner is delivering the pump light from the fiber coupled laser diodes through the fiber bragg grating or double-clad active fiber with low loss. On the other hand, the principle of laser combiner is combining high power lasers without compromising the quality of light. The fabrication of combiner includes seven approaches to integrate double-clad fiber which are side coupling, distributed side coupling, side coupling with bridging fiber, tapered fiber bundle, fiber bundle integrated bridging fiber, side coupled signal fiber and side coupled signal fiber with capillary tube collapsing.

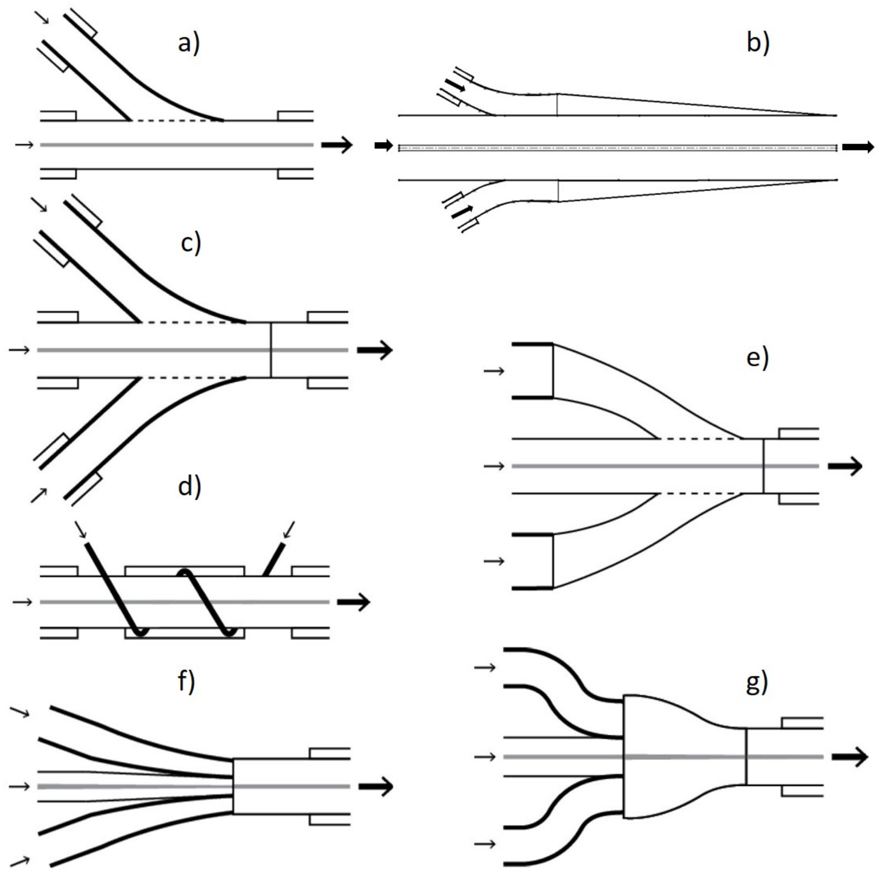

Figure 2.8: Combiner fabrication approaches; a) side coupling, b) side coupling with bridge fiber, c) fusion of MM fibers to signal fiber, d) fusion capillary tube to signal fiber, e) distributed side coupling, f) tapered fiber bundle and g) tapered fiber bundle with bridge fiber

In Figure 2.8a, a side coupling of a multi-mode pump diode fiber to double-clad active fiber is depicted. It is important that the fiber should be integrated with an angle in order to couple pump light into pump core of the fiber [35–37]. In Figure 2.8b, side coupling of multi-mode pump diode fibers using bridging fiber is illustrated. In this concept, up to twelve fibers can be integrated through bridge fiber without changing uniformity of an active fiber [38]. In Figure 2.8c, coupling of multi-mode pump fibers to a single-mode signal fiber is shown. In this concept, side-pumped signal fiber is spliced to the active fiber. In Figure 2.8d, the same integration approach is applied between the signal fiber and the active fiber as illustrated in Figure 2.8c, but in this approach, a capillary tube are collapsed on signal fiber. In Figure 2.8e, distributed side coupling approach is shown [39–41]. The pump fiber is coiled and fused along double-clad active fiber. Besides these side pumping approaches, there are also end-pumping approaches, which are shown in Figure 2.8f and g. In Figure 2.8e, tapered fiber bundle is obtained by tapering the fiber bundle down to the diameter of double-clad active fiber and splicing with it. This is the most common concept among commercial combiners [42–48]. The tapered fiber bundle combiner may include a single-mode signal feed-through the fiber to build amplifier systems or seeding mechanisms. In this thesis, this type of combiner is fabricated and characterized in Section 4.2. Finally in Figure 2.8g fiber bundle integrated to bridging fiber is depicted. This approach is generally used on laser combiner concepts to combine high power lasers which is presented as preliminary data of this thesis. After pump light is guided through the double clad active fiber by combiner, the principles that were mentioned above take place and the signal light trapping in the core of the double-clad active fiber by fiber bragg gratings are introduced below.

Double-clad active fibers are composed of a rare-earth element doped core, an undoped hexagonal, rectangular or d-shaped first cladding as a pump core and a UV-curable, high temperature resistant polymer coated second cladding with low refractive index. In this thesis, we use Yb-doped double-clad (Nufern LMA-YDF-20/400-M) and in-house fabricated active fibers to build up fiber laser that is shown in Section 4.3.

Fiber Bragg gratings (FBG) are made by exposing periodic pattern of UV radiation or femtosecond pulses to the core of single-mode fiber. The working principle of FBG is based on the periodicity of the refractive index of the exposed pattern, which satisfies the Bragg condition where $\lambda_{bragg} = 2n\Lambda$. In that way, the light with a specific wavelength for each index and periodicity can constructively interfere from the grating structure [49].

2.2.2 Power limitations of fiber lasers

Power limitations of fiber lasers are imposed by thermal effects, non-linearity of fiber, facet damage and brightness of the fiber coupled pump diodes [50]. There are several limitations which are caused by thermal effects. The first one is heat conversion of unabsorbed pump light at gain medium. The other thermal effect is melting core by heat power deposition per unit length. The last thermal effect that limits the power is thermal lensing which is created by heat induced temperature gradient in the core of fiber. There are also non-linear effects such as stimulated Raman scattering (SRS), which is a nonlinear response of the optical medium due to vibrational or rotational degrees of freedom, and stimulated Brillouin scattering (SBS), which is caused by generated acoustic phonons related non-linearity of a medium. The facet damage is melting and fracturing of end face of the fiber when the power density is over the breakdown threshold of the glass matrix. Pump diodes have limited brightness for coupling into the optical fiber, number of diodes are limited also due to the limit of maximum input port of pump combiners. All these effects limit the maximum power and quality of high power lasers. These limitations can be overcome by modifying the fiber laser oscillators with cooling equipment or light guiding components such as combiners and end-caps. In order to reach high power levels, there is also another solution which is high power beam combining.

2.2.2.1 High power beam combining

High power beam combining is coherent or incoherent laser beam combining of fiber lasers with free-space or all-fiber components. For coherent beam combining, it is necessary to control the phase of single frequency lasers to let them interfere constructively. Incoherent beam combining can result in several kW level near diffraction limited light combination without controlling phase of lasers. Incoherent beam combining is not only performed with free-space components but also with all-fiber laser combiners which can reach up to $5kW$ power levels with high quality lights [51, 52]. In this thesis, high power beam combining with in-house fabricated combiner and preliminary data for high quality high power laser combiner with tapered bridge fiber is given in Section 5.

2.3 Integration of optical fibers

The integration of fiber laser components and fibers have significant importance to build up robust, monolithic, low loss, high power lasers. In this section, fusion splicing is basically introduced and advantages of CO_2 laser source are discussed in terms of splicing and shaping optical fibers compared to the other heat sources.

2.3.1 Fusion splicing of optical fibers

The fusion splicing of optical fibers is a welding process of two fibers with high-strength, low-loss, long lasting and stable integration point. Unlike the mechanical splicing of two fibers, the fusion splicing are dust-free, alignment-free and temperature independent [53]. Also, fusion splice has many advantages over other interconnection methods of optical fibers such as free space coupling and mechanical splicing. Fusion splicing joints have very tight cross-section areas almost like the original fiber when it is coated with polymer. During the fusion splicing, fiber ends are softened and also viscosity of silica is decreased with increasing temperature [54], then they are merged to each other by melting as the low-loss high strength joint. The fiber softening point is approximately 1800 ^oC as shown in Figure 3.23. In order to reach this temperature limit, there are few heat sources such as flame torch, electrode arc discharge, filament heater and CO_2 laser. All splicing methods have advantages and disadvantages with respect to each other. Flame torch is the oldest method for fusion splicing and tapering process. It has been used from early 1960's to the present. Even if strong splices are obtained [6], it is not useful for fusion splicing anymore because of not having homogeneous and stable heating. The electrode arc discharge [7, 55] and filament heater are common heat sources which are used in recent fusion splicers. A typical tungsten filament is used as a heat source in the filament heater. This method supplies homogeneous heat on the fiber and allows splicing to larger fibers, fabricating couplers and other high-heat applications. However, filaments need to be changed based on the application and they don't work above 50 minutes operation. Also, ablated filament may be deposited on silica glass during splicing or tapering. The electrode arc discharge technique is widely used as a practical source which can heat homogeneously for different size of fibers by creating plasma field of super heated air. This method is reliable and easy to use for many types of fibers. In our laboratory, we are working with electrode arc discharge splicer to build our high power laser systems which are shown in Section 5.2. However, this technique also has a disadvantage that the vaporized silica deposits on electrode tips which leads to contamination on the optical fiber during the splicing process. CO_2 laser splicers are used most recently for advanced splicing as well as tapering, fabrication of end-cap and ball lens and collapsing tubes.

2.3.2 Splicing and shaping of optical fibers with CO_2 laser

CO_2 laser is a very clean heat source for the silica based optical fibers. During the heating process, there is not any contamination and deposition on the fiber surface. Unlike flame, arc discharge and filament source heating mechanisms, which are based on heat radiation and conduction, the heating mechanism of CO_2 laser source exploits strong absorption of light having 10.6 μm wavelength on the silica. This absorption is caused by elastic vibration of oxygen (O) atom between two silicon (Si) atoms. Interaction between CO_2 laser radiation and silica will be explained in detail in Section 2.3.4. Silica based optical fibers can be integrated and processed by using CO_2 laser thanks its stable and repeatable laser power [56]. In this thesis, all glass processes are performed by CO_2 laser splicing system which is introduced in Section 3.1.

2.3.3 Splicing loss

The optical fiber splicing quality may differ according to position, composition, diameter, geometry, alignment and cleaning of the fiber and its end-face. At the end of splicing process, the guided light signal may undergo four fundamental optical effects such as transmitted signal into same mode, reflected signal, transmitted signal into another mode and radiated signal depending on the quality of the integration point. Such optical effects are shown in Figure 2.9 [53]. The

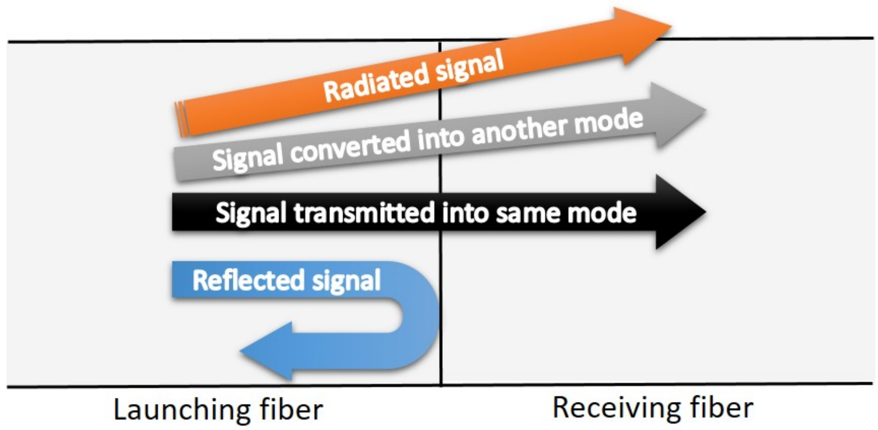

Figure 2.9: Optical effects that may occur at splice points: Radiated signal, transmitted signal into another mode, transmitted signal into same mode and reflected signal.

first effect is the transmission signal into identical mode in which incoming light is guided from the launching fiber to the receiving fiber by preserving its optical mode. This effect is expected when two optical fibers are perfectly welded. Reflected signal from the splice point is observed if the splicing results in bubble, core axial offset, core step or line. According to the reflected signal intensity, interference, parasitic lasing or pulsing may be observed in the optical fiber. Also, the mode field diameter mismatch, curved core, angled core and the splice results that are mentioned above may convert the signal into another mode as an optical loss. If the splicing is performed with serious symptoms, the launched light may be directed towards the outside of fiber. This causes heating of the integration point of the two fibers. The splice loss can be calculated by total launched power and total received power as shown in equation 2.21.

$$\Gamma_{Splice}(in\ dB) = 10log\frac{P_{Launched}}{P_{Received}} \tag{2.21}$$

Losses from 0.1 dB to 0.05 dB can be discussed as a good splice. In this thesis, splice loss of all the fibers, which we have worked with, yielded values in the range mentioned above.

2.3.4 CO_2 laser radiation - Silica interaction

Silica (SiO_2) is the main ingredient of most glasses and has a tetrahedral structure which means four oxygen (O) atoms surround a silicon (Si) atom at the center as shown in Figure 2.10. Structure of silicon dioxide allows forming glass on its own

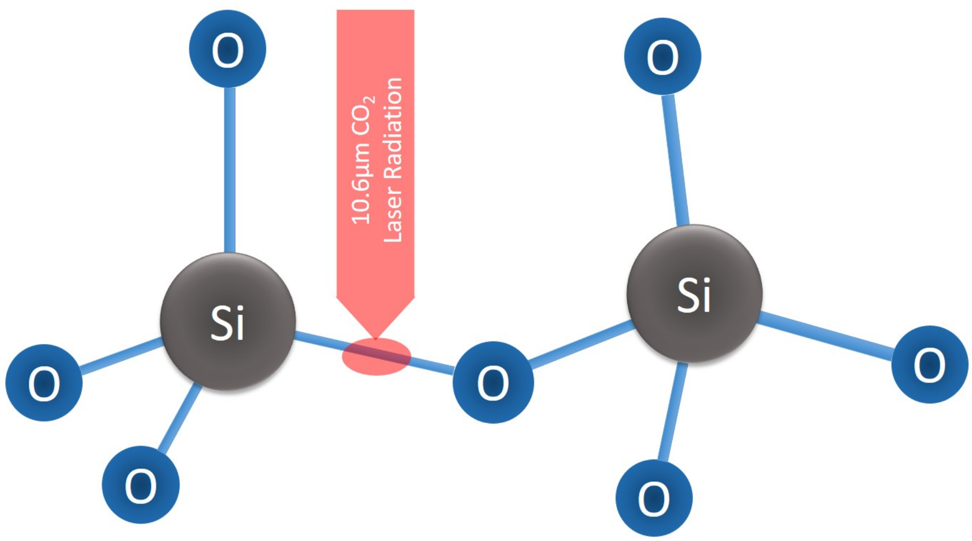

Figure 2.10: Illustration of Silicon Dioxide (SiO_2) lattice structure and (CO_2) Laser radiation on ($Si - O$) bond.

and also supports the base for many oxide glasses such as sodium oxide (NaO_2), calcium oxide (CaO), magnesium oxide (MgO), aluminum oxide (Al_2O_3), boron trioxide (B_2O_3), or lead oxide (PbO) [57]. Pure silica glass has a very high melting point, high chemical durability and low thermal expansion coefficient. These properties of silica glass can be modified by composing oxide glasses with silica. Composition of them can provide better chemical durability, lower melting point, higher refractive index and viscosity of glass. Therefore, silica-based fibers have many advantages over fibers which are formed with other types of glass. These fibers demonstrate almost all properties of silica and additionally support very high damage thresholds, low optical nonlinearity, mechanically robustness, high bending tolerance [58]. Hence, silica based fibers are commonly used for fiber laser applications, especially in high power fiber laser systems.

In this study, fibers that are used for CO_2 glass processing applications are generally made of fused silica. Fused silica (fused quartz) is silica glass having amorphous (non-crystalline) structure and it is produced by fusing (melting) high-purity silica sand. In general, there are three types of manufacturing fused silica. The first one is the electric fusion, which is the most commonly used one. The second one is flame fusion, which is a process consisting of trickling silica sand into high temperature flame. The third one is the flame hydrolysis which is a process (synthetic production) consisting of highest purity fused silica nano-droplets formed by hydrolysis of silicon tetrachloride ($SiCl_4$) inside a hydrogen oxygen torch [59]. For all types of product, silica has a wide range of high optical transparency from ultraviolet (UV) wavelength 0.2 μm to infrared (IR) spectral region wavelength 3.5 μm. This transparency range limitations can be changed from 0.2 μm to 0.4 μm and 3.5 μm to 2.5 μm by modifying silica glass. Light absorption of glass in the range below 0.3 μm is dominated by electronic excitation of molecules, while molecular vibrations are dominated in the IR range [60]. For successful laser glass processing, choice of laser source is restricted with the absence of available laser sources which are working on exceeded limit wavelengths. In the UV regime, F_2 laser is operating at 157 nm and excimer laser is operating at 193 and 247 nm and these lasers strongly couple energy into glass via defects or near-band edge states, providing one approach for micro-machining glass or driving refractive index change on nanosecond or longer time scales [61]. In IR regime, there is only CO_2 laser source working at 10.6 μm wavelength band.

Figure 2.11 shows transmittance of fused silica glass in the range of 2.5 μm to 12 μm and the band between 9.4 μm and 10.6 μm is shaded because it refers to operating spectrum of common CO_2 laser sources [63]. As it is clear from this figure, fused silica absorption range (8 μm and 10.6 μm) is matched with CO_2 laser source emission wavelength indicated in the figure above. The tetrahedral structure that is shown in Figure 2.10 forms around negatively charged silicon atom and it has a certain geometrical shape likewise gravity center of positively charged atoms. Energy of the IR electromagnetic field will be absorbed as a result of generated dipole by molecular vibration of the structure defined above.

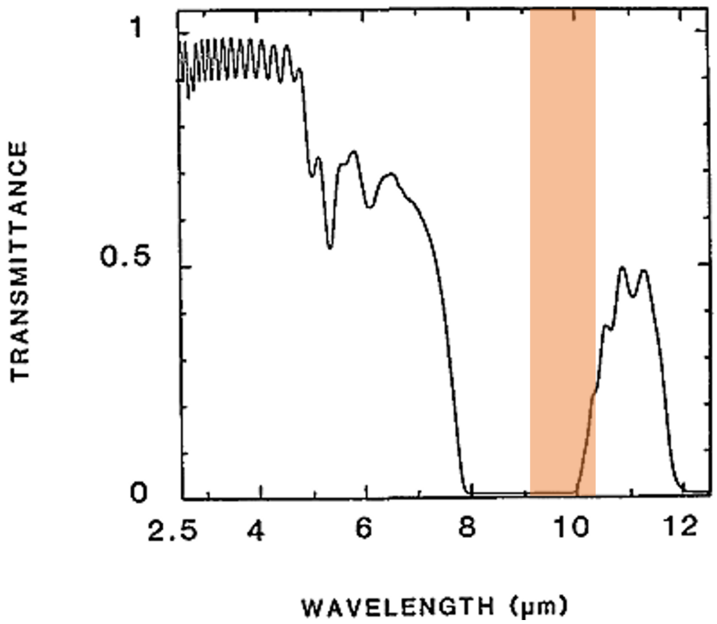

Figure 2.11: Transmission spectra of a pure fused silica (Suprasil) sample in range of 2.5 μm to 12 μm [62].

The movement of the oxygen atom which is bonded to adjacent silicon atom with $Si - O$ bond results in coupling of the two $Si - O$ vibrations. Bond strength and vibration frequency both depend on the Si and O atoms in the bond and on the other neighbors of the silicon atom [64]. The band of high absorption in the range of specific wavelengths is attributed to the bond-stretching vibration between the Si and O atoms in a $Si - O - Si$ bridge structure.

According to the composition of silica, the absorption peak position and its shape of stretching vibration modes can vary as shown in Figure 2.12. In this Figure, absorption coefficient peaks of SiO_x shifts from 940 cm^{-1} to 1150 cm^{-1} while oxygen content increases. It is also proved that CO_2 laser is a very efficient source for processing silica based glass. Laser processing of silica glass has continuing attention as part of the improvement of new technologies for micro-optical fabrication applications and for building up stable, robust, high power fiber lasers and their components.

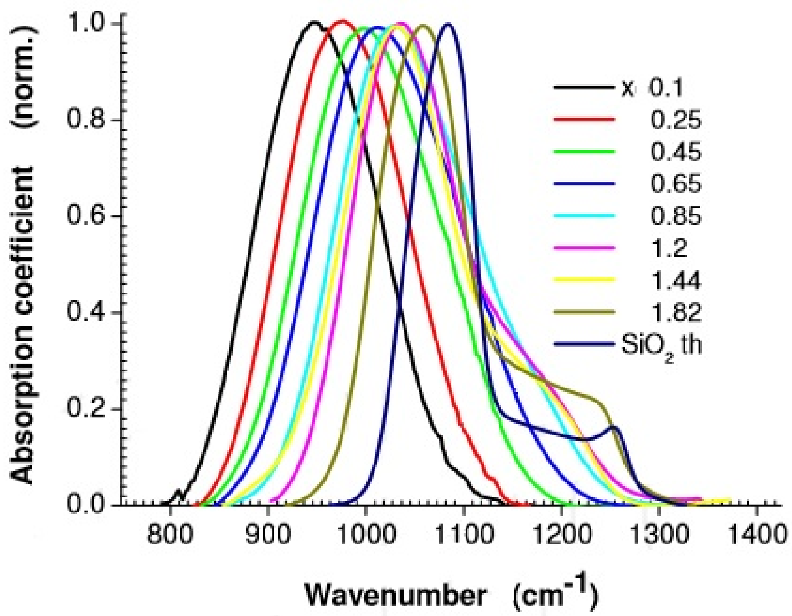

Figure 2.12: Position and shape of the absorption peak assigned to the stretching vibration mode of the $Si{-}O{-}Si$ bridge are dependent on the oxygen content [64].

Chapter 3

CO_2 laser glass processing of optical fibers

In this chapter, applications of CO_2 laser processing of optical fibers that are made up of fused silica will be mentioned. Applications begin with low loss integrations of optical fibers which have same cladding diameters, different cladding diameters and core offset. Then, fiber tapering will be described and examples of fabrication will be shown. The chapter also describes two applications of CO_2 laser glass processing on optical fibers. The first one is end-cap fabrication and the second one is ball lens fabrication on optical fibers.

3.1 Integration of fiber optics with CO_2 laser

In chapter 2.3.1, integration types of optical fibers are introduced and potential splice loss symptoms are exhibited. Solutions and examples for low loss integrations will be mentioned briefly in this section. We will first start introducing integration of optical fibers with same cladding diameters, different cladding diameters and also we will show the integrations of core offset fibers by CO_2 laser.

For all applications in this thesis, the *AFL LZM-100 LAZERMaster Laser Splicing System* is used as a CO_2 laser source. The main structure of the laser system is shown in Figure 3.1. As presented in this figure, CO_2 laser radiation having

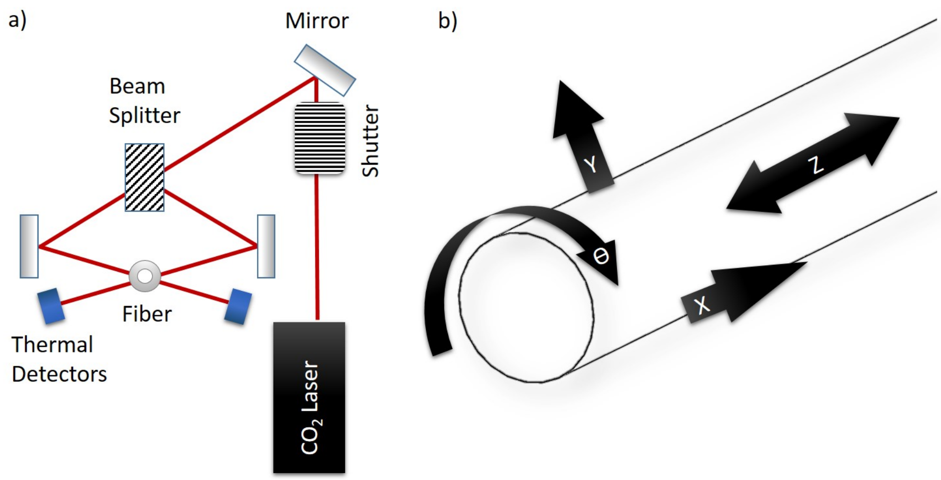

Figure 3.1: (a) Depiction of the CO_2 Laser source, (b) Available coordinates of movement of the fiber in this system.

4 mm beam spot, surrounds the fiber to heat it homogeneously. Power (max. $30W$) and wavelength ($10.6\mu m$) stability of this laser provides low loss integrations and high quality components. In order to prevent integration losses, there are few steps to be carried out including stripping and cleaving fiber.

Optical fibers are generally polymer coated right after drawing in order to protect them from subsequent handling damage. Mechanical stripping is the process of removing the protective polymer coating from the optical fiber. The polymer coating needs to be removed from the fiber just before the cleaving or splicing procedure. There are several methods for stripping the polymer like using hand-held mechanical tools, motorized strippers and sulphuric acid or a controlled flow of hot air. We have worked with all the methods that are mentioned and we are also capable to stripping fiber with high quality. Although all techniques result in qualified strips, motorized strippers and chemical striping that are found to be more applicable for better results. In Figure 3.2, one of the bad and good results of stripping are shown. At the end of the good striping process, fiber and polymer should be well contacted and the shape of the stripping should ideally be conic, because if you have cracked polymer after the stripping process as figure 3.2a, bubbles will form inside the polymer during the re-coating process.

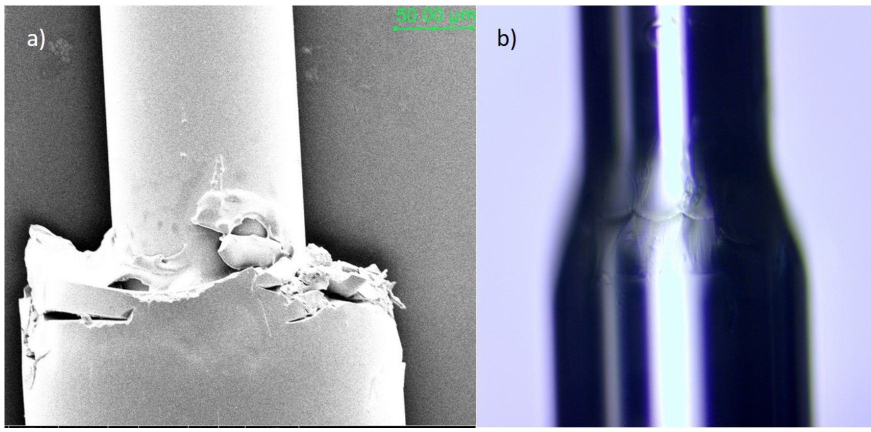

Figure 3.2: a) Scanning Electron Microscope (SEM) image of optical fibers with hand-held mechanical stripper and b) Differential interference contrast (DIC) mode image with motorized mechanical stripper.

Fiber cleaving is a controlled breaking procedure through perpendicular to longitudinal axis of fiber to get a clean, flat and smooth fiber-end surface. It is one of the crucial steps in the area of fiber optic integration. Before optical fiber is connectorized or fusion-spliced or the light is launched into the fiber, the fiber ends need to be well prepared. Surface of end face of fiber should be as flat as possible and the cleave angle should be approximately 0^0. Unoptimized (Figure 3.3a) and optimized (Figure 3.3c) cleave results are shown and successful results of cleave angles (Figure 3.4) are given in Figure 3.3 and 3.4.

3.1.1 Splicing of fibers with same cladding diameters

In this section, CO_2 laser splicing of same cladding diameter fibers will be demonstrated. For building up a simple monolithic high power fiber laser, different types of fibers can be used in the splicing process. Low loss oscillators and amplifiers

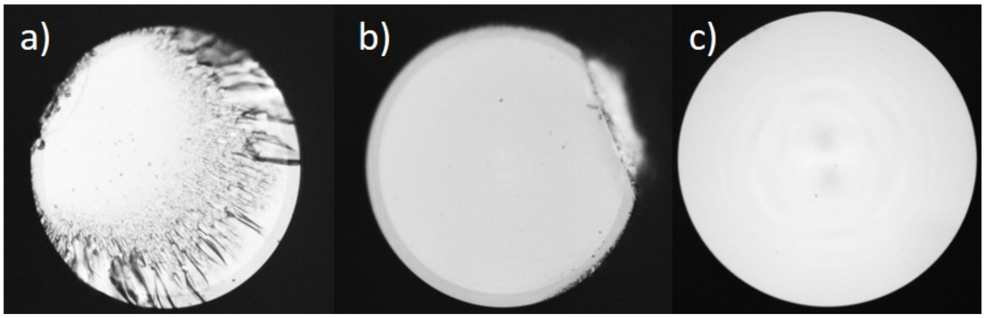

Figure 3.3: Optical microscope images of cleaved fiber's end surface having a) cracks, hackles and sparkles b) blade cracks c) smooth and clean surface.

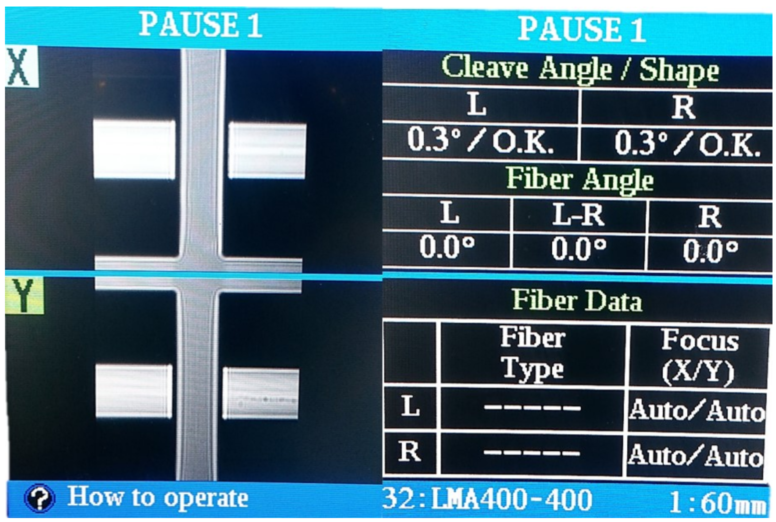

Figure 3.4: Measured cleave angles of 400 μm cladding fibers.

begin with laser diodes at the bottom. Usually, commercial laser diodes come with output fibers having 105 μm, 200 μm, 400 μm core diameter. Then, integration between laser diode fiber output and combiner or FBG input takes place. In Figure 3.5, possible fiber integration types are shown on specific fiber laser oscillator. These possible cladding diameter fiber splice points can be listed as 105/125 μm- 105/125 μm, 200/240 μm- 200/240 μm and 20/400 μm- 20/400 μm. Similar to basic 105/125 μm- 105/125 splicing, 200/240 μm- 200/240 μm multi-mode fiber splicing is shown in Figure 3.6. Basic splicing starts with gap setting position where well cleaved fibers take vis-a-vis positions like shown in Figure 3.6a. Then, alignment of the fibers begins according to their claddings or cores. After finishing the alignment, lasing starts and images of heated fibers

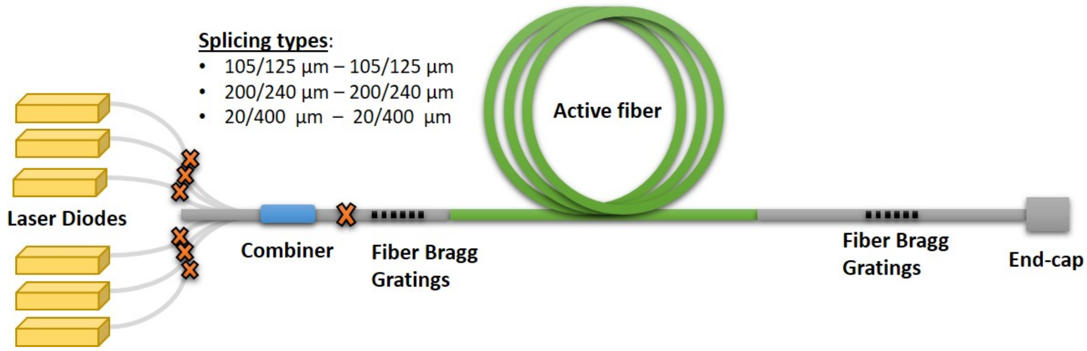

Figure 3.5: Illustration of possible splicing points of fiber having same cladding diameter on the specific concept of high power fiber oscillator.

appear as in Figure 3.6b. At the end of the splicing process, integration point of the fibers are shown as Figure 3.6c with estimated loss and other parameters optionally. Generally, there is white or gray line between integrated multi-mode fibers which comes from the diffusion of doping atoms through the splice point and it is normal for doped multi-mode fibers as long as the line stays in the core region. So, multi-mode fiber splicing is sufficient for high power applications in Figure 3.6c.

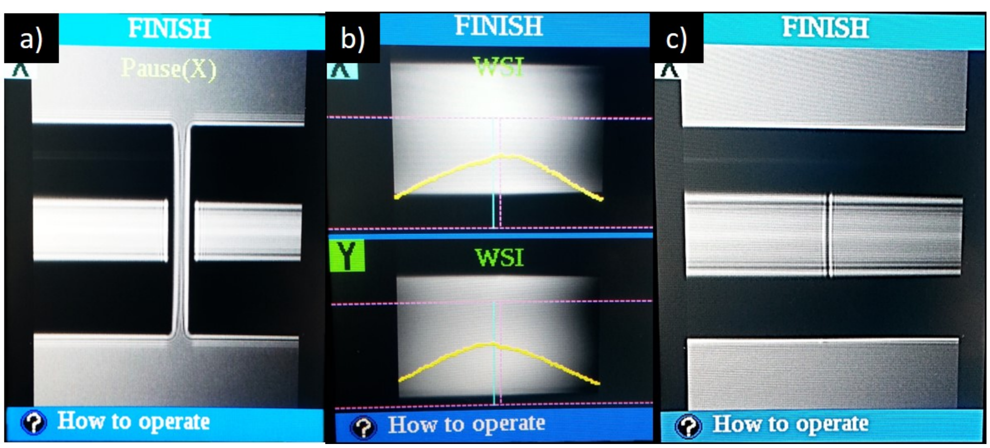

Figure 3.6: Splicing of 200 μm core - 240 μm cladding fibers. a) Gap setting position of well cleaved fibers, b) heat distribution of fibers while CO_2 lasing and c) integrated fibers

In order to splice low loss large mode area (LMA) or single mode (SM) fibers, cleaving and splicing parameters should be well optimized. Any cracked or high angled cleave can cause symptoms like bubbles, curved core or angled core mentioned in chapter 2.3.3. In Figure 3.7, demonstration of bad splicing between similar 20/400 μm fibers is given. Cleaves, in Figure 3.3b, can cause crater of bubbles at the integration point as in Figure 3.7a.

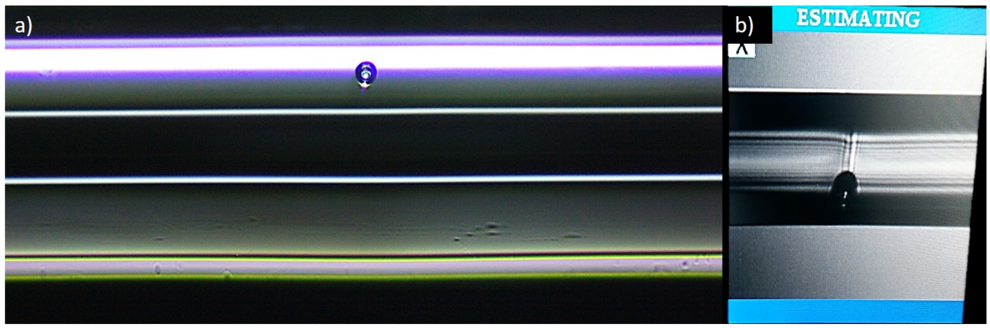

Figure 3.7: a) Optical microscope image, b) splicer screen-shot of bubble symptom at 20/400 μm fiber splicing.

In order to obtain good integration between the fibers, well optimized cleaving and splicing parameters should be used and the the core and the cladding of the fibers should be aligned precisely. A successful splicing between 20/400 μm fibers is shown in Figure 3.8. It is hard to detect the splicing point of fibers with optical microscope image shown in Figure 3.8a. It can be seen that the alignment between the cores of the fibers are almost confined after splicing process in Figure 3.8b.

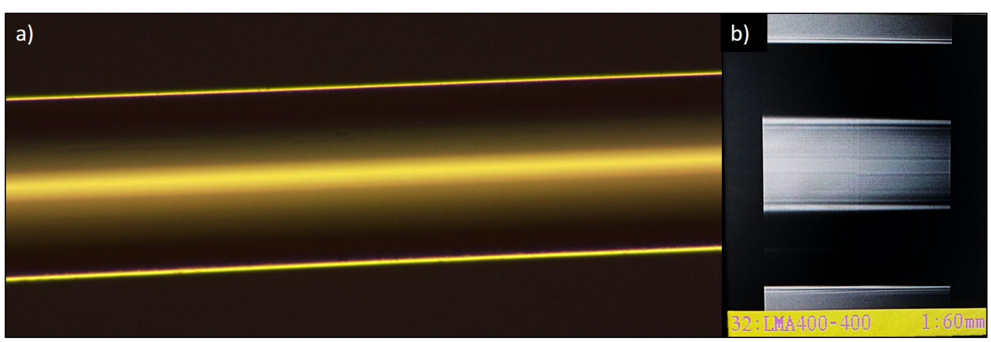

Figure 3.8: a) Optical microscope image, b) splicer image of successful integration of 20/400 μm splicing.

3.1.2 Splicing of fibers with different cladding diameters

In the previous section, possible fiber splicing points are shown on the illustration of a typical high power fiber laser oscillator concept (Figure 3.5). In this section, CO_2 laser splicing of different cladding diameter fibers will be demonstrated. In Figure 3.9, different fiber splicing types are shown on the same high power laser concept such as 105/125 μm- 200/240 μm, 200/240 μm- 220/242 μm, 200/240 μm- 20/400 μm 20/400 μm- 1000 μm and spherical shape 20/400 μm - hexagonal shape 20/400 μm fibers.

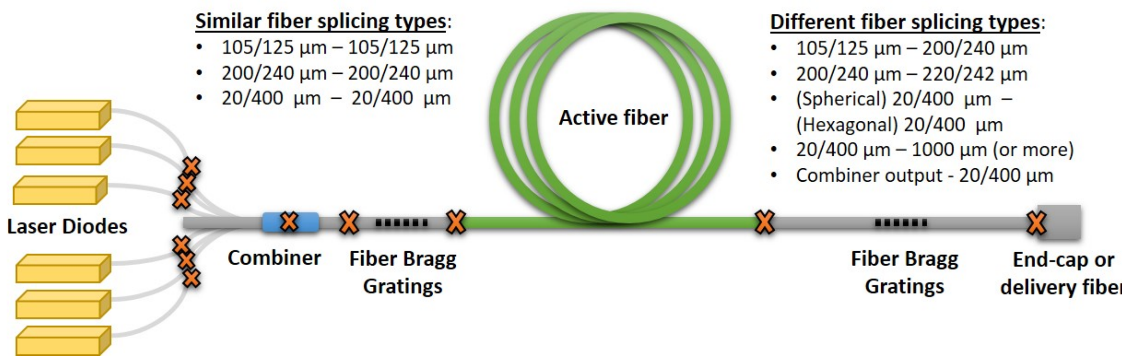

Figure 3.9: Possible integration points between fibers with same or different cladding diameters in a typical high power fiber laser system

These types of integration are usually used for laser diode - combiner input, FBG - Yb-doped active fiber, FBG - end-cap and FBG - QBH delivery fiber optic cable. Depending on the heat in splice processing, there are two types of splicing among different diameter fibers; namely, cold splice and hot splice. In cold splice process, two fibers are joint without changing their shapes and their structure as it is shown in Figure 3.10 a. Cold splices are generally fragile splices but both fibers' core-cladding diameters and numerical apertures (NA) are conserved. On the other hand, hot splices are strong splices, however, numerical apertures and mode field diameters of both fibers change while melting under a heat source. Illustrations of cold splicing and hot splicing are shown in Figure 3.10.

In Figure 3.11, the splices between 240 μm - 600 μm, 125 μm - 400 μm cold splicing and 125 μm - 600 μm splicing for end-cap applications that will mentioned

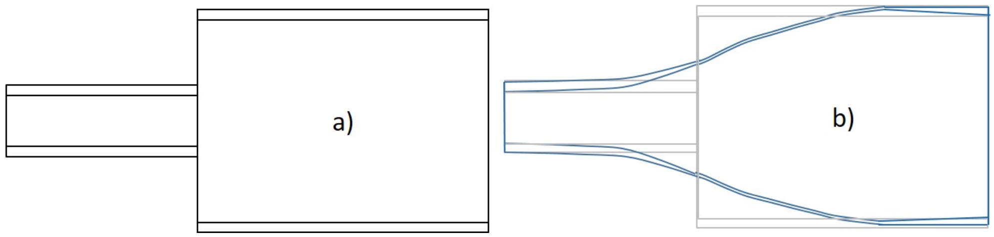

Figure 3.10: Illustration of a) cold splicing and b) hot splicing.

at Section 3.2 are shown. Also, Figure 3.11d shows 125 μm - 240 μm hot splicing that works for diode fiber-to-combiner fiber integration applications. 300 μm delivery - 400 μm hexagonal shape active fiber splicing is demonstrated in Figure 3.11e, additionally. In this splice, a high quality laser couples into a delivery fiber with 100/300 μm core/cladding diameter and it is necessary for QBH cable integration to fiber laser. Integration of fibers with different diameters will also be

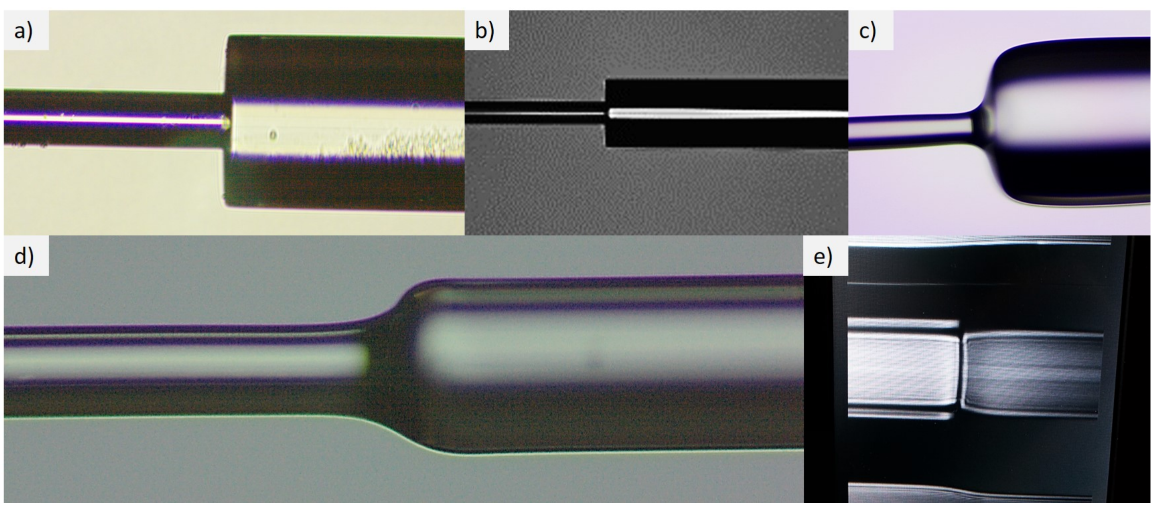

Figure 3.11: (a) 240μm - 600μm cold splicing. (b) 125μm - 400μm cold splicing. (c) 125μm - 600μm Splicing. (d) 125μm - 240μm hot splicing. (e) 300μm delivery - 400μm hexagonal shape active fiber splicing.

exhibited in section 4.2 as a splice between combiner cleaved end-face and 20/400 μm delivery fiber to complete the combiner fabrication process. Furthermore, another integration point which combines two high power laser sources will be shown in section 5.2. In this splice 20/400 μm fiber output is integrated with 200/240 μm multi-mode fiber as an input of 3x1 combiner.

3.1.3 Low loss integration of core offset fibers

In this section of the thesis, integration of core offset fiber will be shown. While preparing active fiber preforms before drawing the operation, there is a polishing step in order to shape the preforms. Claddings of preforms can be polished as D-shape, hexagonal, elliptical and rectangular. In this polishing step, centering the core is a critical point to get low loss integration. In our institute (Bilkent University, National Nanotechnology Research Center (UNAM)), Yb-doped active fibers are fabricated in the fiber optic facility by Prof. Mehmet Bayındır group. Unoptimized prototypes of active fibers are demonstrated in Figure 3.12. It is clear that 10 μm core offset from center of fiber is due to uncentered preform polishing. Before obtaining optimized active fibers from Prof. Mehmet Bayındır group, we were able to build a high power fiber laser with in-house fabricated unoptimized active fiber, which will be introduced in Section 4.4.

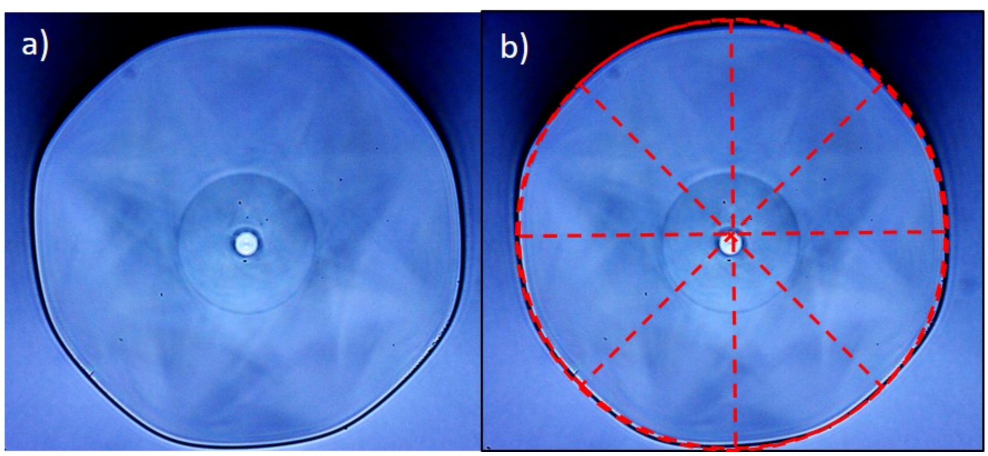

Figure 3.12: Prototype of in-house drawn Yb-doped active fiber image of a) end-face and b) 10 μm core offset.

Splicing the FBG with an offset-core hexagonal shape active fiber is a critical point in building a high power laser. In Figure 3.13a, gap setting position before alignment of these two fiber is shown. After the lasing process, fibers' cores are well aligned and integrated to each other (Figure 3.13b). The splicer machine measures the core offset of fibers before and after the splicing process and results of core offset are about 500 nm in total (Figure 3.13c). The cladding of active fiber is 10 μm larger than passive FBG fiber. In addition, the core alignment

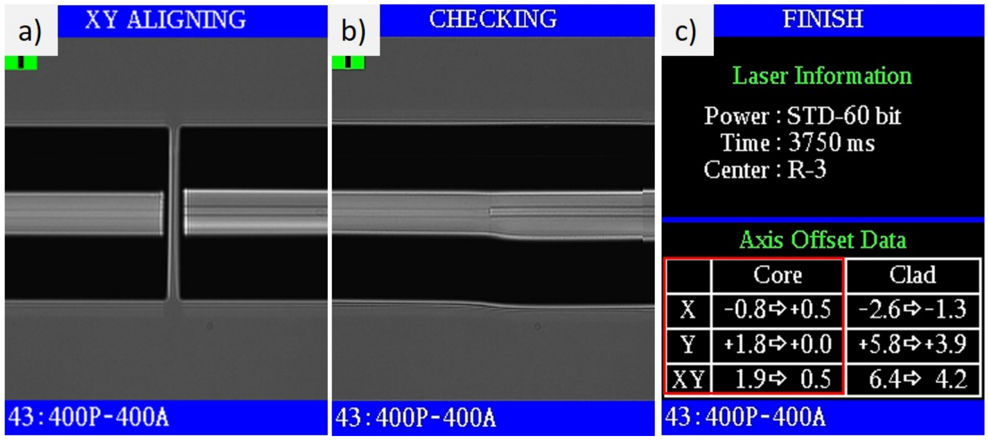

Figure 3.13: Splicing process of FBG tile and hexagonal shape active fiber. a) Gap setting position, b) spliced fibers, c) measured core offset before and after splicing

procedure itself causes increment on their claddings offset. Matching not only their cores, but also their claddings is of great importance. Figure 3.14 shows optical microscope images that the cladding of the active fiber is melted on the FBG well enough.

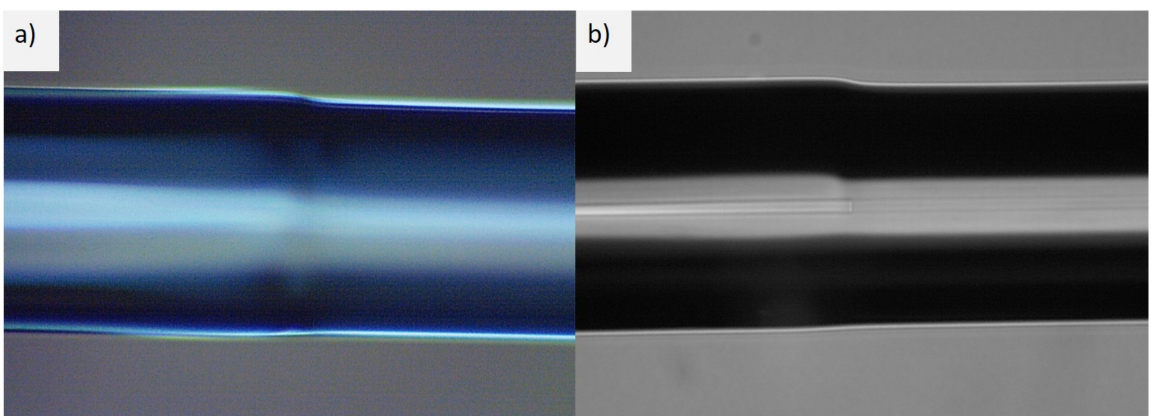

Figure 3.14: Optical microscope images of splicing in a) differential interference contrast (DIC), b) dark field (DF) mode.

3.2 End-cap fabrication with CO_2 laser

End-cap is a core-less fiber rod which can have a diameter from 125 μm to 3 mm with a length of few millimeters. It is generally used as a component for fiber lasers and amplifiers. According to its length, end-caps expand the beam through the larger diameter of light beams. In Figure 3.15, typical end-cap for LMA fiber is shown.

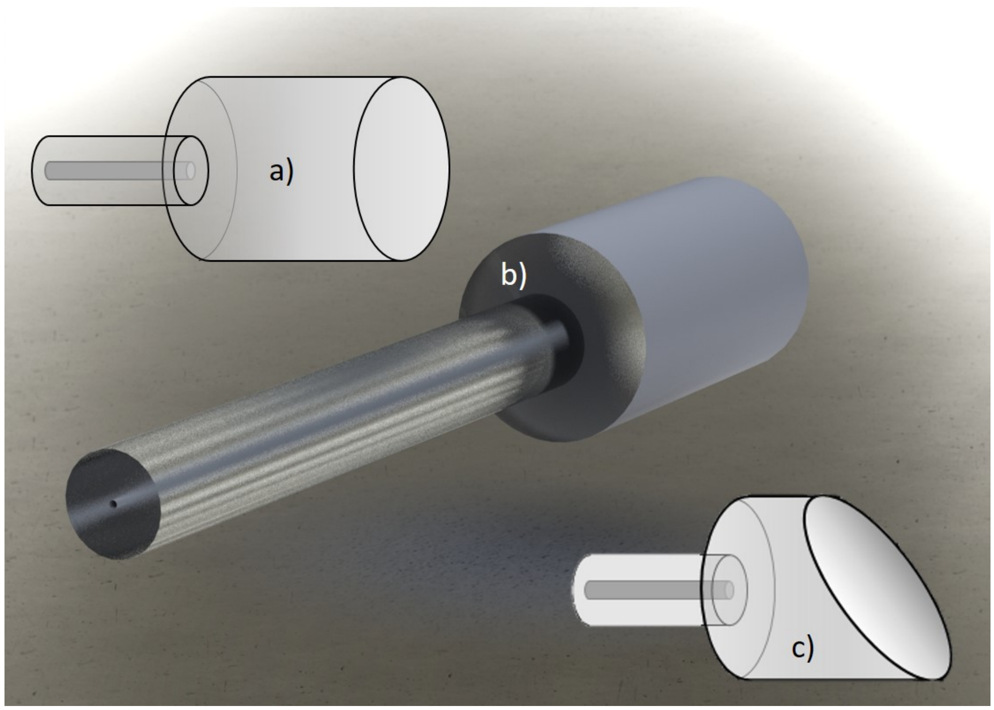

Figure 3.15: Image of a) end-cap with flat end, b) SolidWorks design of end-cap, c) angled end-cap.

Using end-caps has several advantages. The first advantage is protecting the end-face from optical damages. Optical intensity decreases at the glass-air interface, so fiber end-face can be damaged depending on the given optical power and source type (pulsed or continuous). The second advantage is the elimination of Fresnel reflection, fibers or end-caps having flat end results with Fresnel reflection from end-face about 4%. Using angled end-cap, as shown in Figure 3.15c, can eliminate Fresnetel reflection that can result in suppression of parasitic lasing in high-gain fiber amplifiers. Also, for photonic crystal fiber applications end-cap has advantages in terms of protect these fibers from environmental effects by covering the end-face of the fiber.

In this section, designing, numerical simulation and fabrication steps of end-cap will be shown. Designing of end-cap is studied with 3D CAD Design software *SolidWorks* (©2015 Dassault Systemes SolidWorks Corporation, USA) and it is shown in Figure 3.15b.

In order to ensure the length of the end-cap that should be integrated to the fiber end, optical design software Zemax (2015 Zemax, LLC All Rights Reserved, Germany) is used and expected results is shown in Figure 3.16. In Figure 3.16a,

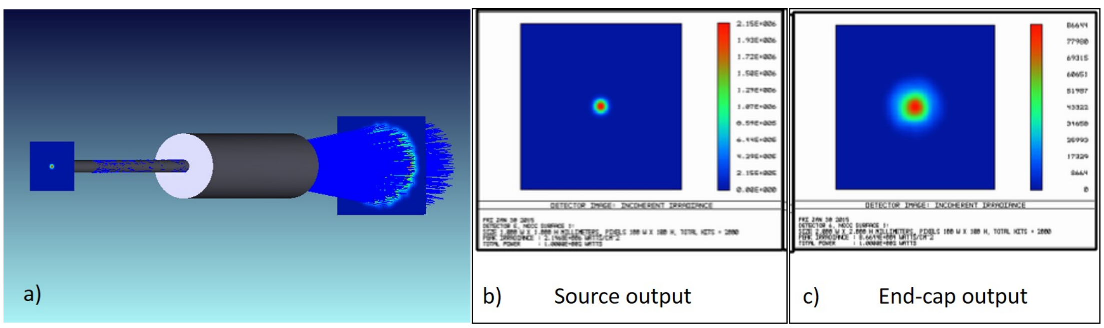

Figure 3.16: (a) Ray tracing simulation geometry: single mode source coupled SM fiber and 600 μm end-cap. (b) Simulated beam profile of SM source and end-cap.

ray tracing simulation of integrated SM (9/125 μm core/cladding diameter) fiber with 600 μm coreless end-cap is studied. End-cap length is determined by the NA of the SM fiber output and the point where TIR occurs for the first time. Simulated and expected beam profiles after source output (3.16b) and after end-cap output (3.16c) are also shown. The diameter of the source output beam is increased at the end of the end-cap.

End-cap fabrication starts generally with splicing of fibers having different cladding diameter (Section 3.1.2). In Figure 3.17, typical processing of splicing is demonstrated. Alignment of the glass rod and the fiber about the center is critical to obtain unscattered beam profiles. After the alignment process, CO_2 laser radiation starts to melt the fibers and merges them to each other as shown

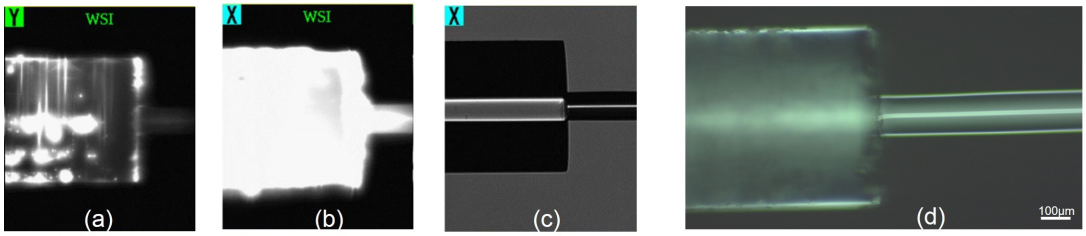

Figure 3.17: Splicing process: (a) starting to melt 600m and 9/125m fibers with CO_2 laser, (b) melting and splicing of two fibers, (c) after splicing and proof test. (d) Optical microscope image of the splicing point of the end-cap.

in Figure 3.17a and b. There is also different size (”400-125” and ”2000-125”)

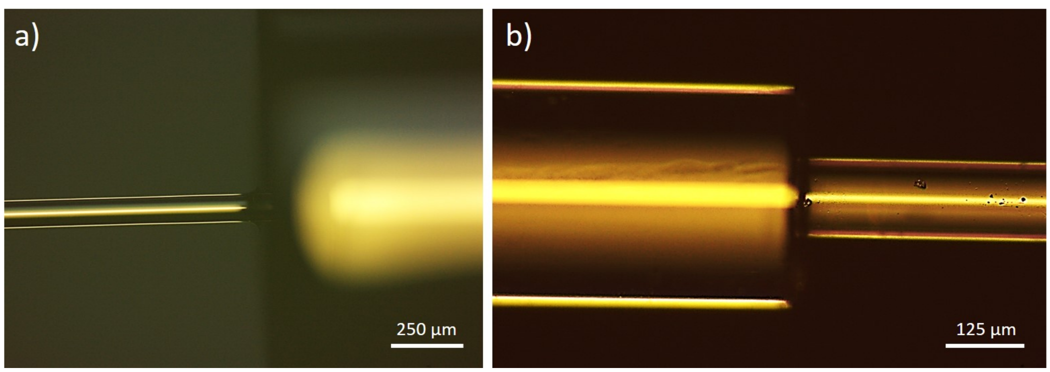

Figure 3.18: Splicing of a) 2000 μm rod and 125 μm SM fiber b) 400 μm MM fiber and 125 μm SM fiber

end-cap splicing in Figure 3.18. In this Figure, 2000 μm rod and 125 μm SM fiber are spliced to each other, also 400 μm MM fiber is spliced to 125 μm SM fiber. In this thesis, we spliced the rods with different cladding diameters with 125 μm SM fiber. In the future, we will integrate end-caps to LMA high power laser outputs in order to protect them from end-face damages.

3.3 Ball lens fabrication with CO_2 laser

Ball lens is an optical component which is spherically shaped with a CO_2 laser radiation. They are generally used to collimate or focus light which comes from the fiber output. Ball lenses are utilized for increasing light coupling between fibers, emitters and detectors. They are also used in medical and sensor applications. In this section, ball shaped lensing on fiber will be introduced and fabrication results for different diameter lenses will be given.

Figure 3.19: CAD design of ball lens

In Figure 3.19, CAD design of ball lens is illustrated. It is important that fabricated ball lens should have a symmetrical and spherical shape. Fabrication procedure of ball lens starts with aligning the fiber according to all x,y and z axis as in Figure 3.20. Accuracy of this alignment provides homogeneous CO_2 lasing on the fiber.

After centering the fiber with respect to the axis, the lasing process takes place for shaping the fiber. There are several parameters to optimize the lensing procedure such as "Feeding speed: Moves fiber on z axis through center of laser while fiber getting its shape", "Laser power: Adjust starting power", "Relative power: Vary power of laser with respect to given function", "Pre-heat time: Adjust time to heating before main lasing", "Rotator angle: Adjust rotation speed" and "Motor Positions: Adjust starting positions".

In Figure 3.21, changing 400 μm fiber end shape through 1000 μm ball lens

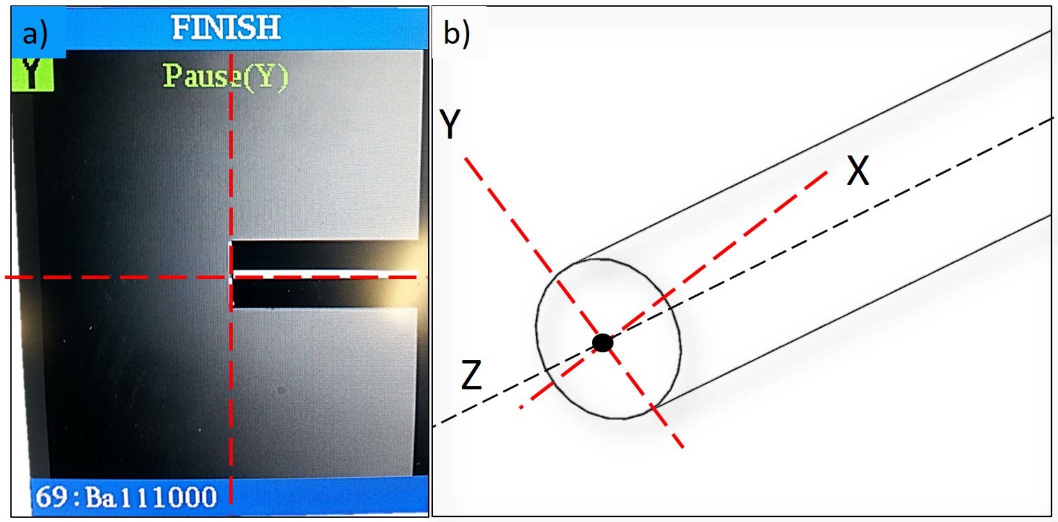

Figure 3.20: a) Alignment of fiber according to y and z axis on the laser source system. b) Sketch of fiber position according to x-y-z coordinates.

(3.21a) and 750 μm (3.21b) ball lens with time is shown. Homogeneous heat distribution on ball lenses is obvious in this figure.

Optical microscope images of ball lens with 1000 μm and 750 μm diameters are shown in Figure 3.22a and b, respectively. In addition to microscope images, light source integrated ball lens shaped fiber image is shown in Figure 3.22 c.

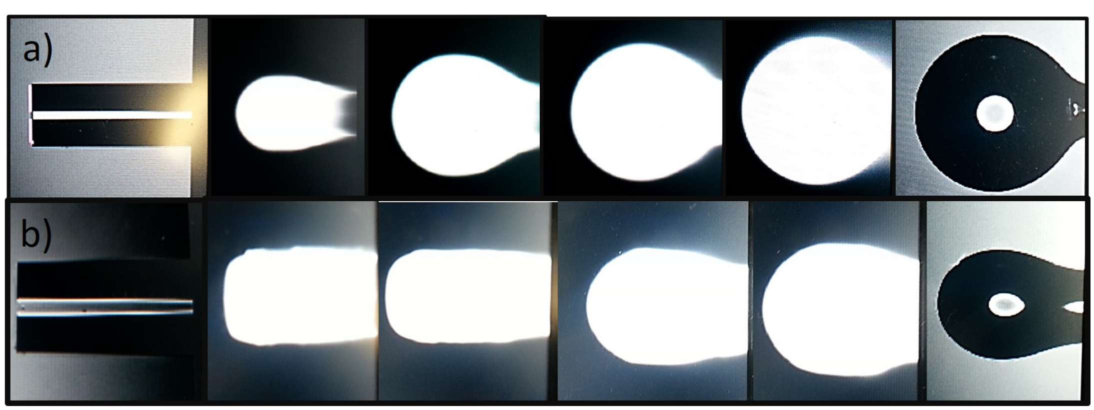

Figure 3.21: a) 1000 μm ball lens shaping images under continuous CO_2 lasing of 400 μm fiber, b) 750 μm ball lens shaping images under continuous CO_2 lasing 400 μm fiber.

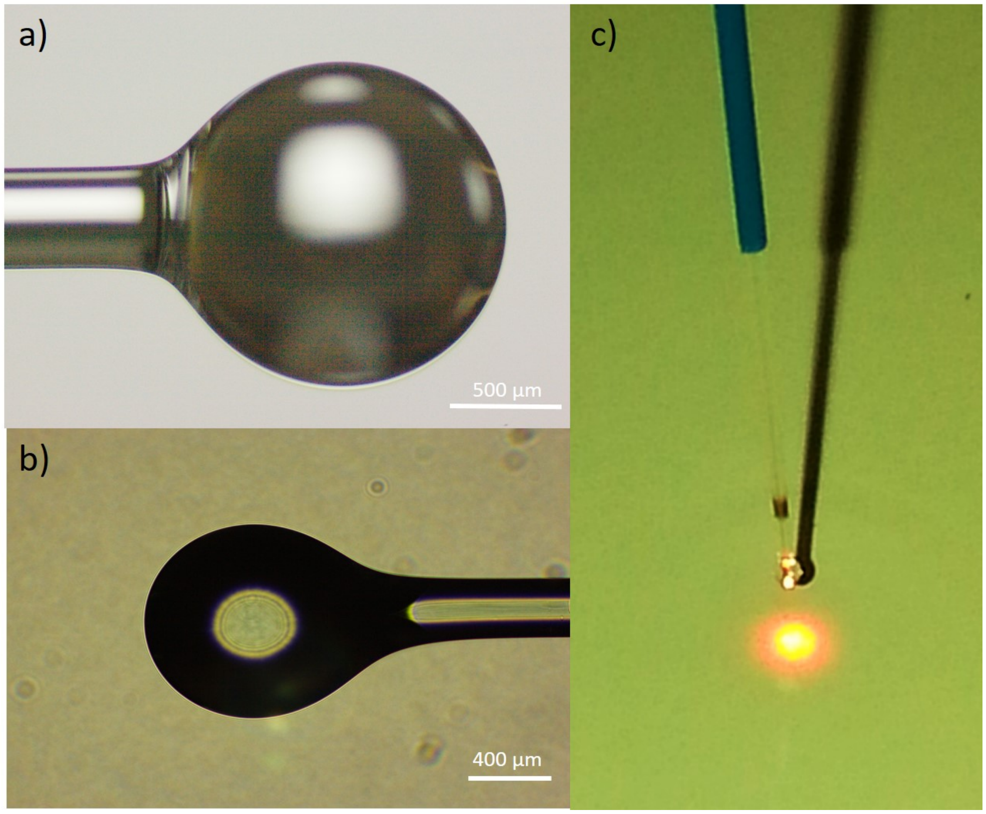

Figure 3.22: Optical microscope images of a) 1000μm ball lens, b)750 μm ball lens on 400 μm fiber. c) Image of light deflection from 750 μm ball lens.

3.4 Fiber tapering with CO_2 laser

Mode field diameter (MFD) of integrated fibers mentioned in the previous sections, should generally be matched to eliminate transition loss between fibers. If light will be guided through less MFD fiber, then one should use another technique before splicing which is called tapering, as it is mentioned in Section 2.1.1. In this section, demonstration of tapered fibers, capillaries and combiners will be presented and precision of tapering process will be discussed.

Fiber tapering process differs from splicing process in terms of its working temperature. During the splicing process, fiber is heated up to its melting point, whereas the temperature of the fiber reaches its softening point in the tapering process. In Figure 3.23, viscosity vs. temperature graph [57] of fused silica is shown to understand the difference between the melting point and the softening point of the optical fiber.

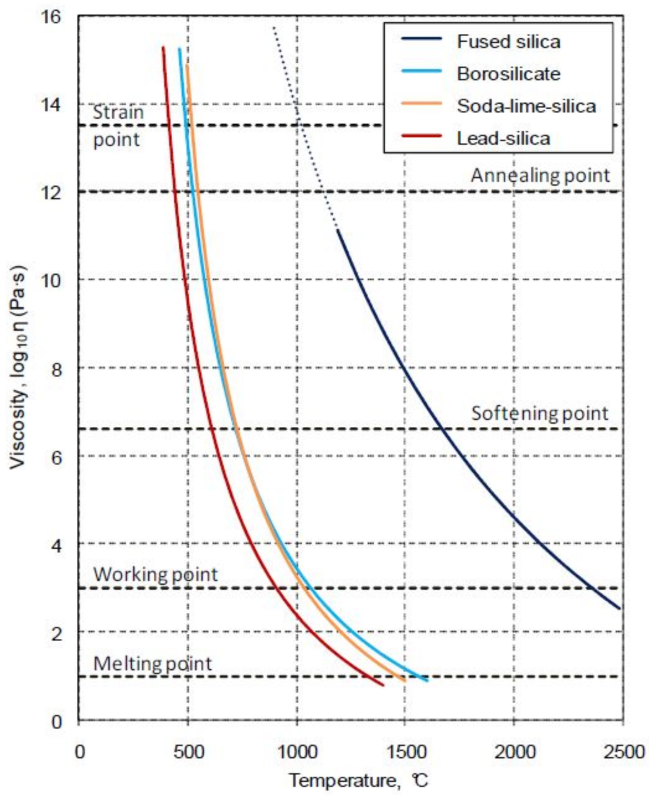

Figure 3.23: Viscosity vs. temperature graph of fused silica, borosilicate, soda-lime-silica, lead-silica. [57]

Thanks to the rotation and micron precision movement that is available in CO_2 laser system, we are able to taper fibers and fiber bundles with accuracy of 5 μm and also capable of shaping fibers in the range between 100 μm - 2000 μm. In Figure 3.24, tapering of 400 μm fiber to 125 μm is shown. Pink line in Figure 3.24b refers to the designed ideal curve of the tapering process whereas green and orange ones refer to diameters of the fiber in x-y axis.

It is clear that the fiber taper region is smooth and $x - y$ diameters of the tapered fiber are equal as shown in Figure 3.24a and 3.24b.

Tapering is also applied to spherical capillary tubes having approximately 150

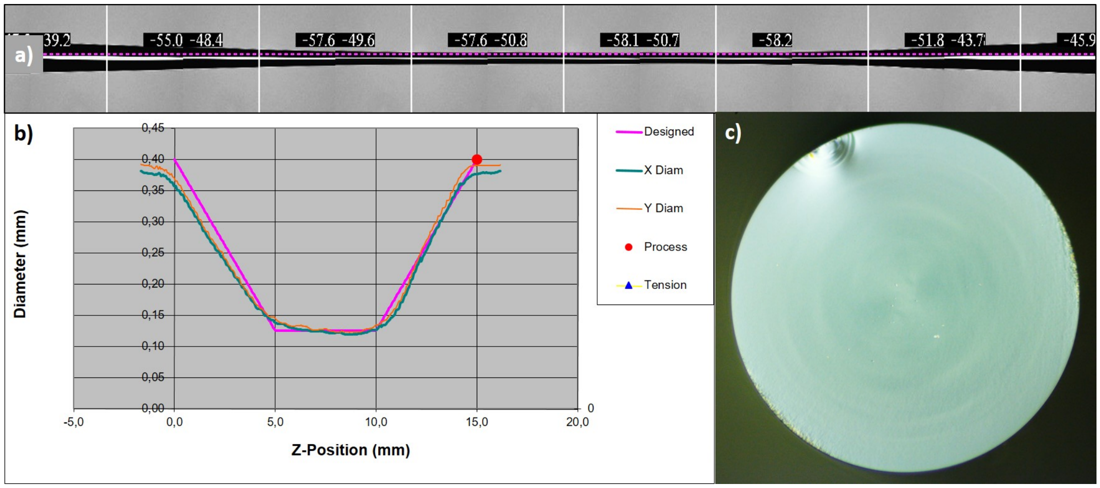

Figure 3.24: Tapering of 20/400 μm fiber a) scanned taper region image, b) measured and expected diameter vs. z-position graph and c) cleaved end-face from the middle point of the taper.

μm wall thickness. In Figure 3.25, tapering of capillary tube is exhibited. As seen in this figure, it has a smooth and symmetric taper region. When capillary is cleaved from its thinnest part, end-face looks clear and spherical as expected.

Tapering of the fiber bundle that is inserted into the capillary tube is a challenging process due to the unique material composition of each glass. Although the capillary is formed by pure fused silica, it may cover the impure optical fibers. Therefore, softening points of capillary and fiber differ from each other. Inside the combiner, heat does not flow from the outer side to the inner side homogeneously as it is distributed within the fiber due to air gaps inside the fiber bundle. Rotation factor of CO_2 laser system takes place in this step. Rotation of the fiber bundle provides homogeneous heat distribution inside the bundle. Figure 3.26 demonstrates a successful tapering of a combiner. When it is investigated; fiber symmetry, homogeneity of contact points, taper length, end-face diameter, smoothness of taper and surface roughness are well enough to fabricate high power combiners for the fiber laser.

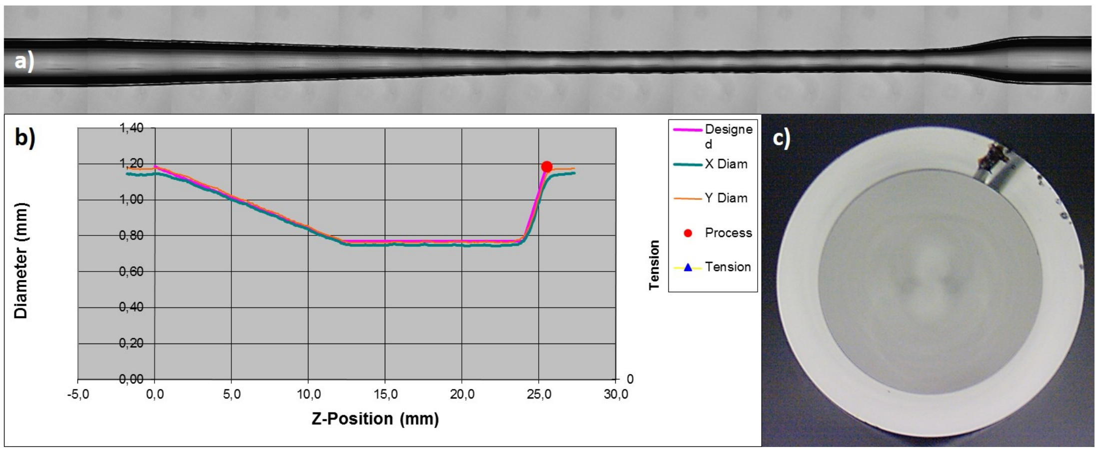

Figure 3.25: Tapering of 1100 μm capillary a) scanned taper region image, b) measured and expected diameter vs. z-position graph and c) cleaved end-face from the middle point of the taper.

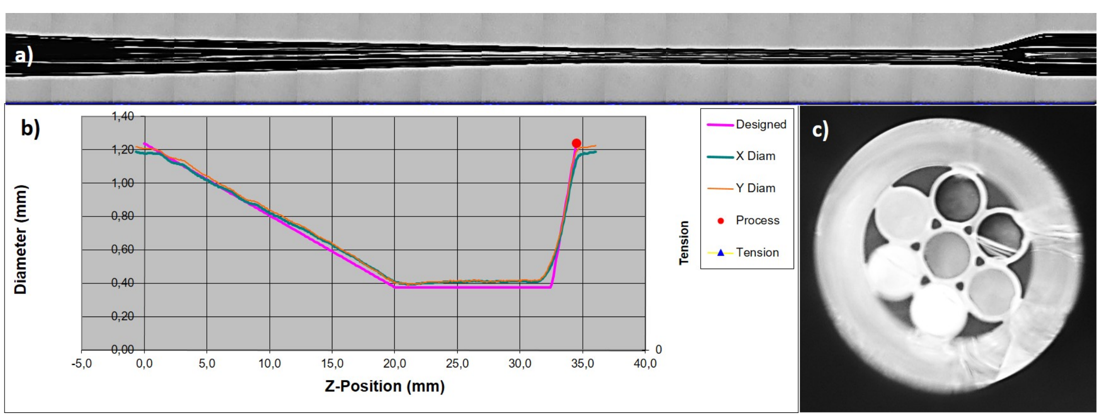

Figure 3.26: Tapering of 7x1 combiner a) scanned taper region image, b) measured and expected diameter vs. z-position graph and c) cleaved end-face from the middle point of taper.

In order to obtain results that match with expected values, there were long optimization processes for each fiber, capillary and combiner. Along the optimization process, "Tapering time", "pulling speed", "taper length", "laser power", "variable laser power", "pre-heat", "rotation speed" parameters were optimized for each size of glass. Optimization procedure for combiner and capillary tapering will also be given in Section 4.2.

3.5 Summary

In this chapter, high quality integration of fibers with same or different cladding diameter were exhibited. Low loss integration of core offset fiber challenges were discussed and integration of these types of fibers were shown. Fabrication of end-cap and ball lens by CO_2 laser radiation were demonstrated. Finally, fiber tapering, kind of a mode field adapter, was introduced and results of fiber, capillary tube, and combiner tapering were shown.

Chapter 4

Pump combiners for high power fiber lasers

In this chapter, design and numerical study of 7x1 pump combiners, optimization route for combiner development, their fabrication and characterization will be studied. Construction of a high power fiber laser operating at 1080 nm with 600 W average output power using in-house fabricated 7x1 pump combiner and a high power fiber laser operating at 1064 nm with 420 W average output power using in-house fabricated 7x1 pump combiner and active fiber will be presented. The physics and the structure of combiner was already mentioned in section 2.2.1, so we will begin with the design and the numerical study of pump combiners.

4.1 Design and numerical study

Fabrication of a combiner starts with designing its structure. Seven fibers are used as an input because spherically shaped capillary tube allows this particular number of fibers to fit into the fiber bundle's symmetrical geometry. First of all, the taper ratio of one of the fibers of combiner is calculated adiabatically as in section 2.1.1 to obtain the minimum taper length of the combiner. Then, the combiner is technically drawn to visualize its untapered and tapered diameter parts by 3D CAD software (SolidWorks). 3D drawing of a typical combiner is shown in Figure 4.1. The initial untapered diameter of fiber bundle is important to taper capillary tubes through exact dimensions. After modeling the 7x1 combiner, ray tracing software (Zemax) is used to check if adiabatic criterion of the taper region works. In Figure 4.2, the light guiding from each input of combiner through the taper region is traced. According to Figure 4.2c, it is obvious that coupled light is guided into the taper medium without any scattering through glass.

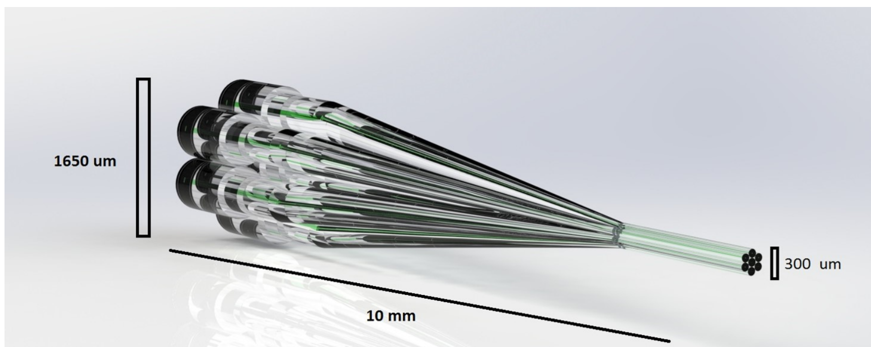

Figure 4.1: Solidworks design of a typical combiner

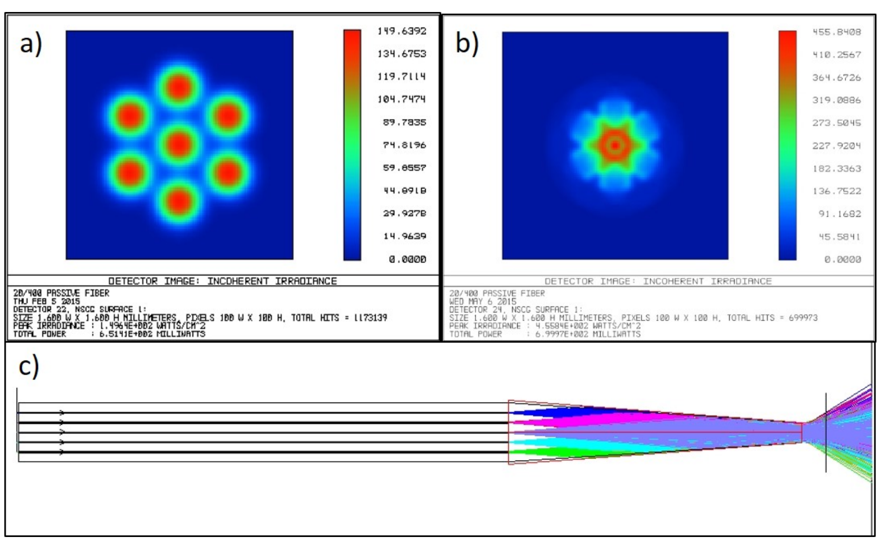

Figure 4.2: Ray tracing simulation of a) source cross-section b) output cross-section c) tapered region.

Even if the fiber bundle is tapered adiabatically, there can be scattering light from the taper region caused by dirt inside the capillary. Also, there is Fresnel reflection that comes from the splicing point between the tapered fiber bundle and the delivery fiber. All these reasons lead to heat in a taper region. In order to manage the thermal load on the tapering and splicing region, a heat sink for combiner is designed and fabricated with the help of calculated dimensions, shown in Figure 4.3.

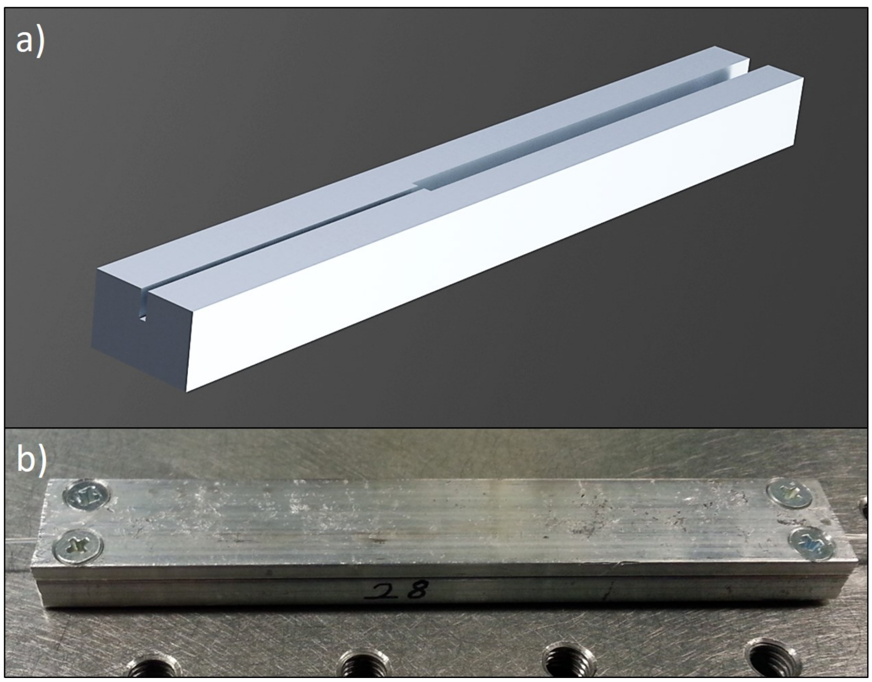

Figure 4.3: a) Designed heat sink of combiner, b) fabricated housing of combiner with top cover.

4.2 Fabrication and Characterization of 7x1 Pump Combiners

In this section, fabrication, optimization and characterization of 7x1 pump combiners will be discussed and results will be shown. Three types of pump combiners which have 105/125 μm, 200/240 μm and 220/242 μm input fibers, 400 μm output fiber will be exhibited.

4.2.1 Fabrication and optimization

Fabrication of a typical combiner is performed in several steps including tedious optimization of tapering, cleaving and splicing processes. In order to produce a combiner, the first step is preparing its capillary tube that will cover fiber bundle. Types of capillary tubes may change with input fiber diameter or designed fiber bundle diameter. We use capillary tubes, which have fluorine doped inner walls to get lower refractive indices, fabricated by Prof. Mehmet Bayındır group in our institute. In Figure 4.4, fluorine doped capillary is shown. The refractive index difference between the outer cladding of the fiber bundle and the inner wall of the capillary tube provides low loss transmission through tapering region [65].

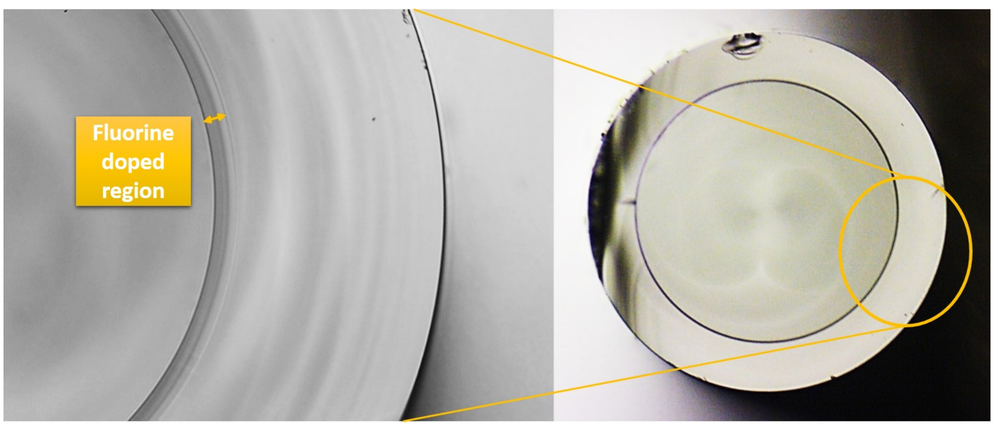

Figure 4.4: Optical microscope image of cross-section of fluorine doped capillary tube.

In order to shape the fiber bundle as a symmetrical hexagon, fibers should fit inside capillary tube as shown in Figure 4.5. Therefore, optimization of the capillary tube tapering constitutes a critical point for the fabrication of the combiner. Unoptimized capillaries generally have bending points, rough and wavy taper region, unwanted inner diameter and elliptical cross-section. Depending on the diameter of the input fiber, capillary tubes are optimized by adjusting laser and motorized system parameters. One of the well optimized capillary tubes is shown in Figure 3.25a.

Another step of fabrication is inserting the fiber bundle into the capillary tube. Before this process, it is important that all fibers are well cleaved and cleaned to prevent contaminations caused by broken or dirty fibers. There is no specific set-up for inserting the fibers, so fiber holders and v-grooves are modified for this purpose. As it is known that the uncoated fibers are very fragile and vulnerable to outside effects, insertion process should be very gentle. All bundles can successfully be inserted into the tube with our set-up.

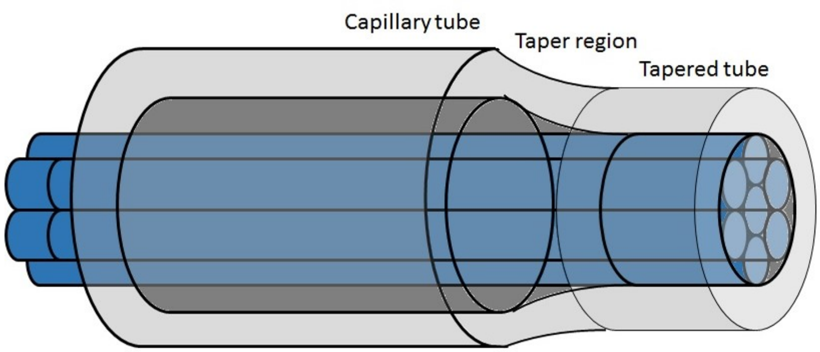

Figure 4.5: Illustration of untapered and tapered capillary tube which covers fiber bundle inside.

The next step of fabrication is tapering the combiner with laser through the desired diameter. CO_2 laser has an advantage for this specific taper process, because laser radiation does not directly affect the air that can be present between the capillary tube and the fiber bundle. Tapering the fiber bundle is quite challenging because it contains lots of design parameters such as fiber types, fiber diameters, capillary tube types, wall-thickness of capillary tubes, geometrical order of fiber bundle and so on. Combiner tapering is optimized for each input types and one of the well optimized tapering results were shown in Figure 3.26. Also, optimization process of tapered combiners are figured in 4.6.

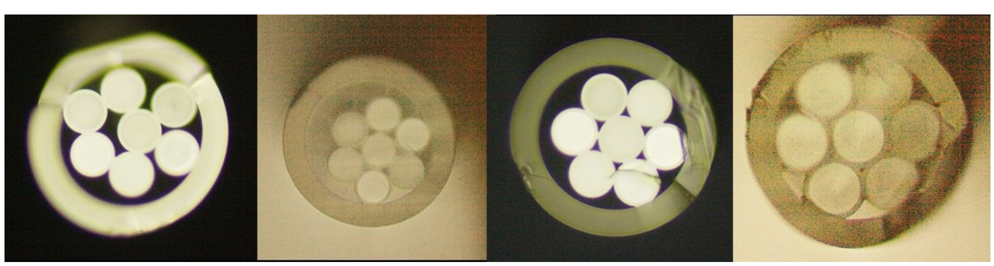

Figure 4.6: Optimization stages of combiner production with cross-section images.

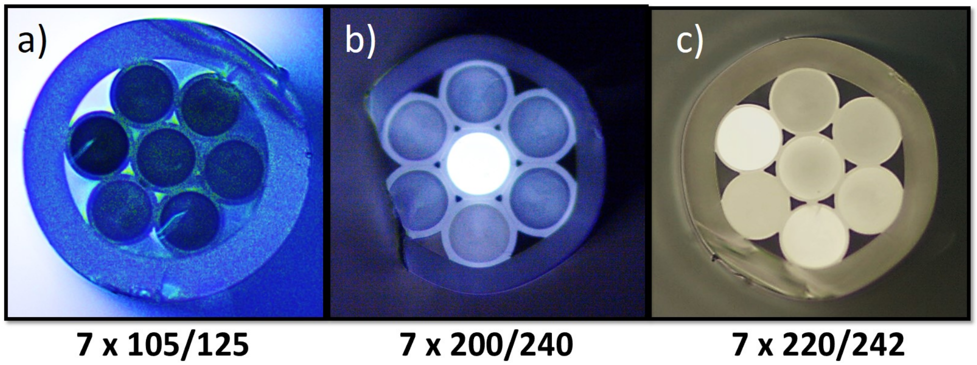

Figure 4.7: Cross-section of combiners that have a) 105/125 μm, b) 200/240 μm and c) 220/242 μm input fibers.

All types of combiners that have input fibers 105/125 μm, 200/240 μm and 220/242 μm are tapered down successfully to the desired waist diameter. In Figure 4.7, these combiners' cross-sections are shown. It is clear that the fiber symmetry, shape and homogeneity of the contact points meet all the expectations by the help of adjusted parameters.

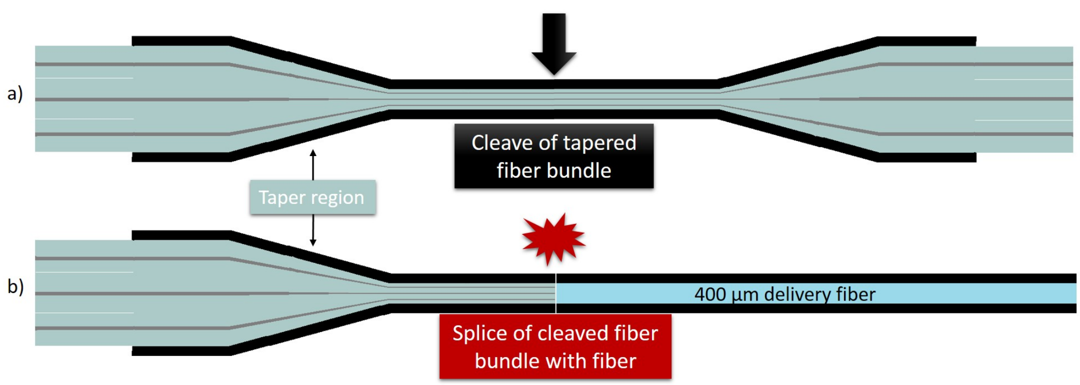

Figure 4.8: Illustration of a) cleaving fiber bundle after tapering process, b) splicing between fiber bundle and 400 μm delivery fiber.

Fabrication continues with cleaving and splicing steps. As shown in Figure 4.8a, tapered fiber bundle is cleaved into the middle of taper region for splicing. Cleaving is a crucial step to build low loss integration in that region. Also, cleaving optimization process begins right after fiber bundle tapering optimization. Cleaving enhancement is exhibited in Figure 4.9. In this cleaving process, the capillary tube that covers the fiber bundle should not be broken or cracked, as in

Figure 4.9a and b, also angled cleaves (Figure 4.8c) may cause failures in splicing between combiner output and delivery fiber. Parameters of the best cleaving (Figure 4.9c) for each fiber type are adjusted.

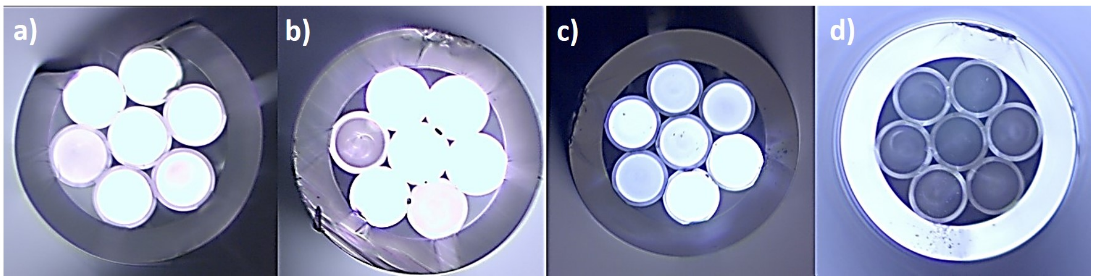

Figure 4.9: Cleaving progress of tapered fiber bundle cross-section. Images of cleaving with a) broken capillary tube, b) cracked capillary tube and fibers c) angled cleave d) nothing.

Combiner delivery fiber types may differ depending on the requirements. We were able to taper the combiner output from 600 μm to 125 μm, however, in this work 20/400 μm passive fiber utilized in fiber oscillators will be used and mentioned in section 4.3 and 4.4. After optimization of cleaving, the following step is splicing the fiber bundle to the combiner output fiber as shown in Figure 4.8b. In this splice, all fiber bundle fibers and capillary tubes should be joined to 400 μm delivery fiber without any defect. Any contamination or imperfection can result in explosion of the integration point, especially in high power applications. Well integrated fiber bundle and combiner output are shown in Figure 4.10. It is

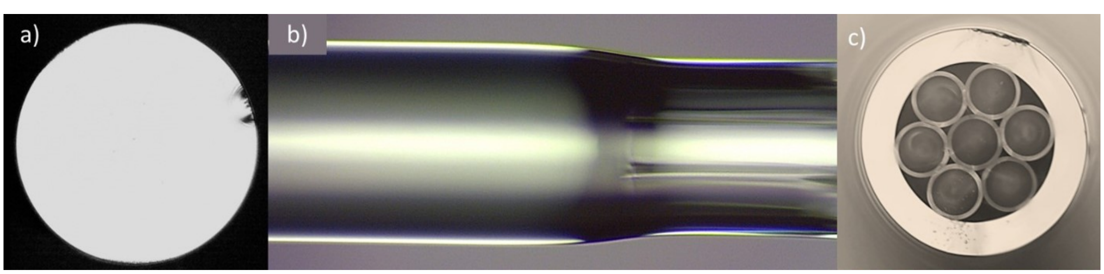

Figure 4.10: Optical microscope images of a) 400 μm delivery fiber cross-section b) splicing region and c) well cleaved fiber bundle cross-section.

obvious that the integration point between them is very smooth and symmetrical and also does not contain any imperfections.

The final step of a 7x1 pump combiner fabrication is packaging the integrated combiner with housing. In Figure 4.11, combiner is inserted into its metal housing which is designed and produced (4.3).

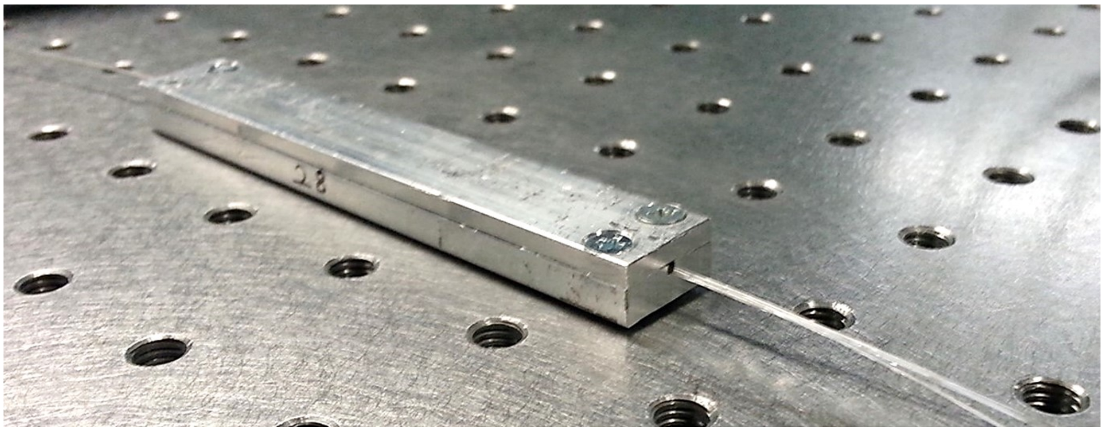

Figure 4.11: Fabricated 7x1 (105/125 μm input fibers) pump combiner that is inserted into its metal housing.

4.2.2 Characterization

In this part, characterization of the fabricated combiners mentioned in the previous section will be demonstrated. Characterization progress may be divided into three parts: Structural, optical and thermal characterization.

4.2.2.1 Structural characterization

In structural characterization, fiber symmetry, homogeneity of contact points, taper length, end-face diameter, smoothness of taper and surface roughness are investigated. In order to study these properties, we use optical microscope, several image processing techniques and scanning electron microscope (SEM). In the previous sections, we characterized the quality of the cross section of tapered fiber bundles with optical microscope, as in Figure 4.9 and 4.10. Also, image processing technique which is a feature of CO_2 laser system is used to characterize the dimensions and smoothness of the taper region formed during the fiber bundle tapering process (Figure 3.26a and b). In addition to these techniques, SEM characterization is also used to investigate surface roughness of tapered and cleaved fiber bundles as shown in Figure 4.12.

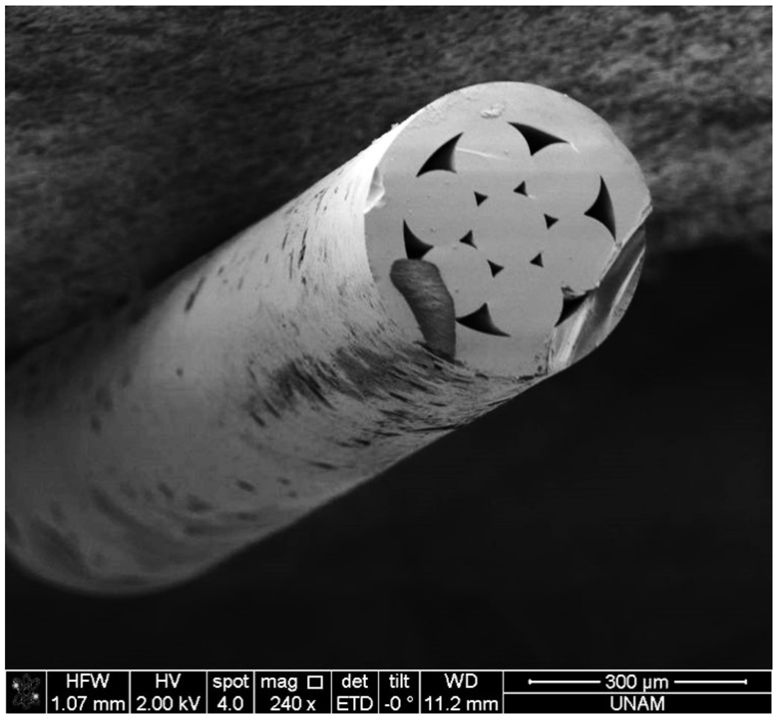

Figure 4.12: Scanning electron microscopy (SEM) image of combiner output.

4.2.2.2 Optical characterization

Optical characterization of the combiner consists of transmission measurements and optical power capacity of each port. Transmission characterization set-up is shown in Figure 4.13. Firstly, each laser diode which will be used in the setup is characterized (Figure 4.13a) in terms of current, voltage, output power, wavelength and diode cooling temperature. We use six *JDSU (JDS Uniphase Corporation)* laser diodes which have specifications as follows; 915 nm central operation wavelength, 140 W maximum output power and 105/125 μm output fiber. In table 4.1, similar values for all six laser diodes are given.

All the diodes are, then, subsequently integrated into the combiner input ports

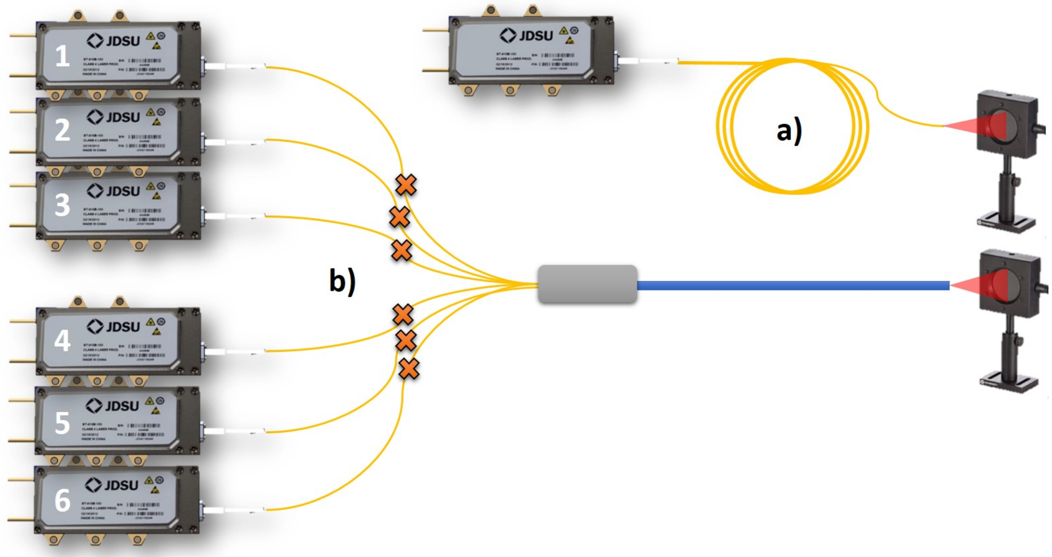

Figure 4.13: Transmission characterization, a) First step is the power measurement of the laser diode output, b) Second one is the power measurement of the combiner using characterized laser diode.

that are characterized one by one and output powers are measured from the combiner output fiber (Figure 4.13) with *Thorlabs S350C* (1mW resolution) powermeter. In Figure 4.14, combiner output powers versus laser diode powers graph is demonstrated. This graph shows that all input ports of the combiner operate with the same efficiency and can handle up to 140W pump power, individually. Although there are seven inputs of combiner, six of them are used due to power supply limitations. However, the unused port is also characterized with diode 1 and its transmission efficiency is 97.4%. The overall efficiency of the combiner was calculated 98%. These results match with the efficiency of commercial high power pump combiners. It is demonstrated that the combiner can handle 851.4 W pump power which is limited by maximum diode powers. In section 4.3, a high power fiber laser system that includes this pump combiner will be presented.

Current (A)	Voltage (V)	Diode Cooling Temperature (^0C)	Wavelength (nm)
1	19,82	17	913,51
2	20,21	17	914,29
3	20,59	17	914,91
4	20,94	17	915,98
5	21,28	18	916,49
6	21,6	18	917,11
7	21,9	18	917,92
8	22,2	18	918,78
9	22,48	18	919,39
10	22,74	18	920,64
11	23	19	921,49
12	23,24	19	922,37
13	23,47	19	923,39

Table 4.1: Operation parameters of the laser diodes used in the setup

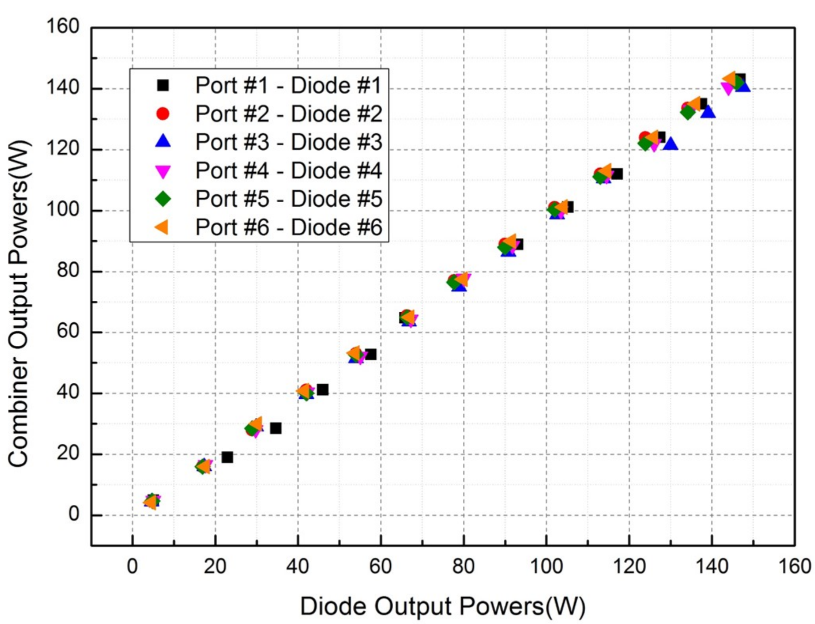

Port No.	Transmission Efficiency
1	98.4%
2	98.1%
3	97.9%
4	97.6%
5	98.2%
6	98.4%

Figure 4.14: Combiner output powers vs. laser diode output powers graph for each input port and laser diode. Calculated transmission efficiency of each input port of combiner.

4.2.2.3 Thermal characterization

In this part, thermal load on the combiner will be investigated and results will be given. All thermal measurements are performed by *FLIR ThermoVision A40M* infrared camera (Figure 4.15a) in this thesis. The laser diode sources and the combiner integration region are the main heat sources in this characterization, so they should be held in stable temperature to work in a safe and reliable manner. Hence, both diodes and combiner housing are actively cooled by a heat sink as shown in Figure 4.15b and c. Each heat sink works with circulating water inside

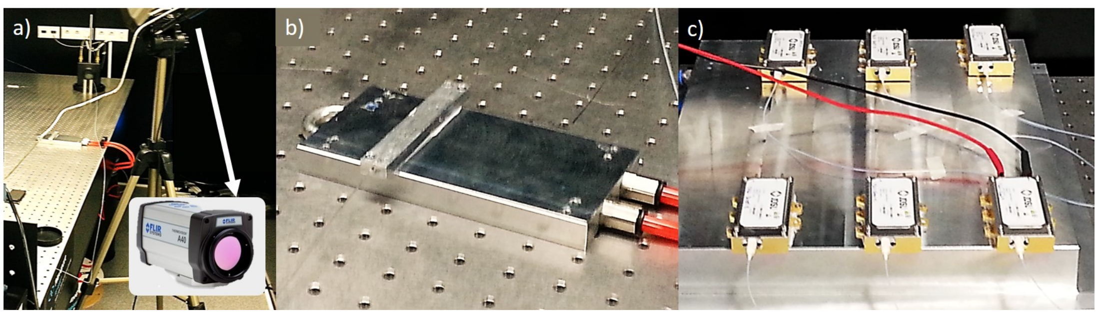

Figure 4.15: Image of a)Thermal characterization setup and thermal camera, b) heat sink integrated combiner housing, c) laser diodes on heat sink.

it and the operation temperature is about $18 \pm 1\ ^0C$. In Figure 4.16, the thermal load is exhibited on the diode and the combiner while characterizing the input port with 140 W laser diode power. As we can understand from Figure 4.16a, the internal temperature of the combiner is almost equal to the inlet water temperature which is 19 ^0C. When the diode power is increased up to its maximum value of 140 W, internal temperature of the combiner increases up to 24 ^0C and stays stable at this level. Increase in the temperature of each port of the combiner is about 5 ^0C when it operates at the maximum power. In the next section, it will be shown that housing can provide thermal management, reducing the thermal load by 6 ^0C while all the diodes are working.

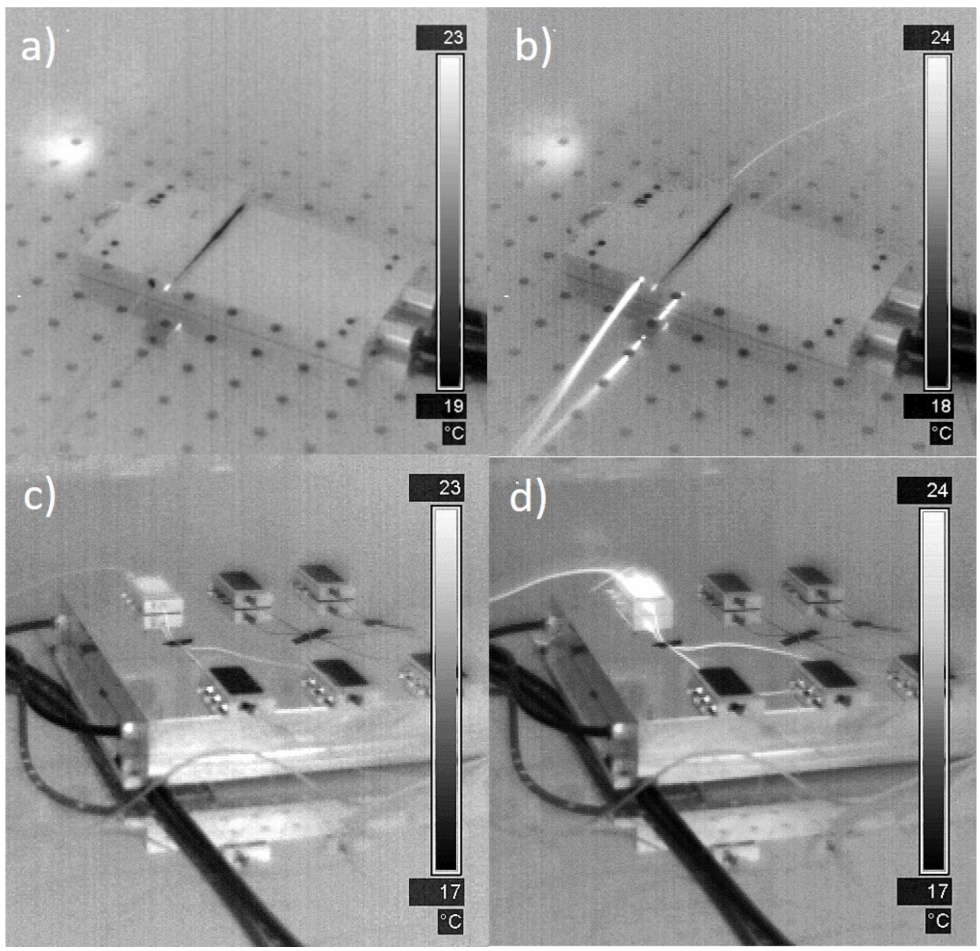

Figure 4.16: Thermal images of 7x1 pump combiner (a) and laser diode (c) working at low power, (b) and (d) at high power

4.3 Development of high power fiber laser operating at 1080 nm with 600 W average output power built with in house fabricated 7x1 pump combiner

In this section, construction of a "1080 nm 600 W High Power Fiber Laser" using the in-house fabricated 7x1 pump combiner which is characterized in section 4.2, will be demonstrated and the results will be discussed.

As the 7x1 pump combiner was characterized and proven to handle optical power up to 140 W from each port, it is used as a pump combiner of $Yb-$doped active fiber to construct a high power fiber laser working at 1080 nm. The structure of this fiber laser is shown in Figure 4.17. Laser diodes are the same ones used in the characterization process. In this setup, an FBG, with 99,9% reflectivity at 1080 nm central wavelength, which can handle high powers is used as a highly reflective mirror. In the following step, the FBG is integrated to 20/400μm combiner output with almost zero clad offset between these fibers. After splicing the FBG and the combiner, 40 m hexagonal shape Nufern LMA-

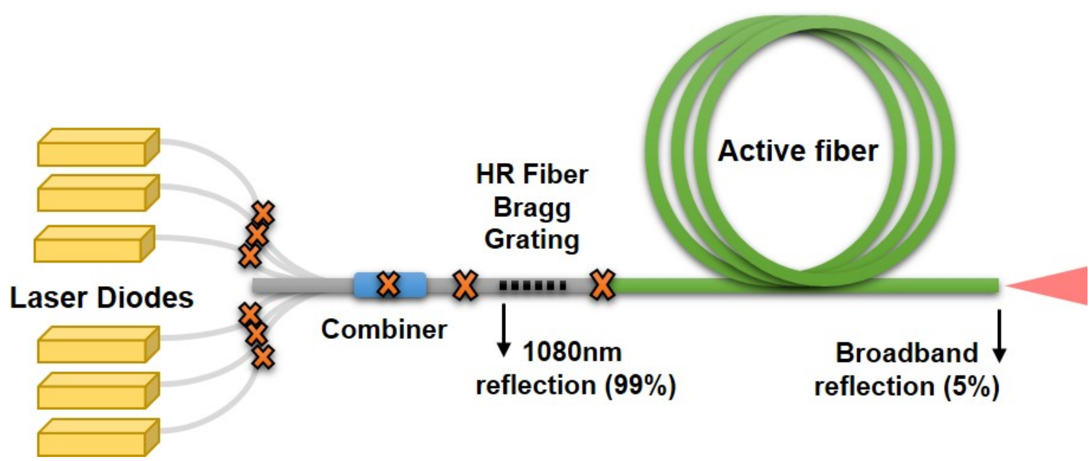

Figure 4.17: Structure of 1080 nm high power fiber laser.

YDF-20/400-M Ytterbium doped fiber and spherical shape FBG output tail are spliced to each other with core-to-core integration technique as mentioned in section 3.1.3. The end of the active fiber, which serves as the output of laser, acts like a broadband mirror with a 4-5% reflectivity due to cleaving process.

Fiber laser is simulated by *RP Photonics software, fiber power package (©RP Photonics Consulting GmbH)*. The simulation result is exhibited in Figure 4.18. According to this graph and the numerical results, 915 nm 851.4 W pump power is absorbed in 40 m active fiber and 636 W of 1080 nm laser is generated with 21 W unabsorbed pump light. In total, simulated laser power and efficiency are

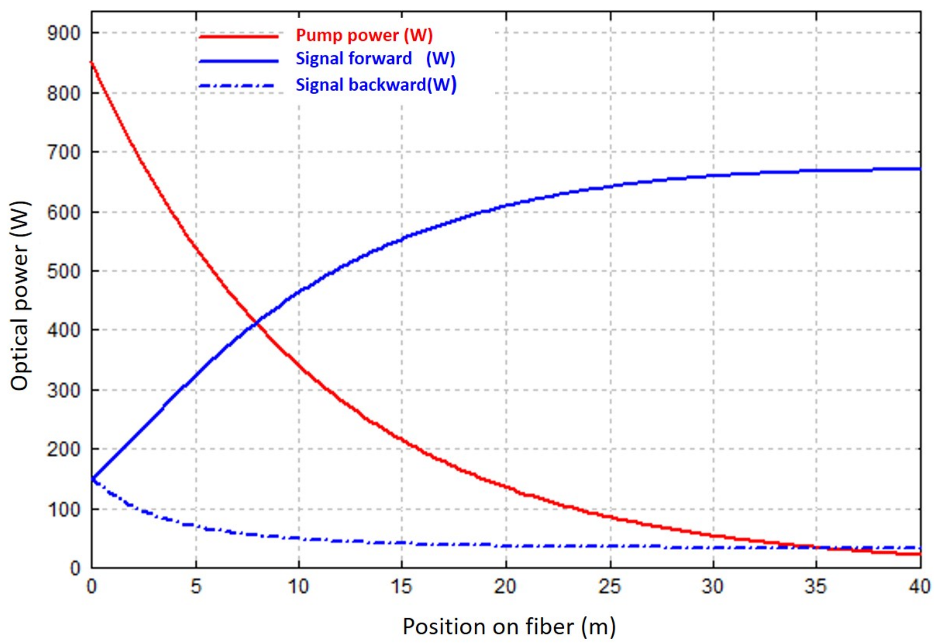

Figure 4.18: 1080nm high power laser simulation graph is plotted by Optical power vs. Position on fiber.

657 W and 77.1% without stripped unabsorbed pump, 636 W and 74.7% with stripped pump light.

The high power fiber laser setup is constructed as depicted in Figure 4.17 and demonstrated in Figure 4.19. All components and their integration points of the fiber laser are actively cooled with aluminum heat sinks. Also, the active fiber and its splice with the FBG fiber are wrapped onto a compact 10 cm diameter water-cooled cylindrical coil.

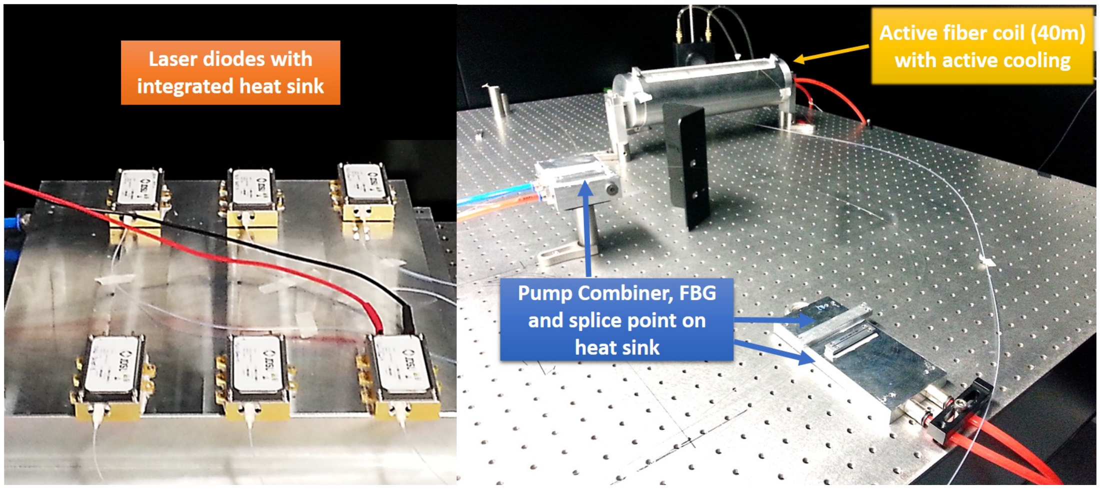

Figure 4.19: Fiber laser setup with cooled laser diodes, splicing points, combiner and compact active fiber coil.

The constructed high power laser with the in-house fabricated 7x1 pump combiner is operated with maximum power ($851.4W$) supplied by the laser diodes. The output power is recorded with and without stripped unabsorbed pump light. The optical spectrum of the output light with and without stripped unabsorbed pump light is shown in Figure 4.20. Also output power and efficiency according to the launched power with stripped unabsorbed pump are shown in Figure 4.21.

According to the these Figures, the central wavelength of the output laser is 1079.85 nm with 2.45 nm bandwidth. The central pump wavelength is 923.50 nm with 10 nm bandwidth because of insufficient cooling of laser diodes, so the pumping laser with this wavelength causes decrement on the efficiency of the fiber laser as in Figure 4.21. Laser output power without stripped light is 656 W consisting of 46 W unabsorbed pump light and 610 W laser light. The efficiency is about 71.64% if pump light is stripped, otherwise it is 77.04%. Our experimental data for the total power is matched with the simulated one which is 657 W. However, there is a difference between the simulated unabsorbed pump power and the experimental one which is about 25 W and this difference is caused by the pump wavelength shift from the original pump light wavelength.

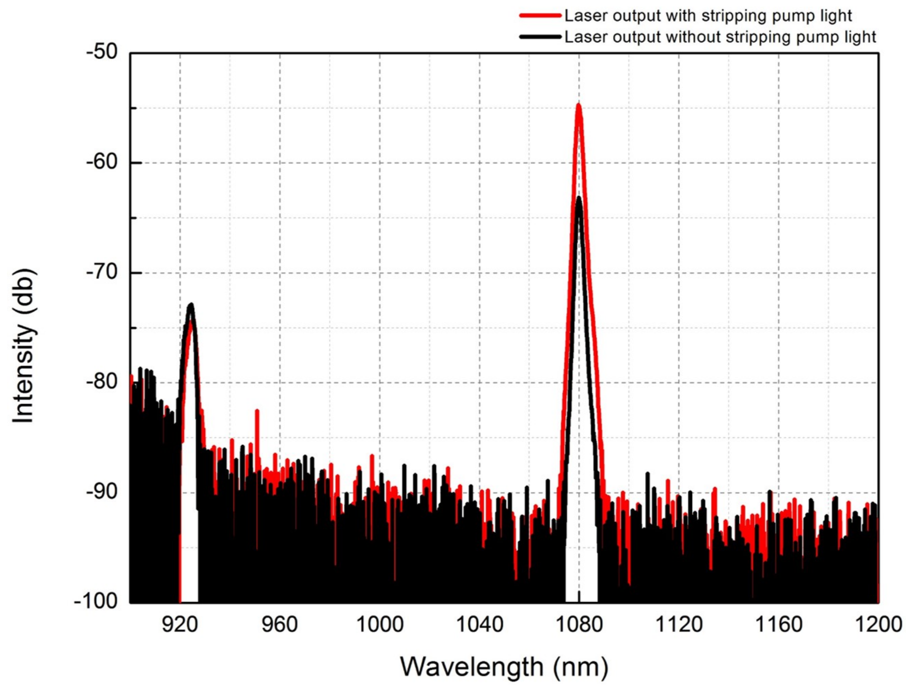

Figure 4.20: Optical spectrum of output laser with and without stripped pump light.

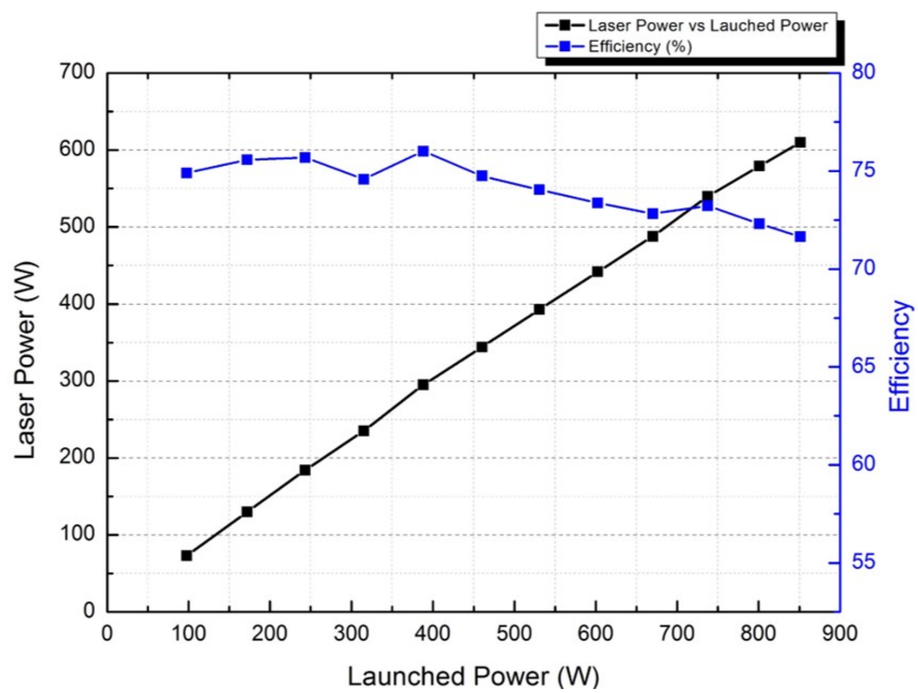

Figure 4.21: Output power with stripped unabsorbed pump light versus Launched power graph with their calculated efficiencies.

In the simulation, center pump wavelength is adjusted to 915 nm, however, our laser pump wavelength is shifted 8 nm from expected value due to lack of cooling system that is integrated to the laser diodes. Therefore, the absorption (0.35 dB/m) of the active fiber at 923 nm is less than the absorption at 915 nm which is 0.40 dB/m.

Operation of the fiber laser is also monitored by a thermal camera in order to detect possible defects on the system and to characterize 7x1 pump combiner under maximum power. The thermal image of the laser system is shown in Figure 4.22. The thermal load on the combiner is 8 ^oC while it is operating under 850

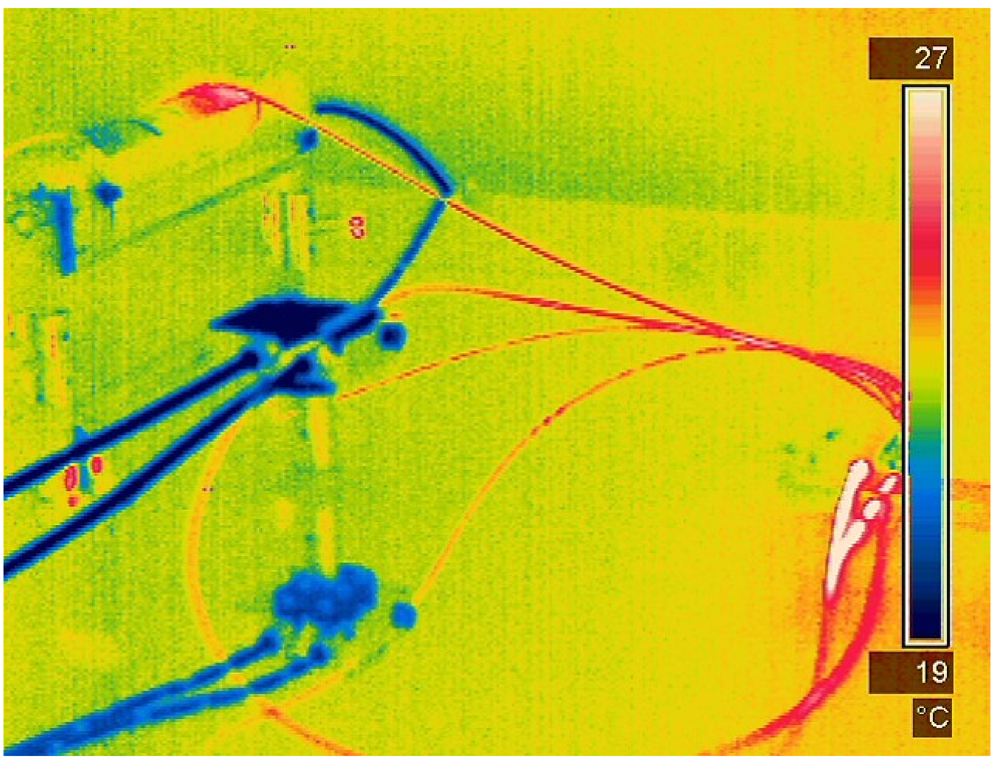

Figure 4.22: Thermal camera image of 1080 nm fiber laser sytem operating with maximum power.

W pump power. Results show that the combiner housing distributes the thermal load homogeneously and it can maintain the temperature stable even if the input port number is increased.

We proved that the fabricated 7x1 pump combiner can handle 850 W pump power without observing any significant temperature increment. Although we are limited with the pump power, it is clear that this combiner can handle multiple kW level pump light with respect to the results above.

4.4 Development of high power fiber laser operating at 1064 nm with 420 W average output power built with in-house fabricated 7x1 pump combiner and active fiber

In this section, a 1064 *nm* 420 *W* high power fiber laser built with in-house fabricated 7x1 pump combiner and active fiber will be introduced. The results will be presented and discussed.

The 1064 *nm* fiber laser has a similar structure as the 1080 *nm* fiber laser that we have demonstrated in the previous section. The fabricated 7x1 pump

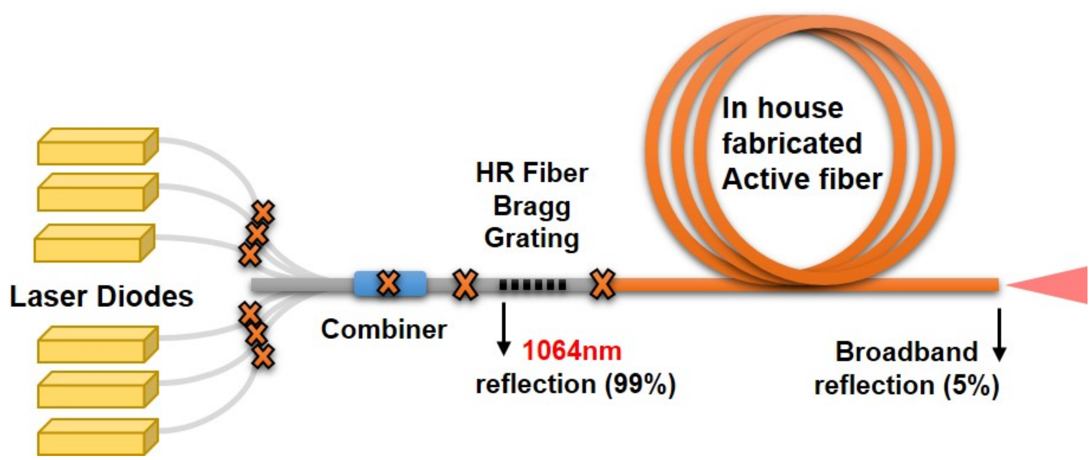

Figure 4.23: Structure of 1064 *nm* high power fiber laser.

combiner is again used in this concept of fiber laser, but the FBG is replaced with a 1064 *nm* high reflective grating which can handle 500 *W* power. Also, the active fiber is replaced with a 27 *m* Yb-doped hexagonal shaped fiber which is drawn at fiber tower by Prof. Mehmet Bayındır Group at UNAM (section 3.1.3).

Cross-section images of the fiber and integration with the FBG fiber were shown in Figures 3.12 and 3.13. Yb doping concentration of this in-house fabricated active fiber is higher than that of Nufern LMA-YDF-20/400-M active fiber, so we used shorter active fiber of 27 m. In Figure 4.24, the constructed high power fiber laser setup is shown. In this setup, the active fiber is wrapped around 10

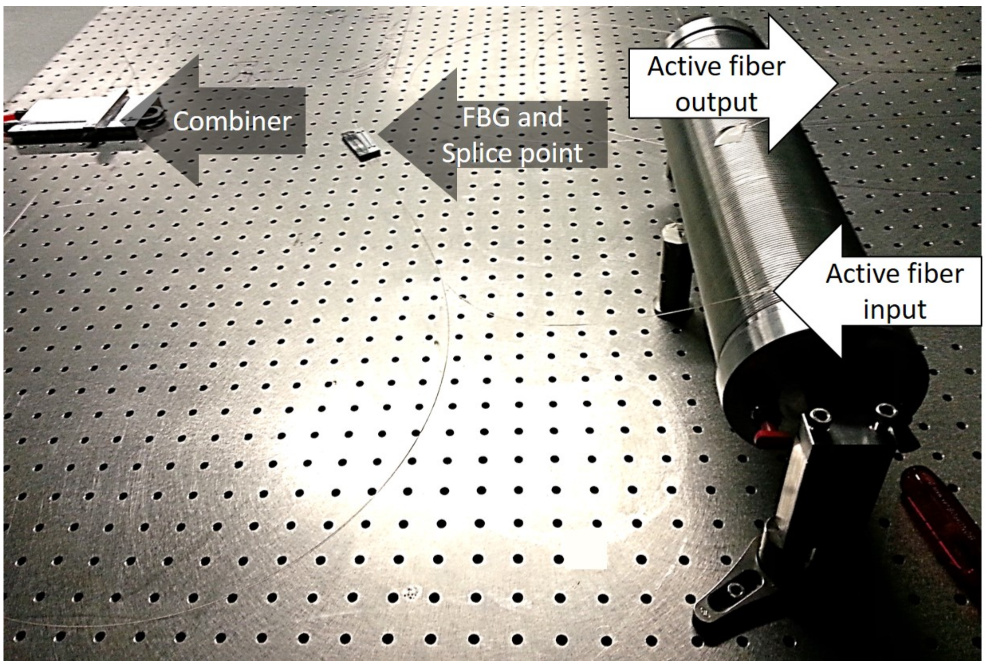

Figure 4.24: 1064 nm fiber laser setup with cooled combiner and compact active fiber coil.

cm diameter coil as shown in the previous concept and actively cooled like the combiner. However, the splice point and the FBG are passively cooled. When fiber laser is operated up to 420 W, thermal loads on components of fiber laser are acceptable and don't exceed 29 ^oC as shown in Figure 4.27. Since there is no need for active cooling of these components, the experiment continues with passive cooling. Optical spectrum characterization results of laser output are given in the Figure 4.25. According to the optical spectrum, the fiber laser is operating at 1064.33 nm with a bandwidth of 1.66 nm. The pump wavelength of laser diodes is centered at 918.93 nm. The difference between the laser and the pump power is about 18 dB.

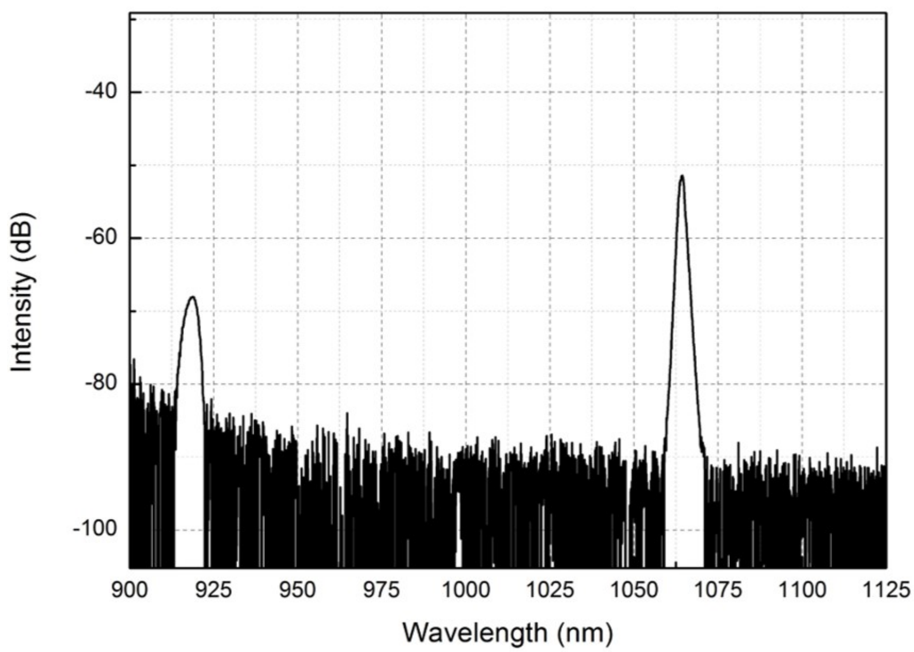

Figure 4.25: Optical spectrum of high power fiber laser operating at 1064 nm wavelength with 420 W average output power.

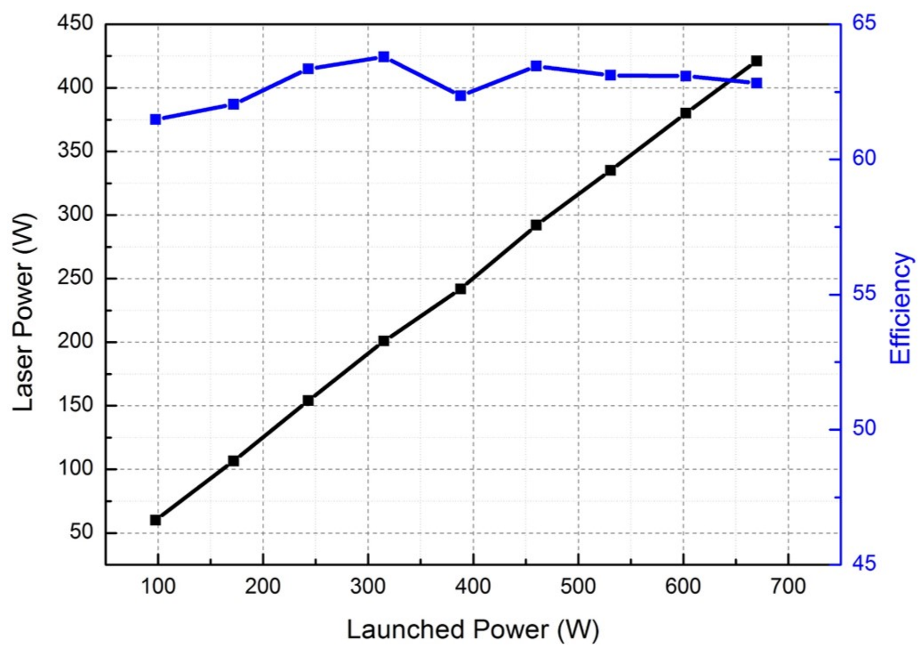

Figure 4.26: Laser output power vs. launched power graph with calculated efficiency.

Neither amplified spontaneous emission (ASE) nor spontaneous raman scattering (SRS) effects are observed as seen in Figure 4.25. The graph of the laser output power versus launched power is presented in Figure 4.26 and calculated efficiencies for each step are also shown. The laser output power is 421 W when 672 W pump power is launched with efficiency 62.6 %. The optimization process for higher efficiency is under the progress. Although the laser diode power limit is 850 W, we are limited with optical power handling of the FBG which is about 500 W.

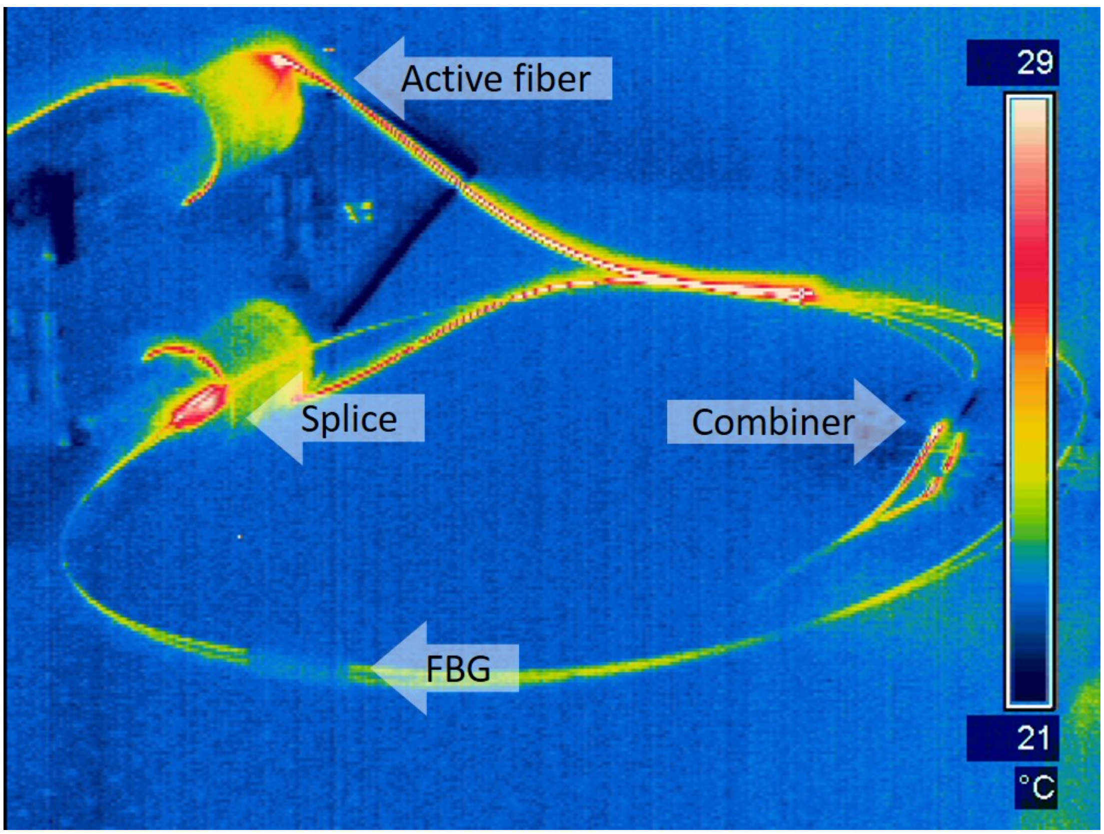

Figure 4.27: Thermal camera image of 1064 nm fiber laser operating at 420 W laser power.

4.5 Summary

In this chapter, designs and numerical calculations of a 7x1 pump combiner for high power fiber laser were studied to fabricate a low loss combiner. Fabrication and characterization steps were introduced for a 7x1 pump combiner. All important steps of fabrication such as cleaving, splicing and tapering process of capillary tube and fiber bundle were demonstrated in detail. Structural, optical and thermal characterization of the fabricated combiner was carried out. In addition, a 1080 nm 600 W high power fiber laser was built with in-house fabricated combiner successfully. Its structure and output laser characteristics were discussed in detail. Finally, a 1064 nm 420 W high power fiber laser was successfully built with in-house fabricated pump combiner and active fiber.

Chapter 5

Signal combiners for high power fiber lasers

In this chapter, all-fiber 3x1 signal combiner will be introduced and its fabrication will be detailed. Combination of two in-house built high power fiber lasers with output powers of 1 kW and 690 W at 1080 nm wavelength will be explained. In addition, a 7x1 laser combiner fabrication and its results will be presented. Finally, fiber laser combiner fabrication with bridge fiber technique will be introduced and preliminary data for this combiner will be shown.

5.1 3x1 kW-class fiber laser combiner fabrication and characterization

In this section, fabrication and characterization of 3x1 laser combiner with 200/240 μm input fiber and the characterization will be demonstrated.

5.1.1 Fabrication

Fabrication of the combiner starts with the capillary tube tapering process. Before tapering, the initial and the final diameters of the capillary tube are designed and calculated as in section 4.1 such that the fibers can properly be fitted into the capillary tube. The images of the capillary tube tapering process are shown in Figure 5.1. It is clear that the tapering region is smooth and well optimized

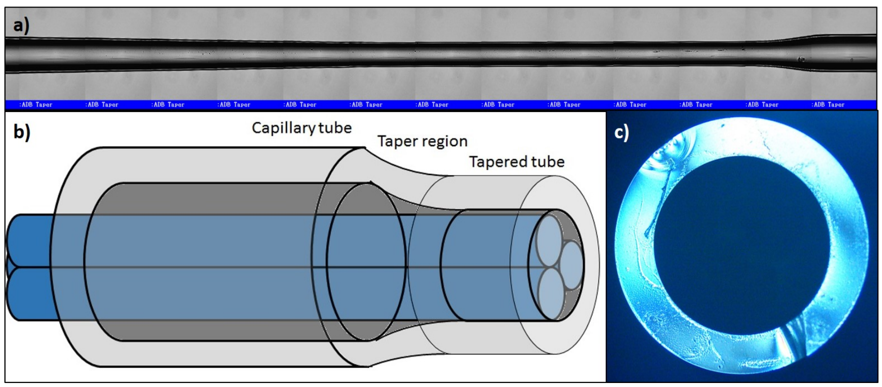

Figure 5.1: a) 3x1 capillary tapering region image, b) designed capillary tube tapering image and c) cleaved capillary tube tapering

(Figure 5.1a) and the waist diameter is same as the designed diameter in Figure 5.1b. Input of the capillary tube should be well cleaved (Figure 5.1c) before inserting the fibers to eliminate cracks or scratches on the fibers. The next step is the insertion of the fibers into the capillary tube. In this process, 200/240 μm fibers are inserted into the tapered tube and the fibers are fitted tightly as seen in Figure 5.1b. After that, the prepared fiber bundle is tapered with CO_2 laser by using the optimized parameters. Tapering and cleaving results of the combiner are given in Figure 5.2. The fiber bundle tapering yields a high quality tapered region as shown in Figure 5.2a; it is smooth and well shaped as expected. Also, cleaving the tapered bundle is successfully performed and the cross-sections are matched with the designed ones. It was planned to get a triangle-like shape for the fiber end-face because stretching the capillary tube in this way results in less air gap between the fibers and the inner wall of the capillary tube. There is one more step to finalize the fabrication process which is splicing the delivery fiber (20/400 μm) to the end-face of cleaved fiber bundle. The splicing procedure is

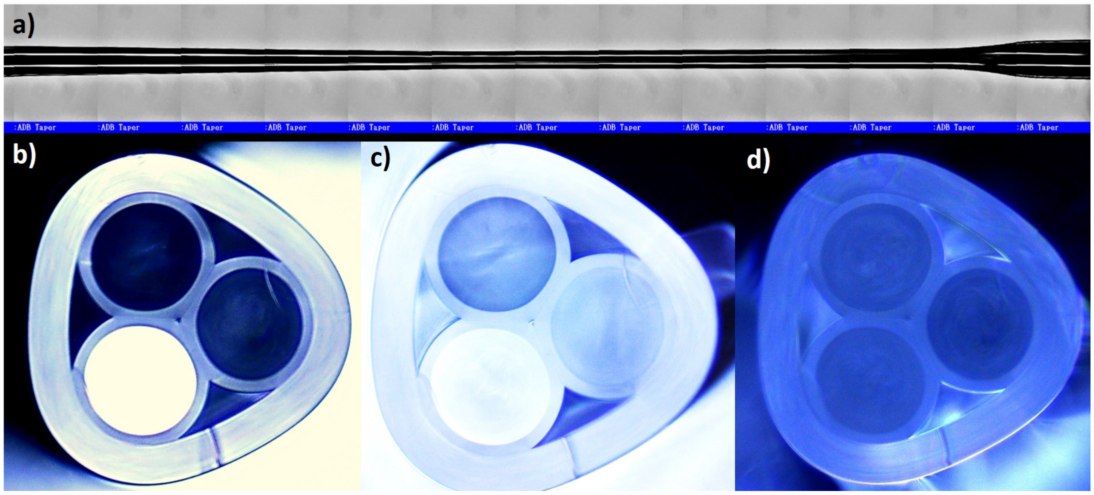

Figure 5.2: a) 3x1 combiner tapering region image. Optical microscope images of 3x1 laser combiner's well cleaved cross-sections in b) transmission mode c) reflection - bright field mode d) dark field mode.

almost same as the one which is applied to the 7x1 combiner splice as described in Figure 4.8. The optical microscope image of this splice is shown in Figure 5.3. The integration images before splicing and during splice process are demonstrated in Figure 5.4. Based on these results obtained above, we can claim that the tapering of the capillary tube and the fiber bundle and the insertion of input fibers into the capillary tube are performed successfully. Furthermore, the cleaving and splicing process of the fabricated 3x1 laser combiner yielded satisfactory results. The fabrication of the combiner ended with the integration to the metal

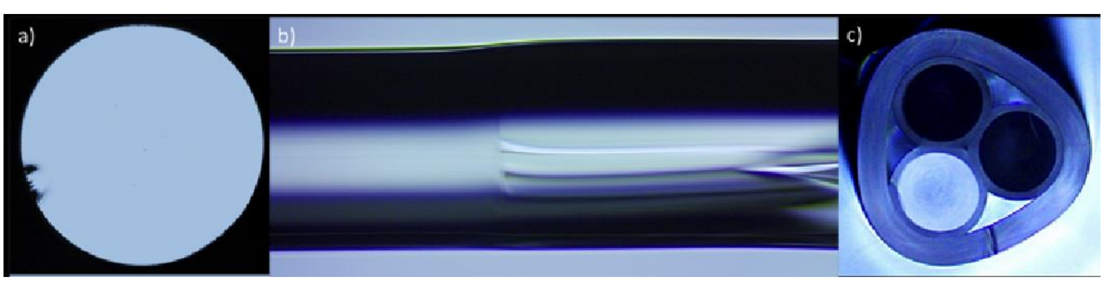

Figure 5.3: Optical microscope images of a) 400 μm delivery fiber end-face, b) splicing 3x1 fiber bundle to 400 μm delivery fiber, c) fiber bundle end-face.

housing. The integrated housing is the same as the one used in fabrication of the 7x1 pump combiner (figure 4.11)

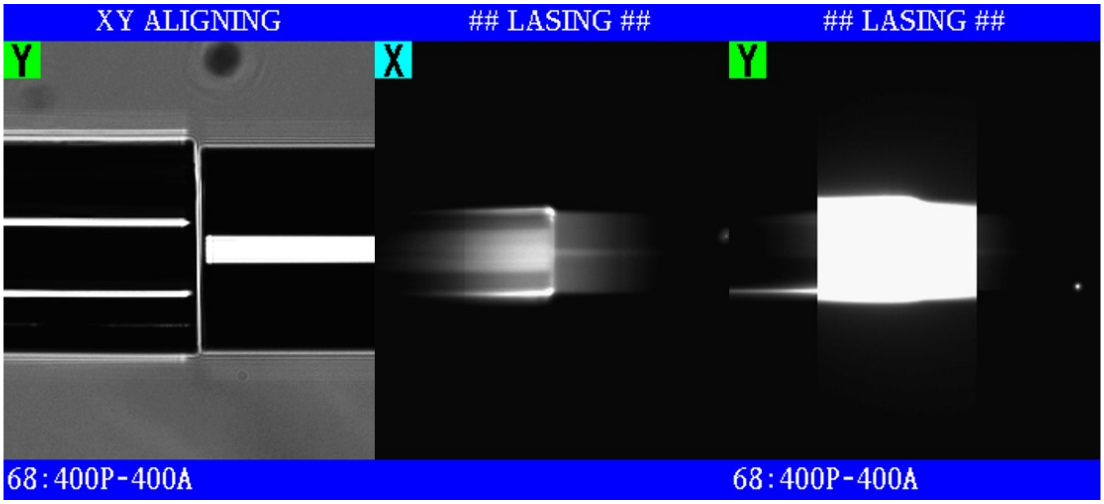

Figure 5.4: Splicer screenshots of 3x1 tapered fiber bundle splicing with 400 μm delivery fiber.

5.1.2 Characterization

Characterization of fabricated 3x1 combiner is divided into three subtopics which are structural, optical and thermal characterization.

5.1.2.1 Structural characterization

In the previous sections, we generally characterized the structure of the fiber bundle cross-sections (Figure 5.2b,c and d) and the splice points (Figure 5.3b) by using the optical microscope. The profile of tapered fiber bundle (Figure 5.2) is also characterized with z axis-scanning technique, which is a feature of CO_2 laser system. In addition to these techniques, SEM characterization images are shown in Figure 5.5. It is obvious that the end-face surface of fabricated 3x1 combiner is very smooth and clean. The fiber connection points inside the tube are symmetrical and air gaps between the fibers and the inner wall of the capillary tube are almost equal in size. Therefore, we can say that all structural characterization results are sufficient to continue the progress.

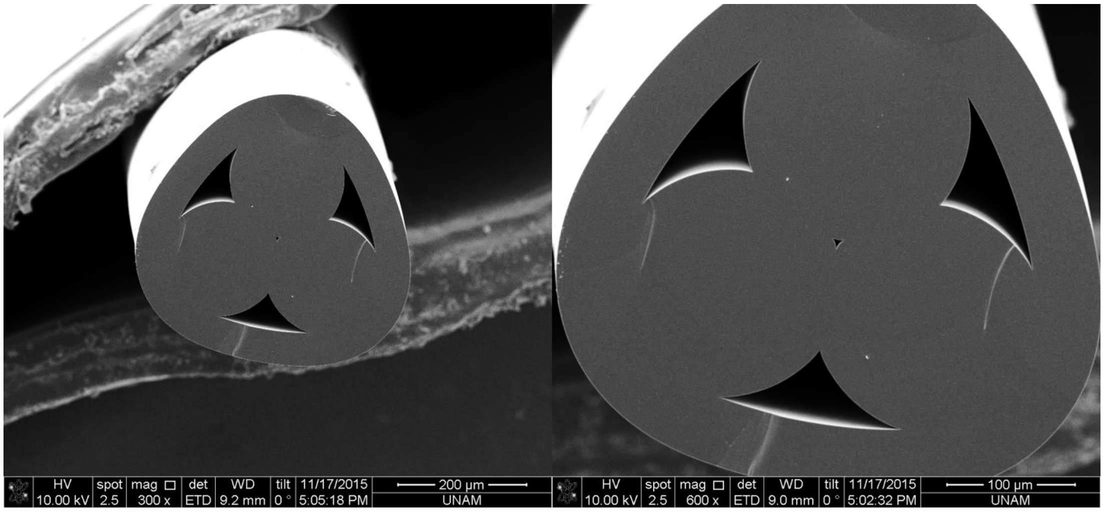

Figure 5.5: Scaning electron microscope images of 3x1 combiner cross-section.

5.1.2.2 Optical characterization

In order to characterize each port of the combiner, a 135 W Dilas laser diode is used. As in the 7x1 pump combiner characterization, the laser diode is first characterized optically, then the diode is spliced to each port orderly to measure the transmission loss. Optical characterization setup is shown in Figure 5.6.

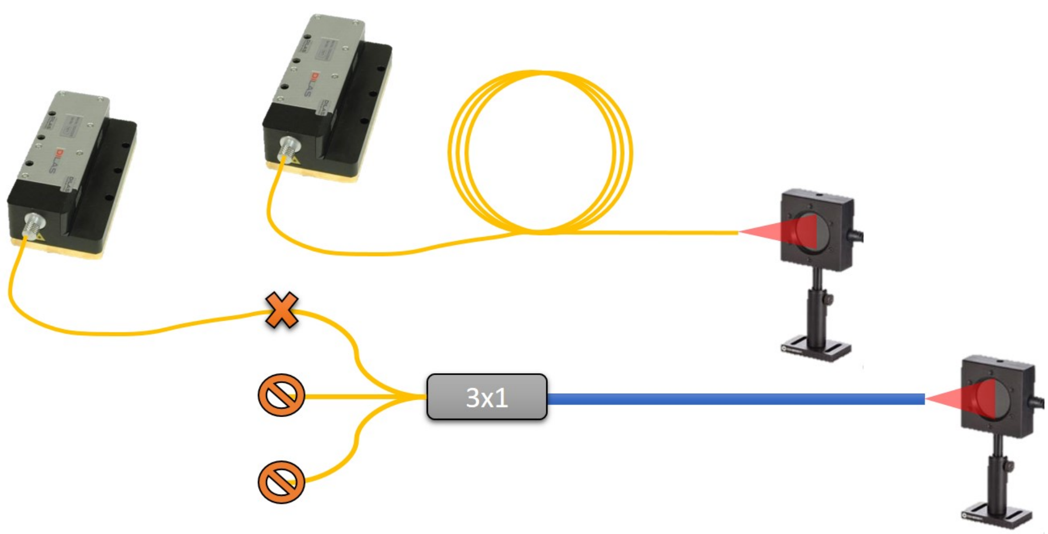

Figure 5.6: 3x1 combiner optical characterization setup

Current (A)	Diode Power (W)	Water Temperature (^oC)	Wavelength (nm)
3	3.9	18	970.83
6	21.27	18	971.32
9	37.65	18	971.56
12	54.2	18	972
15	70.73	18	972.25
18	87.28	19	973.48
21	104.9	19	974
24	123.6	19	974.13
25	129.1	18	974.49
26	134.6	18	975

Table 5.1: 135 W Dilas laser diode characterization results

The characterization of the water cooled laser diode is performed and the results are given in the table 5.1. The maximum output power of the laser diode is 134.6 W at 26 A current and temperature of 18 ^0C. The wavelength of the diode is 975 nm under these conditions. This diode is integrated to each port of the combiner to measure its transmission. Results of the transmission measurement are given in the Figure 5.7. *Coherent Position Sensing Water-Cooled Thermopile Sensor to 5 kW* (1 W resolution) is used in this optical characterization. There is a discrepancy of 2% between the transmission efficiencies of the combiner ports due to the resolution difference of the two powermeters used in the setup. Calculated average transmission efficiency of a fabricated 3x1 laser combiner is about 92.96%.

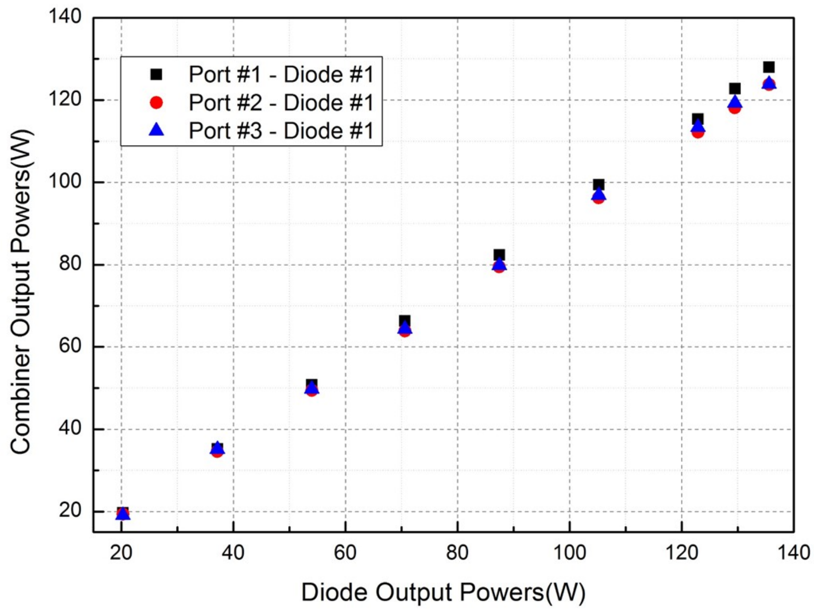

Port No.	Transmission Efficiency
1	94,6%
2	91.9%
3	92.4%

Figure 5.7: Optical output of 3x1 combiner from each port when pump power is launched by laser diode. Efficiencies of different ports are represented by right-hand side.

5.1.2.3 Thermal characterization

The fabricated 3x1 laser combiner is also integrated on the same heat sink that was used for the 7x1 pump combiner as shown in Figure 4.15b. The heat sink is cooled by water at a temperature from 17^oC to 19^oC. Thermal characterization of each port is performed and the increase in the temperature is found to be 7 ^oC, which is the same for all ports, as shown in Figure 5.8. Thermal images are captured before switching on the laser diode (Figure 5.8a) and after adjusting the laser power to its maximum value (Figure 5.8b). These observed thermal increments are similar to that of 7x1 pump combiner and it is an expected thermal load for a typical combiner.

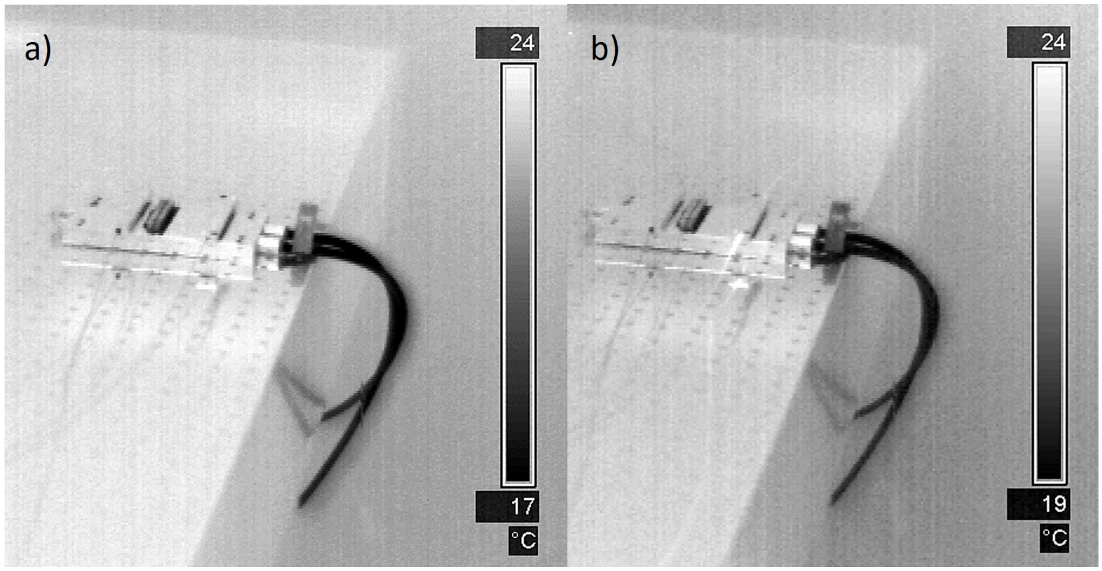

Figure 5.8: 3x1 combiner thermal image when a) unpowered laser diode, b) laser diode at maximum power.

5.2 Combining in-house built two high power fiber lasers with in-house fabricated 3x1 laser combiner

In our laboratory, two compact and monolithic 1080 nm high power fiber lasers which have output powers of 1 kW (976 nm pumped) and 690 W (915 nm pumped) are built. In this section, incoherent combining of these two lasers by the fabricated and characterized 3x1 laser combiner will be demonstrated. The setup of the laser combiner integrated to the high power fiber lasers is shown in Figure 5.9. As it can be understood from figure, the 1 kW laser is located at left-top and the 690 W laser is at right-bottom of the Figure. 20/400 μm output fibers of the lasers are spliced with 200/240 μm input fiber of the laser combiner and these splice points are covered with a metal case in order to prevent any possible damages. Housings of both the splice and the laser combiner are placed in water for active cooling as it is shown in left side of Figure 5.9. The unoptimized splice between the fiber laser output and the combiner input is shown in Figure 5.10. In this splice, the high quality laser light comes from 20 μm core of output fiber

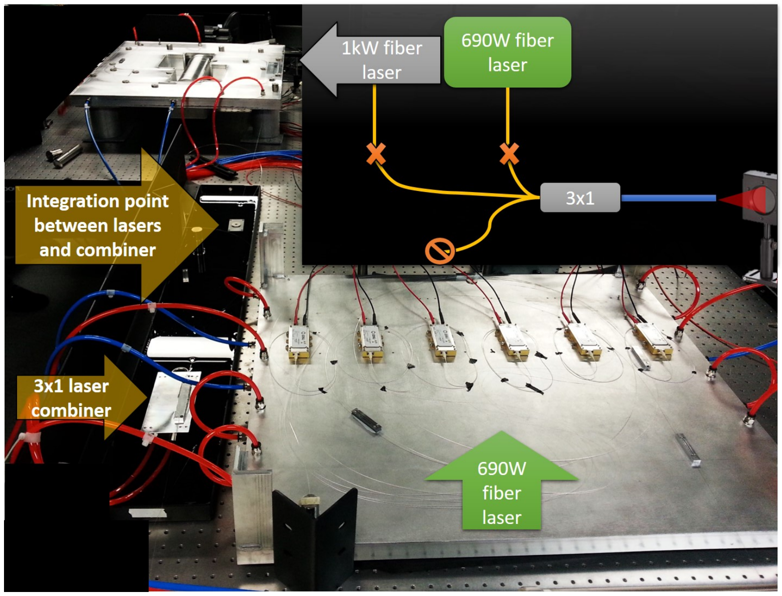

Figure 5.9: Setup of laser combiner integrated high power fiber lasers.

and couples to 200 μm core of the input fiber. However, the unabsorbed pump light also comes from 400 μm cladding of output fiber due to the lack of cladding light stripper on the fiber laser output. Although the splicing region is at almost adiabatic limits, it behaves like the pump light stripper. Therefore, the thermal load on this region can reach critical levels. The graph of the combined laser power versus the total launched power is plotted with their efficiencies and the data for laser powers are listed in the Figure 5.11.

According to the results on figure, 547 W of 690 W fiber laser and 575 W of 1 kW fiber laser are combined with an efficiency of 79,6% and the combination results in 893 W laser power from the combiner output. As the calculated 3x1 combiner efficiency is 93%, the splicing efficiency can also be calculated to be 85,6%. This low efficiency is caused by its pump light stripper-like behavior. We cannot reach higher combination power levels because the splice is not sufficient to handle power above 600 W. However, it is proven that each port of the combiner can handle 450 W and the characterization data show that it can handle more.

According to these results, the laser combiner combines two 1080 nm lasers pumped at 915 nm and 976 nm, yielding a total output power of 893 W. In

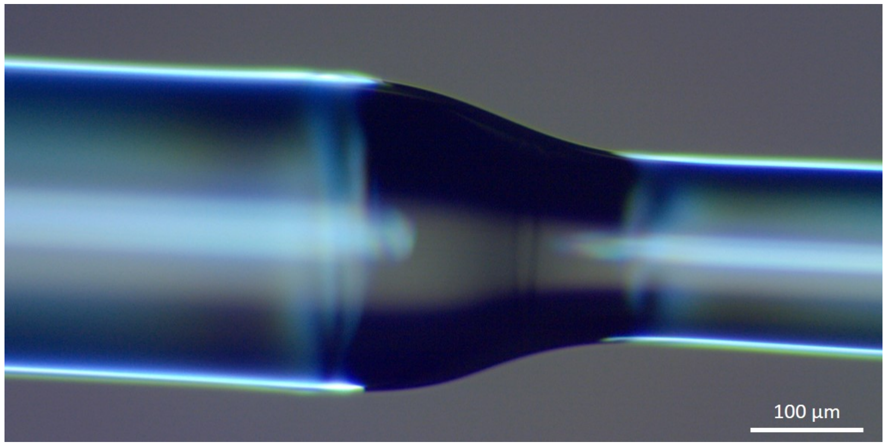

Figure 5.10: Integration point between high power fiber laser output fiber and 3x1 combiner input fiber.

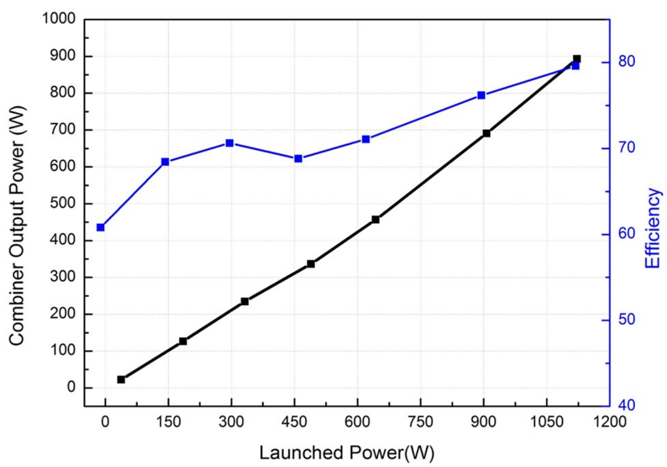

«690W Fiber Laser» Power	«1kW Fiber Laser» Power	Combiner Output Power
17,5W	20W	22,8W
79W	106W	126,6W
139W	193W	234,5W
201W	288W	336,5
260W	383W	457W
429W	478W	691W
547W	575W	893W

Figure 5.11: Combined laser power vs. total launched laser power from fiber lasers with their efficiencies and tabulated data.

Figure 5.12, the optical spectrum from the laser combiner output is given. The narrow-band lasing peak proves that the incoherent combining is successfully performed. Also, we observed that the 915 nm and the 976 nm unabsorbed pump light coming from the lasers is partially stripped at splicing points which we discussed on Figure 5.10.

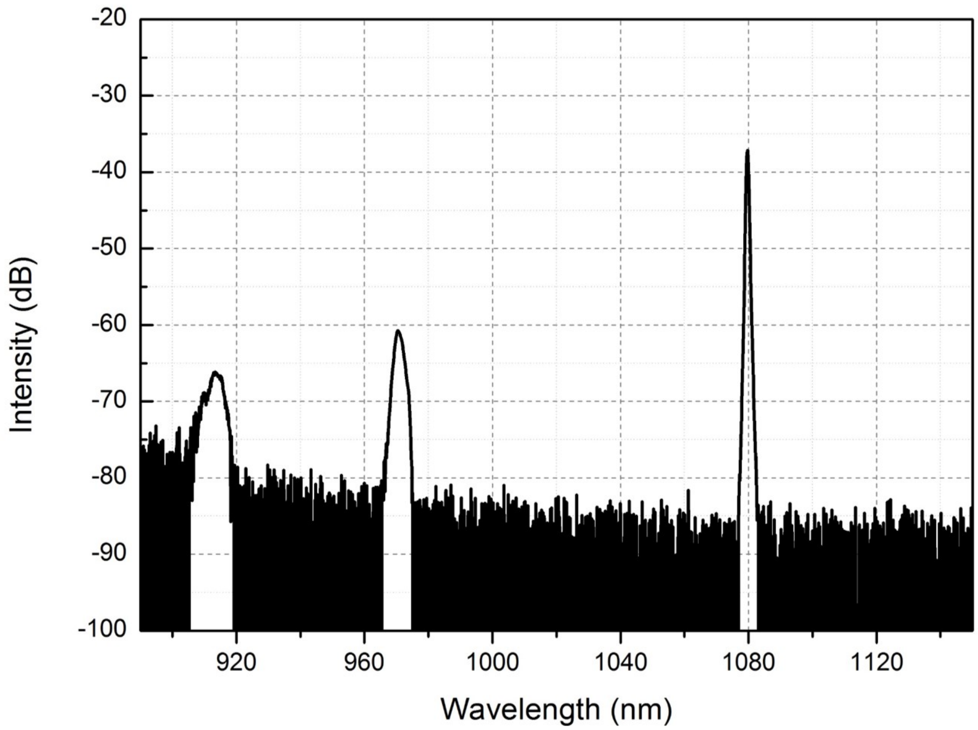

Figure 5.12: Optical spectrum from 3x1 laser combiner output while combining 915 nm and 976 nm pumped two 1080 nm high power fiber laser.

5.3 Preliminary studies for high quality high power fiber laser combining

In this section, there are two different preliminary studies; "7x1 laser combiner fabrication with 10/130 input fibers" and "laser combiner with tapered bridge fiber". These two concepts are important to combine lasers with high quality and low loss. High power beam combining approach with these two concepts are demonstrated in the literature [51, 52]. Following this approach, we have performed preliminary studies and the results will be presented.

5.3.1 7x1 fiber laser combiner fabrication

The 3x1 laser combiner fabrication has been shown in the previous section. Similar to this type of combiner, the 7x1 laser combiners are commonly used to combine the high power lasers. However, different from the 3x1 laser combiner, 7x1 combiner is fabricated with seven single-mode 10/130 μm core/cladding diameter optical fibers in order to achieve diffraction-limited high quality and high power laser light. Fabrication is performed by symmetrical and smooth tapering of the

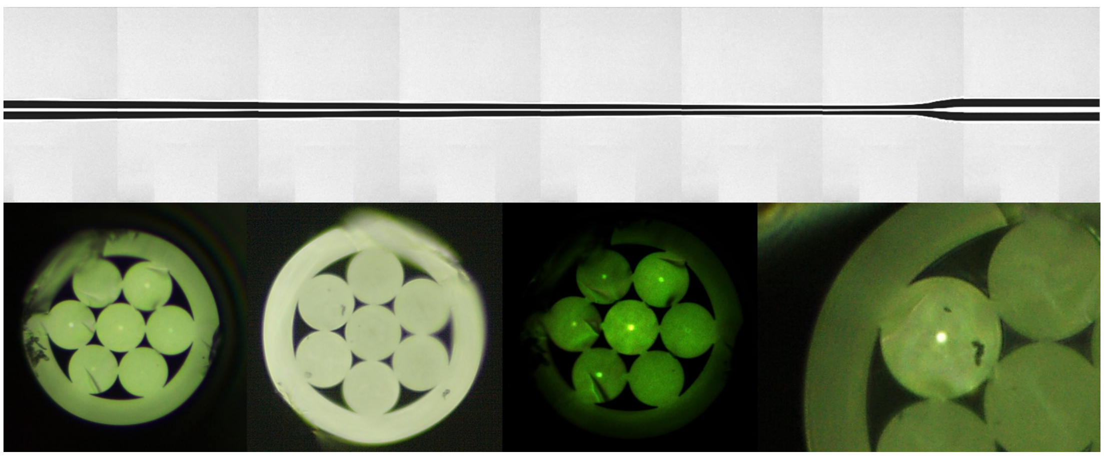

Figure 5.13: Tapering region and cross-section images of laser combiner with 10/130 μm input fibers.

fiber bundle with expected waist diameter of 250 μm. In Figure 5.13, tapered fiber bundle cross-sections are shown and uncleaved taper region is also given. It is obvious that end-face of the cleaved fiber bundle has a symmetrical structure with successfully merged fibers and the inner wall of capillary tube. The optical characterization of this combiner has not been performed yet due to lack of high power laser systems with an output fiber having 10 μm core diameter. In the future, we are planning to perform optical and thermal characterizations of this type of combiner and the other versions of 7x1 laser combiner will be fabricated with different core/cladding diameter optical fibers.

5.3.2 Laser combiner with tapered bridge fiber fabrication

The second concept of high power laser beam combining is fiber laser combiner with tapered bridge fiber. In this concept, delivery fiber or fiber bundle is not tapered but a coreless bridge fiber-a light guiding equipment is tapered and spliced to the delivery fiber and the fiber bundle. In Figure 5.14, structure of the combiner is depicted and preliminary studies of bridge fiber integration and tapering are also presented. It is clear that tapered fiber bundle can be spliced to bridge

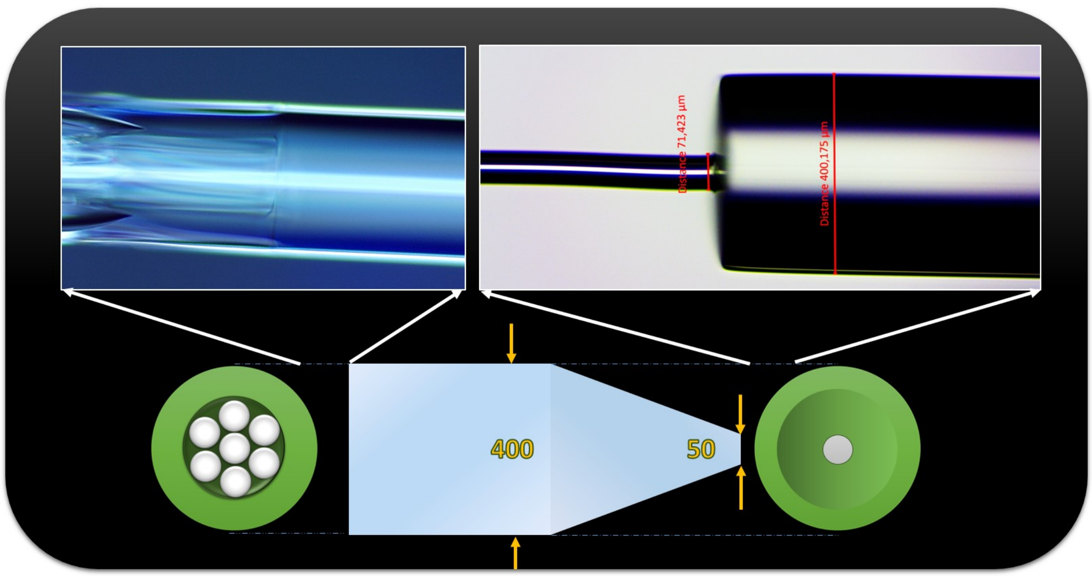

Figure 5.14: Bridge fiber critical integration points between combiner and 400 μm bridge and 50 μm tapered bridge fiber and 50/400 μm delivery fiber.

fiber successfully. In addition, bridge fiber can be tapered down to diameter of 70 μm and it can be spliced to the laser beam delivery fiber. In the literature, both concepts of laser combiner we described in Section 5.3.1 and this section are demonstrated. The first concept resulted with 5.7 kW laser combining with M^2 of 4.2 whereas 5.1 kW laser combining with M^2 of 6 was obtained as a consequence of the second concept [51]. This shows that both concepts are convenient for high quality laser combining. In the future, for the laser combiner with tapered bridge fiber concept, fabrication steps will be optimized and all characterizations will be performed including high power fiber laser integrations.

5.4 Summary

In this chapter, a 3x1 laser combiner were fabricated in order to combine two in-house built fiber lasers with output powers 1 kW and 690 W at 1080 nm wavelength. Structural, optical and thermal characterization of fabricated combiner was carried out. Moreover, combination of the two lasers were successfully realized and incoherently combined output light characteristics were discussed. Finally, a 7x1 laser combiner fabrication was presented and fiber laser fabrication with bridge fiber technique were introduced. Preliminary data for this two concepts were given.

Chapter 6

Conclusion

The aim of this work was to produce high quality, low-loss components and improve their integrations in high power fiber laser systems by tailoring optical fibers with CO_2 laser radiation. In order to construct a compact, robust, efficient high power fiber laser, we tackled integration issues between the optical fibers with same and different cladding diameters, and core offset fibers. These types of optical fibers were successfully integrated. Moreover, the splicing between two fibers which have core offset more than 10 μm was carried out well, even if they have different cladding shape and diameter. Thanks to the optimized splicing processes, end-caps were realized with claddings of 400 μm and 2000 μm based on designs and numerical studies.

Besides the fact that CO_2 laser radiation has prospering results for splicing process, it has proven to be advantageous on long-time glass tailoring operations such as lensing or tapering. In the lensing process, we have manipulated the optical fibers to produce spherically shaped ball lens. We have demonstrated fabrication of the two ball lenses with diameters of 1000 μm and 750 μm. In the other process, we have tapered the optical fibers, the capillary tubes and the fiber bundles. Thanks to the rotation and micron precision movement that is available in CO_2 laser system, we are able to taper them with accuracy of 5 μm. We have optimized tapering of capillary tube and optical fiber for producing high power fiber laser combiners. 7x1 Pump combiner was designed by 3D cad design software SolidWorks and numerically analyzed by ray tracing software, Zemax. Then, this combiner was fabricated and optimized in terms of the tapered fiber bundle geometry and cleaving of the fiber bundle. In addition, structural, optical and thermal characterization was carried out. The 7x1 pump combiner was integrated to the high power fiber laser system we have developed in our laboratory. Pump source limited power handling capacity of this pump combiner was 850 W with an overall efficiency of 98 %. We have also constructed a high power fiber laser which was operated at 1080 nm wavelength and 600 W output power by using this combiner. Furthermore, the same pump combiner was adapted to a laser system which was built by using an in-house fabricated active fiber. This fiber laser was operated at 1064 nm and its FBG-limited maximum output power was 420 W. Additionally, the 3x1 laser combiner was fabricated and characterized in terms of geometrical structure, power handling capacity, thermal load at splice point and its input port efficiency. We have used two ports of this combiner with a launched power of approximately 500 W from each of them. The combined power was measured as 893 W. The overall efficiency of the combiner is 93 %.

Finally, we have studied two concepts which are important to combine lasers with high quality and low loss. The concepts are "7x1 laser combiner fabrication with 10/130 input fibers" and "laser combiner with tapered bridge fiber". For the first concept, we have realized a 7x1 laser combiner structure. For the other concept, it was demonstrated that necessary integration points between the fiber bundle and bridge fiber can be successfully spliced. Besides tapering of bridge fiber diameter down to 70 μm, splicing of tapered bridge fiber and delivery fiber can be properly performed.

In this thesis, we exploit our know-how on CO_2 laser glass processing technology. Based on the results, we are limited with pump source in order to reach high power levels. In the future, we are planing to develop combiners for multi-kW fiber lasers by combining high power pump sources. This advanced fiber optical components could be, also, applicable for multi-kW fiber amplifier systems. In addition, we are motivated to develop different concepts of side-coupling and end-coupling combiners.

Bibliography

[1] D. Gloge, "Optical fibers for communication," *Appl. Opt.*, vol. 13, pp. 249–254, Feb 1974.

[2] C. Jauregui, J. Limpert, and A. Tunnermann, "High-power fibre lasers," *Nat Photon*, vol. 7, pp. 861–867, Nov 2013. Review.

[3] E. Snitzer, H. Po, F. Hakimi, R. Tumminelli, and B. McCollum, "Double clad, offset core nd fiber laser," in *Optical Fiber Sensors*, p. PD5, Optical Society of America, 1988.

[4] S. Poole, D. Payne, and M. Fermann, "Fabrication of low-loss optical fibres containing rare-earth ions," *Electronics Letters*, vol. 21, pp. 737–738, August 1985.

[5] A. Braglia, A. Califano, Y. Liu, and G. Perrone, "Architectures and components for high power cw fiber lasers," *International Journal of Modern Physics B*, vol. 28, no. 12, p. 1442001, 2014.

[6] J. Krause and C. Kurkjian, "Fibre splices with 'perfect fibre' strengths of 5.5 gpa, v¡0.01," *Electronics Letters*, vol. 21, pp. 533–535, June 1985.

[7] D. L. Bisbee, "Splicing silica fibers with an electric arc," *Appl. Opt.*, vol. 15, pp. 796–798, Mar 1976.

[8] H. Fujita, Y. Suzaki, and A. Tachibana, "Method of splicing optical fibers by co2 -laser," Apr. 21 1981. US Patent 4,263,495.

[9] S. Bhme, S. Fabian, T. Schreiber, R. Eberhardt, and A. Tnnermann, "End cap splicing of photonic crystal fibers with outstanding quality for high-power applications," 2012.

[10] U. C. Paek and A. L. Weaver, "Formation of a spherical lens at optical fiber ends with a co2 laser," *Appl. Opt.*, vol. 14, pp. 294–298, Feb 1975.

[11] B. Saleh and M. Teich, *Fundamentals of Photonics.* Wiley Series in Pure and Applied Optics, Wiley, 2007.

[12] R. Quimby, *Photonics and Lasers: An Introduction.* Wiley, 2006.

[13] G. Keiser, *Optical fiber communications.* McGraw-Hill series in electrical and computer engineering: Communications and signal processing, McGraw-Hill, 2000.

[14] M. Artiglia, G. Coppa, P. Di Vita, M. Potenza, and A. Sharma, "Mode field diameter measurements in single-mode optical fibers," *Lightwave Technology, Journal of*, vol. 7, pp. 1139–1152, Aug 1989.

[15] D. Marcuse, "Gaussian approximation of the fundamental modes of graded-index fibers," *J. Opt. Soc. Am.*, vol. 68, pp. 103–109, Jan 1978.

[16] S. Arabasi, "Tapered splice for ecient power coupling to small-core nonlinear fibers," *Blacksburg, Virginia: Virginia Polytechnic Institute and State University*, 2008.

[17] J. Love, W. Henry, W. Stewart, R. Black, S. Lacroix, and F. Gonthier, "Tapered single-mode fibres and devices. i. adiabaticity criteria," *Optoelectronics, IEE Proceedings J*, vol. 138, pp. 343–354, Oct 1991.

[18] A. Snyder and J. Love, *Optical Waveguide Theory.* Science paperbacks, Springer, 1983.

[19] E. Snitzer, "Neodymiumglass laser," in *in Proc. 3rd Int. Conf. Solid Lasers*, pp. 999–1019, 1963.

[20] C. J. Koester and E. Snitzer, "Amplication in a ber laser," *Applied Optics*, vol. 3, no. 10, p. 11821186, 1964.

[21] V. Dominic, S. MacCormack, R. Waarts, S. Sanders, S. Bicknese, R. Dohle, E. Wolak, P. Yeh, and E. Zucker, "110 w fibre laser," *Electronics Letters*, vol. 35, pp. 1158–1160, Jul 1999.

[22] D. Machewirth, V. Khitrov, B. Samson, U. Manyam, K. Tankala, S. Heinemann, C.-H. Liu, and A. Galvanauskas, "All-fiber based linearly polarized single-mode ytterbium fiber laser with >300w output," in *Optical Fiber Communication Conference and Exposition and The National Fiber Optic Engineers Conference*, p. OTuF2, Optical Society of America, 2005.

[23] Y. Jeong, J. Sahu, D. Payne, and J. Nilsson, "Ytterbium-doped large-core fibre laser with 610 w of near diffraction-limited output power," *Electronics Letters*, vol. 40, pp. 1527–1528, Nov 2004.

[24] Y. Jeong, J. K. Sahu, D. N. Payne, and J. Nilsson, "Ytterbium-doped large-core fiber laser with 1.36 kw continuous-wave output power," *Opt. Express*, vol. 12, pp. 6088–6092, Dec 2004.

[25] E. Stiles, *New developments in IPG fiber laser technology.* 5th International Workshop on Fiber Lasers, Dresden, Germany, 2009.

[26] D. J. Richardson, J. Nilsson, and W. A. Clarkson, "High power fiber lasers: current status and future perspectives," *(Invited) J. Opt. Soc. Am. B*, vol. 27, pp. B63–B92, Nov 2010.

[27] J. Limpert, F. Roser, S. Klingebiel, T. Schreiber, C. Wirth, T. Peschel, R. Eberhardt, and A. Tunnermann, "The rising power of fiber lasers and amplifiers," *Selected Topics in Quantum Electronics, IEEE Journal of*, vol. 13, pp. 537–545, May 2007.

[28] R. Paschotta, *Encyclopedia of laser physics and technology*, vol. 1. Wiley-vch Berlin, 2008.

[29] C. Bollig, C. Jacobs, M. J. D. Esser, E. H. Bernhardi, and H. M. von Bergmann, "Power and energy scaling of a diode-end-pumped nd:ylf laser through gain optimization," *Opt. Express*, vol. 18, pp. 13993–14003, Jun 2010.

[30] G. A. Newburgh, A. Word-Daniels, A. Michael, L. D. Merkle, A. Ikesue, and M. Dubinskii, "Resonantly diode-pumped ho3+:y2o3 ceramic 2.1 μm laser," *Opt. Express*, vol. 19, pp. 3604–3611, Feb 2011.

[31] J. Yu, L. Guo, H. Wu, Z. Wang, H. Tan, S. Gao, D. Wu, and K. Zhang, "High brightness laser-diode device emitting 160 watts from a 100 μm/na;0.22 fiber," *Appl. Opt.*, vol. 54, pp. 9385–9389, Nov 2015.

[32] F. Dorsch, V. Bluemel, M. Schroeder, D. Lorenzen, P. Hennig, and D. Wolff, "Fiber-coupled diode laser systems up to 2-kw output power," 2000.

[33] D. M. Grasso, N. Shou, H. Chen, R. Pathak, P. Liang, S. D. Roh, and D. Lee, "Wavelength-stabilized fiber-coupled diode laser with 500 w output and 20 mm mrad beam quality," *Proc. SPIE 8381, Laser Technology for Defense and Security VIII, 83810K*, vol. 9, Feb 2012.

[34] M. Zervas and C. Codemard, "High power fiber lasers: A review," *Selected Topics in Quantum Electronics, IEEE Journal of*, vol. 20, pp. 219–241, Sept 2014.

[35] K. S. Abedin, J. M. Fini, T. F. Thierry, B. Zhu, M. F. Yan, L. Bansal, F. V. Dimarcello, E. M. Monberg, and D. J. DiGiovanni, "Seven-core erbium-doped double-clad fiber amplifier pumped simultaneously by side-coupled multimode fiber," *Opt. Lett.*, vol. 39, pp. 993–996, Feb 2014.

[36] M. Haag, B. Khler, J. Biesenbach, and T. Brand, "Novel high-brightness fiber coupled diode laser device," 2007.

[37] T. Theeg, H. Sayinc, J. Neumann, L. Overmeyer, and D. Kracht, "Pump and signal combiner for bi-directional pumping of all-fiber lasers and amplifiers," *Opt. Express*, vol. 20, pp. 28125–28141, Dec 2012.

[38] C. Jauregui, S. Böhme, G. Wenetiadis, J. Limpert, and A. Tünnermann, "Side-pump combiner for all-fiber monolithic fiber lasers and amplifiers," *J. Opt. Soc. Am. B*, vol. 27, pp. 1011–1015, May 2010.

[39] P. Yan, M. Gong, C. Li, P. Ou, and A. Xu, "Distributed pumping multifiber series fiber laser," *Opt. Express*, vol. 13, pp. 2699–2706, Apr 2005.

[40] A. Grudinin, D. Payne, P. Turner, L. Nilsson, M. Zervas, M. Ibsen, and M. Durkin, "Multi-fibre arrangements for high power fibre lasers and amplifiers," Nov. 30 2004. US Patent 6,826,335.

[41] S. Norman, M. Zervas, A. Appleyard, P. Skull, D. Walker, P. Turner, and I. Crowe, "Power scaling of high-power fiber lasers for micromachining and materials processing applications," 2006.

[42] D. DiGiovanni and A. Stentz, "Tapered fiber bundles for coupling light into and out of cladding-pumped fiber devices," Jan. 26 1999. US Patent 5,864,644.

[43] S. Yin, P. Yan, and M. Gong, "End-pumped 300 w continuous-wave ytterbium-doped all-fiber laser with master oscillator multi-stage power amplifiers configuration," *Opt. Express*, vol. 16, pp. 17864–17869, Oct 2008.

[44] A. Kosterin, V. Temyanko, M. Fallahi, and M. Mansuripur, "Tapered fiber bundles for combining high-power diode lasers," *Appl. Opt.*, vol. 43, pp. 3893–3900, Jul 2004.

[45] D. DiGiovanni and M. Fishteyn, "Method of applying a precursor to an assembled fiber bundle and fusing the bundle together," June 4 2002. US Patent 6,397,636.

[46] M. Fishteyn, "Etched tapered fiber bundle and method of making the same," Apr. 24 2007. US Patent 7,209,615.

[47] C. Headley III, M. Fishteyn, A. D. Yablon, M. J. Andrejco, K. Brar, J. Mann, M. D. Mermelstein, and D. J. DiGiovanni, "Tapered fiber bundles for combining laser pumps (invited paper)," 2005.

[48] F. Gonthier, L. Martineau, N. Azami, M. Faucher, F. Seguin, D. Stryckman, and A. Villeneuve, "High-power all-fiber components: the missing link for high-power fiber lasers," 2004.

[49] E. Wikszak, "Inscription of ber bragg gratings in non-photosensitive and rare-earth doped bers applying ultrafast lasers," *Roubaix, Friederic Schiller Universitat Jena*, 2009.

[50] J. W. Dawson, M. J. Messerly, R. J. Beach, M. Y. Shverdin, E. A. Stappaerts, A. K. Sridharan, P. H. Pax, J. E. Heebner, C. W. Siders, and C. Barty, “Analysis of the scalability of diffraction-limited fiber lasers and amplifiers to high average power,” *Opt. Express*, vol. 16, pp. 13240–13266, Aug 2008.

[51] T. Eschrich, D. Hoh, F. Just, J. Kobelke, S. Unger, M. Jäger, and H. Bartelt, “Incoherent beam combining of 5.1kw using a 7x1 signal combiner into a 50 μm core output fiber,” in *Advanced Photonics*, p. JTu6A.1, Optical Society of America, 2014.

[52] M. H. Muendel, R. Farrow, K.-H. Liao, D. Woll, J. Luu, C. Zhang, J. J. Morehead, J. Segall, J. Gregg, K. Tai, B. Kharlamov, H. Yu, and L. Myers, “Fused fiber pump and signal combiners for a 4-kw ytterbium fiber laser,” 2011.

[53] A. Yablon, *Optical Fiber Fusion Splicing*. Springer Series in Optical Sciences, Springer Berlin Heidelberg, 2005.

[54] R. H. Doremus, “Viscosity of silica,” *Journal of Applied Physics*, vol. 92, no. 12, 2002.

[55] J. Krause, S. Kher, and D. Stroumbakis, “Arc fusion splices with near pristine strengths and improved optical loss,” in *Optical Communication, 1996. ECOC ’96. 22nd European Conference on*, vol. 2, pp. 237–240 vol.2, Sept 1996.

[56] W. Zheng, H. Sugawara, T. Mizushima, and W. Klimowych, “Heating power feedback control for co2 laser fusion splicers,” 2013.

[57] K. L. Wlodarczyk, “Surface deformation mechanisms in laser smoothing and micro-machining of optical glasses,” *Edinburgh, UK: Heriot-Watt University*, 2011.

[58] V. Ter-Mikirtychev, “Physical and optical properties of laser glass,” in *Fundamentals of Fiber Lasers and Fiber Amplifiers*, vol. 181 of *Springer Series in Optical Sciences*, pp. 27–36, Springer International Publishing, 2014.

[59] H. Quarzglas, “Quartz glass nomenclature,” 2015.

[60] D. W. Lane, "The optical properties and laser irradiation of some common glasses," *Journal of Physics D: Applied Physics*, vol. 23, no. 12, p. 1727, 1990.

[61] P. Herman, R. Marjoribanks, A. Oettl, K. Chen, I. Konovalov, and S. Ness, "Laser shaping of photonic materials: deep-ultraviolet and ultrafast lasers," *Applied Surface Science*, vol. 154?155, pp. 577 – 586, 2000.

[62] A. D. McLachlan and F. P. Meyer, "Temperature dependence of the extinction coefficient of fused silica for co2 laser wavelengths," *Appl. Opt.*, vol. 26, pp. 1728–1731, May 1987.

[63] H. Rtger, "D. g. holloway, d. a. tawney. the physical properties of glass. the wykeham science series 24 verlag wykeham publications (london) ltd, london and winchester 1973 220 seiten, 118 figuren, 16 tabellen; broschiert 2.50," *Kristall und Technik*, vol. 8, no. 12, pp. K53–K53, 1973.

[64] N. Tomozeiu, "Silicon oxide (siox, 0¡x¡2): a challenging material for optoelectronics," in *Optoelectronics - Materials and Techniques*, InTech, 2011.

[65] D. Noordegraaf, M. D. Maack, P. M. W. Skovgaard, J. Johansen, F. Becker, S. Belke, M. Blomqvist, and J. Laegsgaard, "All-fiber 7x1 signal combiner for incoherent laser beam combining," 2011.